Fraunhofer
IAF

FRAUNHOFER-INSTITUT FÜR ANGEWANDTE FESTKÖRPERPHYSIK IAF

SCIENCE FOR SYSTEMS No. 21

Daniel Lopez-Diaz

BROADBAND TRANSCEIVER CIRCUITS FOR MILLIMETER-WAVE WIRELESS COMMUNICATION

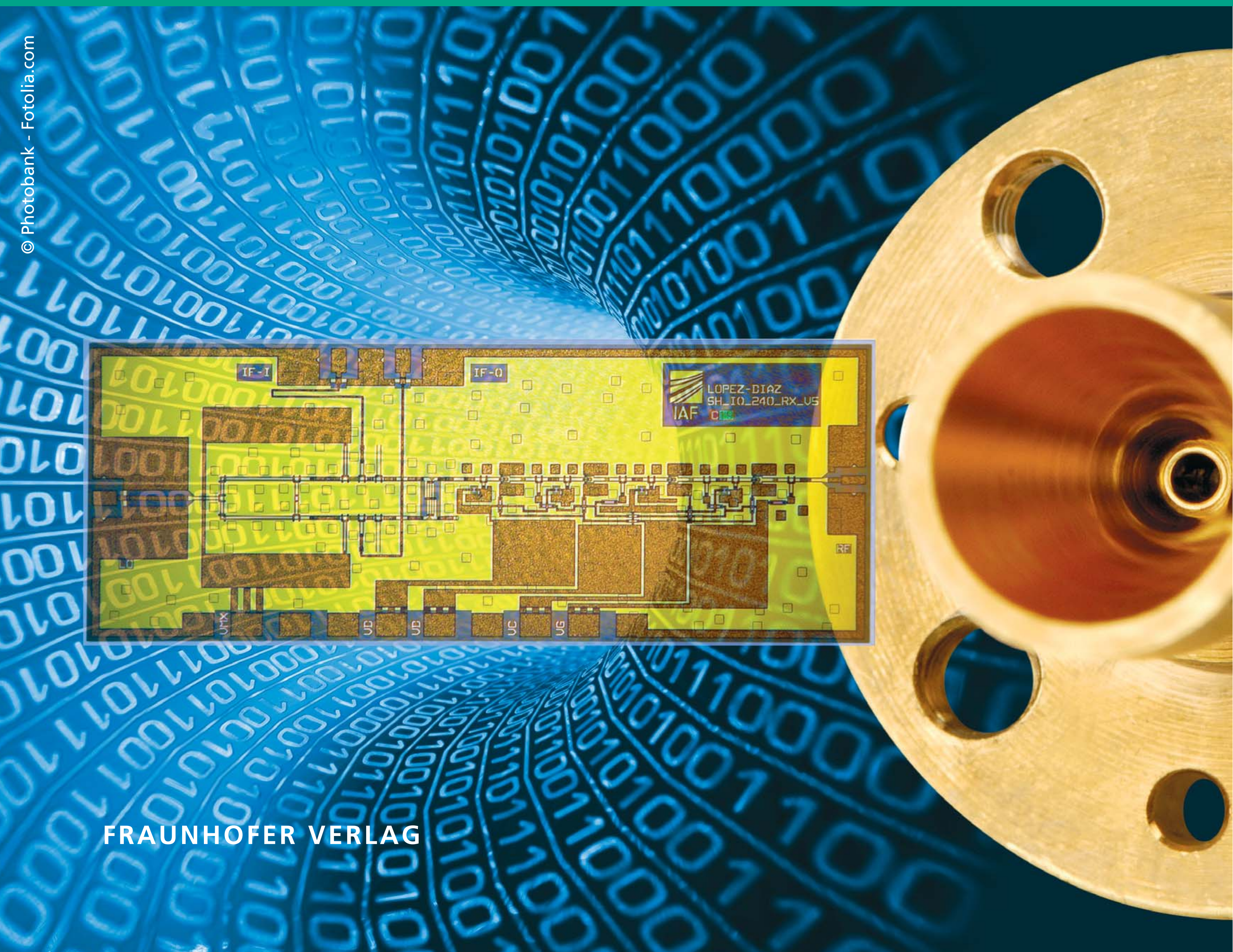

FRAUNHOFER VERLAG

Fraunhofer-Institut für
Angewandte Festkörperphysik IAF

Science for Systems

Band 21

Daniel Lopez-Diaz

Broadband Transceiver Circuits for Millimeter-Wave Wireless Communication

FRAUNHOFER VERLAG

Kontaktadresse:
Fraunhofer-Institut für
Angewandte Festkörperphysik IAF
Tullastraße 72
79108 Freiburg
Telefon 0761/5159-0
Telefax 0761/5159-400
E-Mail info@iaf.fraunhofer.de
URL www.iaf.fraunhofer.de

Bibliografische Information der Deutschen Nationalbibliothek
Die Deutsche Nationalbibliothek verzeichnet diese Publikation in der
Deutschen Nationalbibliografie; detaillierte bibliografische Daten sind im
Internet über http://dnb.d-nb.de abrufbar.
ISBN (Print): 978-3-8396-0834-0

D 93

Zugl.: Stuttgart, Univ., Diss., 2014

Titelbild: © Photobank-Fotolia.com und Fraunhofer IAF

Umschlaggestaltung: Fraunhofer IAF
Druck: Mediendienstleistungen des
Fraunhofer-Informationszentrum Raum und Bau IRB, Stuttgart

Für den Druck des Buches wurde chlor- und säurefreies Papier verwendet.

Fraunhofer-Informationszentrum Raum und Bau IRB
Postfach 80 04 69, 70504 Stuttgart
Nobelstraße 12, 70569 Stuttgart
Telefon 07 11 9 70-25 00
Telefax 07 11 9 70-25 08
E-Mail verlag@fraunhofer.de
URL http://verlag.fraunhofer.de

Broadband Transceiver Circuits for Millimeter-Wave Wireless Communication

Von der Fakultät für Informatik, Elektrotechnik und Informationstechnik der Universität Stuttgart zur Erlangung der Würde eines Doktor-Ingenieurs (Dr.-Ing.) genehmigte Abhandlung

Vorgelegt von

Daniel Lopez-Diaz

aus Weingarten

Hauptberichter:	**Prof. Dr. Ingmar Kallfass**
Mitberichter:	**Prof. Dr. Hermann Schumacher**

Tag der mündlichen Prüfung:	**25.09.2014**

Institut für Robuste Leistungshalbleitersysteme der Universität Stuttgart

2014

Zusammenfassung

In der vorliegenden Arbeit werden breitbandige elektronische Sender und Empfänger für die drahtlose Kommunikation im hohen Millimeterwellen (mmW) Frequenzbereich um 240 GHz untersucht.
Funksysteme in diesem Frequenzbereich werden üblicherweise als "Terahertz"-Kommunikation bezeichnet. Die dort verfügbaren absoluten Bandbreiten ermöglichen höchste Datenraten und schließen somit potentiell die technologische Lücke zwischen schneller, leitungsgebundener und bisher vergleichsweise langsamer, drahtloser Kommunikation. Zu diesem Zweck werden in dieser Arbeit frequenzumsetzende, monolithisch integrierte, Millimeterwellenschaltungen auf Basis des am Fraunhofer Institut für Angewandte Festkörperphysik (IAF) entwickelten metamorphen high electron mobility Transistors (mHEMT) entworfen. Diese Technologie ist aufgrund des niedrigen Eigenrauschens und der sehr hohen Grenzfrequenzen eine der wenigen Halbleitertechnologien, die für aktive integrierte Schaltungen in diesem Frequenzbereich geeignet sind. Die Erschließung der verfügbaren Bandbreite stellt allerdings hohe Ansprüche an das Schaltungsdesign für die breitbandige Frequenzkonversion im hohen mmW Frequenzbereich. Die mHEMT-Transistoren mit ihren hohen Grenzfrequenzen müssen möglichst leistungseffizient und breitbandig als frequenzumsetzende, nichtlineare Bauelemente betrieben und mit passiven und Impedanz-transformierenden Bauelementen zu integrierten Schaltungen erweitert werden. Die besondere Herausforderung stellt dabei die Kombination aus hoher Mittenfrequenz, Bandbreite und multifunktionaler Integration dar. Dabei müssen alle Komponenten, einzeln und im System, die Ansprüche einer digitalen Datenübertragung per Funk wie z.B. hohe Empfindlichkeit und Linearität erfüllen. Mit steigender Frequenz müssen darüber hinaus beim Schaltungsentwurf parasitäre Effekte berücksichtigt werden, die bei niedrigeren Frequenzen vernachlässigt werden können. Dazu zählt unter anderem die Ausbreitung und Kopplung der elektromagnetischen Wellen durch das Halbleitersubstrat. Zur wissenschaftlichen Untersuchung verschiedener Schaltungskonzepte für die Frequenzumsetzung werden in dieser Arbeit Transistor-basierende aktive und passive Mischer analysiert, entworfen und charakterisiert. Oftmals kann in diesem Frequenzbereich die erforderliche Lokaloszillator-Leistung nur mit erheblichem Aufwand erzeugt werden. Aus diesem Grund sind subharmonische Schaltungskonzepte mit einem Lokaloszillator bei kleineren Frequenzen von besonderem Interesse. Die kleinen Wellenlängen in diesem Frequenzband erlauben die on-chip Integration von 0° und 90° Leitungskopplern für Balancierte- und Quadraturmischer. Gleichzeitig steigt bei diesen extrem kurzen Wellenlängen der Einfluss aller Leitungselemente und erfordert die elektro-magnetische Feldsimulation der meisten Leitungsstrukturen während des Schaltungsentwurfs. Die Kombination mit Hochfrequenz-Verstärkern zu multi-funktional integrierten Sendern und Empfängern vereint die Vorteile kompakter Abmessungen, Leistungsfähigkeit und Kosteneffizienz. Die in dieser Arbeit entwickelten, monolithisch integrierten, aktiven Sender- und Empfänger bilden das funktionale Herzstück einer 240 GHz Funkstrecke, mit

der erstmals Daten mit bis zu 40 Gbit/s drahtlos im Single-Input Single-Output (SISO) Verfahren übertragen wurden. Als Teil eines Langstreckendemonstrators ermöglichten sie die Übertragung von bis zu 24 Gbit/s über eine Distanz von 1.1 km. Durch die sehr großen Bandbreiten, wird eine nahtlose Integration in faseroptische Netze möglich, die zum Teil noch einfache und daher breitbandige Modulationsformate wie On-Off Keying (OOK) einsetzen. Neben diesen simplen Modulationsverfahren erlauben die subharmonischen Quadraturmischer auch die Übertragung von spektral effizienter Phasenumtastung (PSK).

Executive Summary

In the present work, broadband millimeter wave (mmW) receiver and transmitter circuits for wireless communication in the frequency range around 240 GHz are investigated. Radio systems in this frequency range are commonly referred to as "Terahertz" communication. The absolute available bandwidths in the mmW frequency range allow high data rates and thus potentially close the technological gap between fast but wired and the comparatively slow and wireless communication. For this purpose, monolithic integrated millimeter wave mixer circuits are designed and analyzed in this work, based on the metamorphic high electron mobility transistor (mHEMT), developed at the Fraunhofer Institute for Applied Solid State Physics (IAF). This technology is one of the few semiconductor technologies which are suitable for active integrated circuits in this high frequency range due to the low noise and high cutoff frequencies. However, the exploitation of the available bandwidth places high demands on the circuit design of broadband frequency conversion circuits in the upper mmW frequency range. The mHEMT transistors with their high cutoff frequencies must be operated efficiently as broadband, non-linear components and extended together with passive and impedance-transforming devices to multifunctional integrated circuits. The major design challenge is the combination of high center frequency, bandwidth, and multifunctional integration. All system components must meet, combined and individually, the demands of a digital wireless data transmission, such as high sensitivity and linearity. With increasing frequency, parasitic effects have also to be taken into account during circuit design which can be neglected at lower frequencies. These include, amongst others, the coupling and propagation of electromagnetic waves through the semiconductor substrate. For the scientific investigation of various circuit topologies for frequency conversion, transistor-based active and passive mixers are analyzed, designed and characterized in this work. In this frequency range, the required local oscillator power can often only be generated with considerable effort. For this reason, circuit designs with a subharmonic local oscillator, located at lower frequencies, are of special interest. The small wavelengths in this frequency band allow the on-chip integration of 0 ° and 90 ° line couplers for balanced and quadrature mixers. At the same time, the influence of all line elements increases with this extremely short wavelength and requires the electromagnetic field simulation of the layout structures during the circuit design. The integration with high-frequency amplifiers combines the advantages of compact size, performance and cost effectiveness. The active monolithic integrated transmitter and receiver, developed in this work, form the functional core of a 240 GHz radio link, which was able to transmit data with up to 40 Gbit/s for the first time in a single-input single-output (SISO) configuration. As part of a long range demonstrator, they allowed the transmission of up to 24 Gbit/s over a distance of 1.1 km. The seamless integration into fiber optical networks, which are partly still using wideband modulation formats such as on-off keying (OOK), is possible due to the very large RF and baseband bandwidths. In addition to these simple modulation methods, the sub-harmonic

quadrature mixers also allow the transmission of spectrally efficient phase shift keying (PSK).

Contents

Acronyms

2DEG	two-dimensional electron gas
AWG	arbitrary waveform generator
ASK	amplitude-shift keying
balun	balanced-to-unbalanced transfomer
BER	bit error rate
BERT	bit error rate tester
BMBF	Federal Ministry of Education and Research
BPSK	binary phase-shift keying (PSK)
BW	bandwidth
CMOS	complementary metal oxide semiconductor
CPW	coplanar waveguide
CPWG	grounded coplanar waveguide
DCA	digital communication analyzer
DEMUX	de-multiplexer
DSB	double sideband
DUT	device under test
DVB	digital video broadcasting
EASY-A	Enablers for Ambient Services & Systems
EM	electromagnetic
ENR	excess noise ratio
EVM	error vector magnitude
FCC	Federal Communications Commission
FET	field-effect transistor
Fraunhofer IAF	Fraunhofer Institute for Applied Solid State Physics
GaAs	gallium-arsenide
HBT	hetero junction bipolar transistor
HD-PE	high-density polyethylene
HEMT	high electron mobility transistor
HFSS	high frequency structural simulator from Ansys Corp.
HPBW	half power beamwidth
IC	integrated circuit
IF	intermediate frequency
IHE	Institut für Hochfrequenztechnik und Elektronik
InP	indium-phosphide
InGaAs	indium-gallium-arsenide
IPQ	Institute of Photonics and Quantum Electronics
I/Q	in-phase/quadrature
ITU	International Telecommunication Union
KIT	Karlsruhe Institute of Technology

LNA	low noise amplifier
LO	local oscillator
LSB	lower sideband
LSSP	large signal scattering parameter (S-parameter)
MBE	molecular beam epitaxy
MOSFET	metal-oxide-semiconductor field-effect transistor
mHEMT	metamorphic high electron mobility transistor
MIM	metal-insulator-metal
MMIC	millimeter-wave monolithic integrated circuit
mmW	millimeter-wave
MSG	maximum stable gain
MUX	multiplexer
NF	noise figure
NFA	noise figure analyzer
NiCr	nickel-chromium
OFDM	orthogonal frequency-division multiplexing
OOK	on-off keying
PCB	printed circuit board
PPG	pulse pattern generator
PSK	phase-shift keying
QPSK	quadrature PSK
QAM	quadrature amplitude modulation
RADAR	radio detection and ranging
RF	radio frequency
RFIC	radio frequency integrated circuit
RMS	root mean square
RPG	Radiometer Physics GmbH
Rx	receiver
SEM	scanning electron microscope
Si	silicon
SiGe	silicon-germanium
SiN	silicon-nitride
SIS	superconductor-insulator-superconductor
SISO	single-input single-output
SNR	signal-to-noise ratio
SOI	silicon on insulator
S-parameter	scattering parameter
SPDT	single pole double throw
SSB	single sideband
TCP/IP	Transmission Control Protocol / Internet Protocol
TV	television
Tx	transmitter
USB	upper sideband
VNA	vector network analyzer
VoD	video on demand

VoIP	voice over IP
WiGig	Wireless Gigabit Alliance
WLAN	wireless local area network
WPAN	wireless personal area network
Y-parameter	admittance parameter

List of Symbols

C	channel capacity
CG	mixer conversion gain
C_{gd}	gate to drain capacitance
C_{gs}	gate to source capacitance
C_{ds}	drain to source capacitance
C_{OFF}	off state capacitance
d	distance
Δf	Bandwidth
ϵ_r	dielectric constant
ϵ_{re}	effective dielectric constant
F	noise factor
f_c	center frequency
f_{LO}	local oscillator frequency
f_{max}	maximum oscillation frequency
f_t	transit frequency
g_m	transconductance
$g_{m,max}$	maximum transconductance
I_b	diode bias current
I_D	diode current
I_D	drain current
$I_{D,max}$	maximum drain current
k	coupling coefficient
k_B	Boltzmann constant: $1.3806488 \cdot 10^{-23}$J/K
L_0	free-space path loss
L_{IF}	IF path loss
λ	wavelength
n	diode ideality factor
P_{IF}	IF power
P_N	noise power
P_{RF}	RF power
q	elementary electric charge: $1.602176565 \cdot 10^{-19}$C
r	even mode and odd mode impedance ratio
R_{ds}	channel resistance
R_{max}	maximum channel resistance
R_{ON}	on state channel resistance
R_S	diode series resistance
T	temperature
T_0	defined standard ambient temperature: 290 K
V_g	gate voltage

V_{gs}	gate to source voltage
V_D	diode voltage
V_D	drain voltage
V_{IF}	IF voltage
V_{RF}	RF voltage
V_T	thermal voltage ($k_B T/q$)
V_{th}	threshold voltage
Y	Y factor
Z_e	even mode impedance
Z_L	characteristic line impedance
Z_o	odd mode impedance
Γ	reflection coefficient
μ	carrier mobility
ω	angular frequency

1 Introduction

1.1 Motivation

The massive increase in global data traffic poses new challenges to the network operators. The driving forces are new innovative devices and services such as smartphones, tablets and cloud computing which also entails a transformation in the consumer behavior [1]. Mobile access to the Internet, email and media, including music, photos and movies are an integral part of modern life. While it was formerly almost exclusively stationary computers that communicated with each other over wired connections, there are today in addition television (TV) sets, game consoles, set-top boxes, smart phones, tablets, etc. connected to the internet [1]. Thanks to packet-oriented protocols such as the Transmission Control Protocol / Internet Protocol (TCP/IP), it does not matter whether these devices are connected to the network by radio, optical fiber or telephone line. These advantages are a major reason for the network convergence which means additional data traffic. Triple play, i.e. the combination of phone, Internet and television was in the past based on three independent networks, which are now bundled available over the Internet due to voice over IP (VoIP) and video on demand (VoD). But exactly these services place greater demands on the network in terms of latency, and especially available bandwidth (BW). These increased bandwidth requirements of modern services also show very clearly the disadvantages of an inadequate network coverage. While in large cities broadband connections are available for many households, the rural areas, with a few potential customers, suffer particularly from slow data connections.
The increase in the data traffic is not only limited to the large networks of the service providers but plays an increasingly important role at home where the usage and sharing of digital media also requires fast network connections. In the past, movies and music were stored on media such as CDs and DVDs while they are today more and more often stored as files on a hard disk. With high resolution media, the rapid distribution to the playback devices, such as TVs or tablets represents a growing problem. Both problems, the cost effective connection of rural areas, as well as the need for high speed short range connections could be ideally addressed by wireless links in the upper millimeter wave frequency range. Up till now, wireless data transmission was mainly focused on frequencies of several GHz. Wireless local area network (WLAN) for example operates at frequencies up to 5 GHz [2] and even the latest microwave backhaul connections operate at frequencies below 100 GHz [3]. For future indoor wireless communication, the unlicensed 60 GHz frequency band is of special interest. Research projects like "Enablers for Ambient Services & Systems (EASY-A)", funded by the German Federal Ministry of Education and Research (BMBF) [4],[93] as well as the commercial Wireless Gigabit Alliance (WiGig) [5] aim to make this frequency band accessible to multi-gigabit wireless links.

The utilization of mmW frequencies above 200 GHz opens up new application areas, wherein this work high speed wireless communication is of particular interest. Broadband short range and long range directional links are two applications which benefit from the large absolute bandwidth available at these frequencies.
When it comes to long range communication, wired high speed data transmission is, up to today, based on optical fiber communication which employs, e.g. on-off keying (OOK) signals. The wireless transmission of such signals requires usually a change in the modulation format to increase the spectral efficiency of the radio signal. With increasing data rates the effort to change the modulation format in real time becomes more challenging and requires sophisticated and power hungry signal processing. The large absolute bandwidths available above 200 GHz enable a new solution to this problem by the direct up- and down-conversion of the OOK signals without a change of the modulation format.
The increasing traffic on communication networks forces the network operators to upgrade their networks constantly. This affects all network levels from the long-haul and backbone networks to the local loop. Installing new broadband connections is cost-intensive and especially in densely developed areas not always possible. Directional radio links in the millimeter wave frequency range are able to provide a solution to this problem by transmitting multi-gigabit signals over the air without the need for heavy construction work as illustrated by figure 1.1 [94].

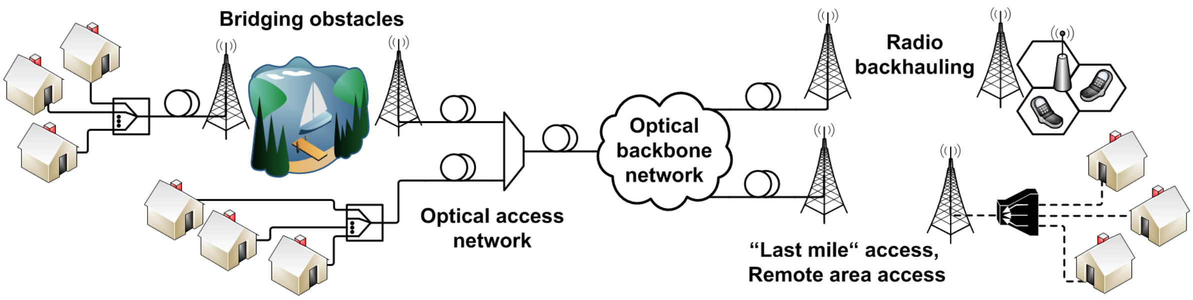

Fig. 1.1: Illustration of different application scenarios for a multigigabit wireless link: last mile access, wireless backhauling and the cost effective connection of optical networks across obstacles like rivers, lakes and valleys (source Koenig, et. al.).

Wireless personal area networks (WPANs), operating at mmW frequencies, are able to provide a solution for high data rate indoor communication by the combination of high throughput based on the large available bandwidth and high frequency reuse factor due to the increased path loss in this frequency range and the signal blocking by walls etc. [6]. The up and down conversion of the high speed baseband signals requires microwave mixers with extremely broadband input and output ports. The advantages of integrated millimeter wave circuits come along with new design challenges at higher frequencies. Effects such as through-substrate coupling or parasitics which could be ignored at lower frequencies must now be taken into account. On the other hand the very high frequencies provide the strong advantage of a higher integration factor due to the smaller wavelength. When the wavelength is in the range of a millimeter, on-chip integrated antennas become eventually possible.

Advances in modern semiconductor manufacturing allow the realization of transistors with increased operating frequencies which are continuously driving towards the Terahertz frequency regime [7–9]. High electron mobility transistors (HEMTs) based on indium-phosphide (InP) composite semiconductors feature currently the highest transit frequencies and are therefore the first choice for monolithic integrated circuits in the high millimeter wave frequency range [7, 10–12].
Although there are many possible application scenarios for integrated mixers in the high millimeter wave frequency range, this work is focused on millimeter wave wireless data transmission. Depending on the intended application, different design goals apply to the circuit design. The specification for a mixer in a radio detection and ranging (RADAR) application differs significantly from the one of a communication receiver. An up or down converter in a data transmission system for example has to feature a large intermediate frequency (IF) and radio frequency (RF) bandwidth while the IF bandwidth in a RADAR application is typically much lower. The presented mixers may be of interest for other applications but those will not be examined in this work.

1.2 Purpose of this work

The main focus of this work is the entire design chain of extremely broadband receiver and transmitter millimeter-wave monolithic integrated circuits (MMICs) and their subsequent system integration. Since mixers form the key element for the frequency conversion within the transmitters and receivers, particular attention is paid to them.
For only few applications, simple single ended mixers are sufficient. Many application scenarios are demanding more sophisticated mixing stages which offer quadrature functionality or increased port to port isolation which cannot be achieved by a single mixer stage. For the design of balanced and quadrature mixers at high millimeter-wave (mmW) frequencies passive coupler structures are needed and are therefore investigated first. Although the research about couplers and hybrids has a long history, new challenges arise, when these designs are used at very high frequencies and integrated on small scale substrates. Coupling through the substrate and over the air are only two effects which play an increasing role as the dimensions become smaller and the operation frequency increases.
The core issue is the design of broadband mixer circuits above 200 GHz and there are many mixer topologies suitable for the design of broadband receiver and transmitter MMICs. Several active and passive mixer concepts are examined and judged based on their figures of merit like conversion gain, isolation, local oscillator (LO) requirement and bandwidth. These investigations are not based only on simulations but are also proven by measurements performed on manufactured MMICs.
On the way to complete receiver and transmitter MMICs, the measurements of the individual building blocks are not sufficient to estimate the performance of a combination of the couplers and different mixer cells. Although measurement based simulations are possible, these simulation cannot take all effects into account which appear in a monolithic integrated circuit. Coupling through the substrate as well as effects of the biasing network are frequently observed during the measurements. The realized mixers and couplers are therefore used to create different balanced and quadrature mixers and

evaluate their performance with respect to port isolation, amplitude and phase imbalance. The most promising combination regarding bandwidth, LO requirement, port isolation and imbalance is then combined with an existing RF low noise amplifier (LNA) to create fully integrated receiver and transmitter MMICs. After manufacturing and characterization, these MMICs are packaged into waveguide modules which require extremely precise manufacturing and state of the art packaging technologies to preserve the on wafer performance of the MMIC in the package.
The packaged receiver and transmitter are then employed to perform data transmission experiments in the frequency range above 200 GHz. The requirements on the receiver and transmitter differ based on the used modulation format. To prove the ability of the broadband mmW receiver and transmitter to transmit exceptionally high data rate signals from an optical fiber network over the air, different transmission experiments with different modulation formats are performed over distances up to 1.1 km.

This thesis is divided into six chapters. The first chapter covers the motivation and purpose of this work. It also includes an overview over the reported state of the art from passive hybrids over integrated mixer circuits to wireless data transmission. In chapter two, the theory of passive and active mixers is introduced and different manufacturing technologies are presented. Among these semiconductor technologies, the Fraunhofer Institute for Applied Solid State Physics (Fraunhofer IAF) metamorphic high electron mobility transistor (mHEMT) technology plays a prominent role and is presented in detail since all circuits of this work are realized using this technology. After manufacturing, the circuits need to be characterized and the different measurement methods are described in chapter three. Chapter four forms the core of this work and covers the design of passive hybrids as well as active and passive mixer circuits. It ends with the presentation of a fully integrated subharmonic in-phase/quadrature (I/Q) receiver (Rx) and transmitter (Tx) chipset. This chipset is then used in chapter five to build a wireless link for data transmission experiments with data rates of up to 40 Gbit/s. The performance of this link with respect to different modulation formats, signal bandwidth and channel attenuation is examined and presented. A summary and an outlook in chapter six conclude this work.

1.3 State of the Art

Although there are only a few technologies available to create active integrated RF circuits above 200 GHz, there has been a significant amount of scientific work in this field. This fact points up the increasing interest from scientific as well as commercial institutions in this frequency range.
This chapter summarizes recently reported work around the main building blocks, needed to create integrated circuits for mmW communication, such as couplers and hybrids, mixers and fully integrated receiver and transmitter circuits. The chapter concludes with an overview about recently reported data transmission experiments between 200 - 300 GHz.

1.3.1 Couplers and Hybrids

Couplers and hybrids are essential building blocks and can be found in virtually any microwave system. Depending on their center frequency, they are either realized as discrete components or are monolithically integrated. The very short wavelengths in the mmW frequency range reduces the size of most couplers to less than a square millimeter and enable the on chip integration of power dividers and couplers.
Important figures of merit of integrated power dividers and couplers are the operation frequency, bandwidth and insertion loss. Major issues are the increased losses at higher frequencies. Usually, higher operation frequencies require thinner substrates to prevent the propagation of unwanted modes and, in case of grounded coplanar waveguide (CPWG) transmission lines, smaller ground to ground spacing which leads to a smaller center conductor with increased attenuation [13]. Table 1.1 gives an overview over reported integrated couplers in the frequency range from 170 to 320 GHz.

f_c [GHz]	Type	Coupling Ratio [dB]	Insertion Loss [dB]	BW [GHz]	Rel. BW [%]	Ref.
170	Lange	3	0.7	70[1]	51.8	2009 [14, 15]
180	Branch-line	3	1	60	33.3	2006 [16]
220	Coupled line	3	0.6[2]	>80[2]	>36.4[2]	2012 [17]
320	Tandem	3	1.2	100	37.03	2010 [18]

[1]based on S_{21} only
[2]simulated

Table 1.1: Reported mmW couplers above 100 GHz.

1.3.2 Monolithic Integrated mmW Mixers

Besides the passive components, mixer cells are a key element of receiver and transmitter MMICs. Different topologies and manufacturing technologies are available which have all their individual advantages and disadvantages. While InP based HEMTs offer the highest transit and oscillation frequencies, silicon (Si) based technologies feature a higher scale of integration and a more mature model basis. An overview over reported integrated mmW mixer circuits in the frequency range from 150 - 300 GHz is given in table 1.2.

f_c [GHz]	Type	Technology	CG [dB]	IF-BW[1] [GHz]	Rel. IF-BW [%]	Year and Ref.
300	fund. resistive	mHEMT	-20	N/A	N/A	2009 [95]
245	4th harm. transcond.	SiGe	-13[2]	1.5	0.6	2012 [19]
220	fund. resistive	mHEMT	-7.9	14	6.3	2008 [20]
220	sub-harm. Gilbert	SiGe	+2[3]	10	4.5	2011 [21]
200	fund. resistive	mHEMT	-8	>24	>11.4[4]	2011 [22]
200	single bal. resistive	mHEMT	-12.2	>18	>9.8[5]	2011 [22]
200	fund. resistive	mHEMT	-11.7	N/A	N/A	2009 [23]
200	active MOSFET-C	90 nm CMOS	-13.4[6]	3	1.5	2012 [24]
180	single bal. active	45 nm CMOS	-4	13.7	8.6[7]	2011 [25]
156.3	double bal. resistive	45 nm CMOS	-12	>26	>16.6	2011 [25]

[1] 3-dB bandwidth.
[2] Conversion gain of the mixer core, based on simulated IF buffer gain.
[3] Conversion gain of the entire receiver minus LNA gain.
[4] f_{LO}=209 GHz
[5] f_{LO}=184 GHz
[6] Conversion gain of the receiver minus TIA gain at the IF ports.
[7] f_{LO}=184 GHz

Table 1.2: Reported monolithic integrated mmW mixers

The conversion gain of the reported mixers as a function of their center frequency is illustrated in figure 1.2. It can be seen that the frequency range above 200 GHz is exclusively dominated by silicon-germanium (SiGe) and other compound semiconductor technologies while complementary metal oxide semiconductor (CMOS) technology catches up and allows already the realization of mixers up to 200 GHz [24]. Nevertheless, the HEMT based technologies offer outstanding noise and speed performances which make them the first choice for the realization of broadband mixers.

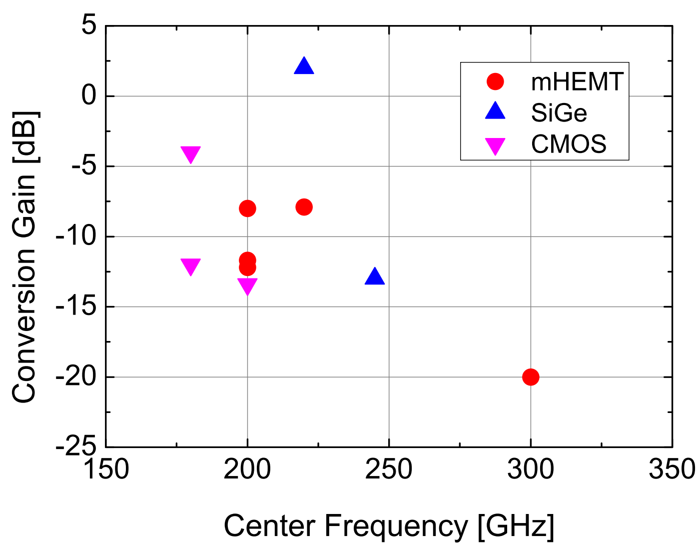

Fig. 1.2: Conversion gain of reported integrated mmW mixers, realized in different semiconductor technologies, as a function of the center frequency.

1.3.3 Receiver and Transmitter MMICs above 200 GHz

Together with other active circuitry, the passive components and the mmW mixers enable the design of single-chip receiver and transmitter MMICs. Similar to the mixer cells, the upper mmW frequency range above 200 GHz is dominated by SiGe and compound semiconductors. Table 1.3 summarizes reported receiver MMICs above 200 GHz.

f_c [GHz]	f_{LO} [GHz]	Technology	CG [dB]	NF [dB]	IF-BW[1] [GHz]	Rel. IF-BW [%]	Year and Ref.
650	162.5	SiGe	-13	42	4	0.6	2010 [26]
320	17.7	SiGe	-14	36	8	2.5	2012 [27]
300	100	mHEMT	13.7	N/A	N/A	N/A	2011 [28]
220	110	SiGe	16	15	10	4.5	2011 [21]
220	110	mHEMT	2	8.4	4.5	2.0	2008 [29]
220	55	mHEMT	3.5	7.4	6	2.7	2011 [30]
200	100	mHEMT	7	6.9	N/A	N/A	2009 [23]

[1] 3-dB bandwidth

Table 1.3: Reported monolithically integrated mmW receiver circuits

To transmit high speed data wirelessly over the air a chipset consisting of a receiver as well as a transmitter is required. As illustrated by the summary in table 1.4, compound semiconductors are able to provide more gain, larger bandwidth and higher output power above 200 GHz compared to CMOS and SiGe technologies.

f_c [GHz]	f_{LO} [GHz]	Technology	IF-BW[1] [GHz]	CG [dB]	P_{Out} [dBm]	Year and Ref.
630	210[2]	InP HBT	15	-24	-30	2012 [31]
245	-[3]	SiGe	-	-	1.4	2012 [32]
220	110	mHEMT	20	-3.6	1.4	2011 [96]
220	55	mHEMT	10	-8	-6	2011 [30]

[1] 3-dB bandwidth.
[2] On-Chip PLL with external 21 GHz reference oscillator.
[3] On-Chip VCO

Table 1.4: Reported electronic based integrated mmW transmitter circuits

1.3.4 Wireless Data Transmission employing mmW Technology

The wireless transmission of high speed digital signals in the range of several tens of Gbit/s requires very broadband receiver and transmitter circuits. These large absolute bandwidths are only available in the mmW frequency range. Millimeter wave communication has gained increasing interest of commercial and scientific organizations which results in ever faster data rates transmitted wirelessly [30, 33–37][94, 96–99]. Table 1.5 gives an overview over reported all MMIC based wireless data transmission above 100 GHz.

f_c [GHz]	Data Rate [Gbit/s]	Distance [m]	Modulation Format	Year and Ref.
200[1]	1.25	2.6	ASK	2010 [33]
220	12.5	0.5	-	2011 [30]
220	30	-	BPSK	2012 [34]
220	25	10	OOK	2012 [99]
220	20	0.5	OOK	2012 [94]
220	9	0.5	OFDM-QPSK	2012 [94]
250[1]	8	0.5	ASK	2009 [35]
295.2	0.096	52	OFDM-64QAM	2010 [36]
300[1]	24	0.5	ASK	2012 [37]

[1]Employing a photonic transmitter.

Table 1.5: Reported wireless transmission experiments between 200 and 300 GHz based on mmW technology

The transmitted data rate as a function of the carrier frequency is plotted in figure 1.3. The numbers next to the marks specify the distance of the data transmission. Due to the high path loss and small output power in the upper mmW frequency range, the links are only able to bridge distances of several tens of meters.

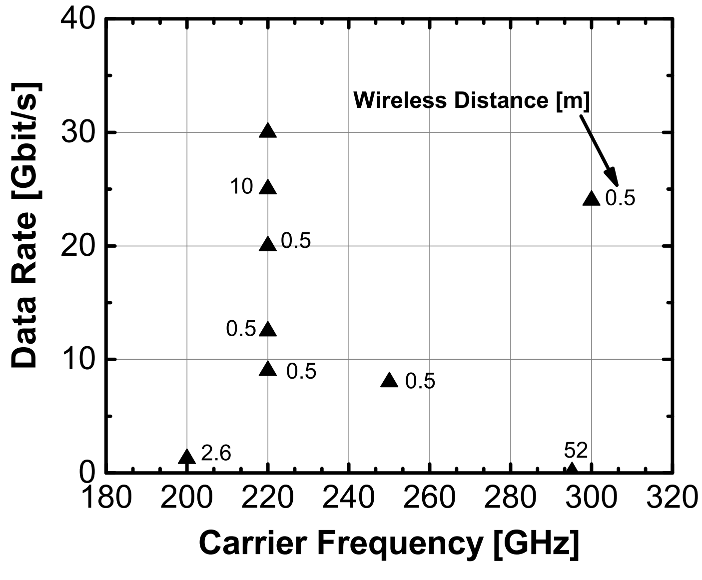

Fig. 1.3: Overview of reported wireless transmission experiments in the mmW frequency range as a function of the carrier frequency.

To overcome the short distances and further increase the bandwidth of the wireless data transmission, improved mixing stages need to be investigated as they convert the low frequency baseband signals to RF signals and vice versa. Prior to the circuit design, the fundamental theory behind active and passive mixers is described in the following chapter.

2 mmW Mixer Topologies

Frequency conversion is, besides amplification, a key element of any mmW receiver and transmitter system. Mixers are used for the up or down conversion of the IF and RF signals respectively, and different topologies for mmW mixers can be found in the literature.
The fundamental concept of a mixer is based on the multiplication of two signals which yields to sum and difference frequencies at the output. A mixer is therefore a three port device. The following trigonometric identity illustrates the frequency mixing by signal multiplication:

$$sin(\omega_1 t)sin(\omega_2 t) = \frac{1}{2}\left[(cos((\omega_1 - \omega_2)t) - cos((\omega_1 + \omega_2)t)\right] \tag{2.1}$$

As described, the multiplication results in the sum and the difference frequencies which is an important fact and must be taken into account during the design process. In many cases, the mixer output contains unwanted spectral components which need to be filtered afterwards.
In this work, the ports of all mixers are named according to the commonly used nomenclature:

- RF: Input port in a receiver or output port in a transmitter integrated circuit (IC). Generally a modulated small signal with a receiver and a modulated large signal with a transmitter in the mmW frequency range.
- LO: Local oscillator, input port in the same frequency range as the RF signal in fundamental mixers. In subharmonic mixers, the LO is situated at half of the RF center frequency.
- IF: Intermediate frequency, output port in a receiver or input port in a transmitter. Normally a much lower frequency signal.

The diagrams in figure 2.1 show the signals for an up conversion scenario (a) and a down conversion scenario (b). The LO port is in all configurations an input port while the IF port is the output in a down converter and an input in an up converter.

2.1 Unbalanced and Balanced Mixers

From a system perspective, the mixer has always the three terminals described above. Form the designer's point of view, there are three main circuit topologies to realize a mixer independent of the employed mixing device (e.g. diode, metal-oxide-semiconductor field-effect transistor (MOSFET) or high electron mobility transistor (HEMT)):

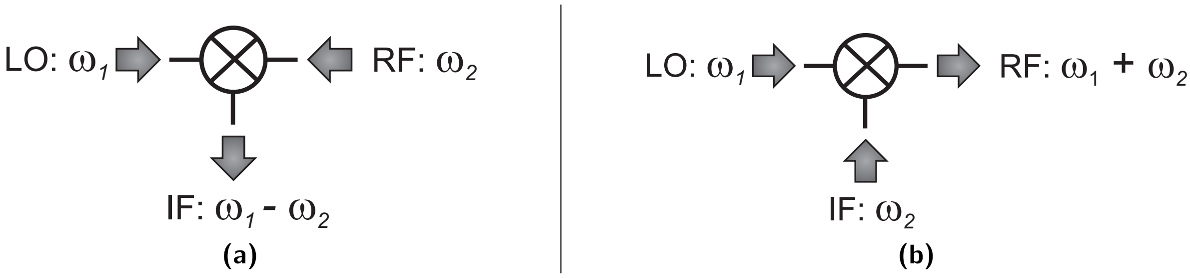

Fig. 2.1: A Mixer used as down converter (a) and up converter (b)

- Unbalanced or single-ended: all input signals are single-ended.
- Single balanced: one of the input signals is a differential (balanced) signal.
- Double balanced: all signals are differential.

The advantage of balanced mixers over unbalanced is the improved port isolation. While with a single balanced mixer only the balanced port is isolated (e.g. the LO from the RF but not the IF from the RF) are in a double balanced structure all ports isolated from each other as long as the balanced signals are 180° out of phase and the mixing devices are identical.
While most mixers at microwave frequencies are double balanced structures, many mixers in the upper mmW frequency range are single-ended or single balanced mixers like those presented in this work.
The two main reasons for this are the less available LO power at those high frequencies as well as the great frequency spacing between the IF and RF or LO ports. The generation of a strong LO signal in the upper mmW frequency range is challenging and in addition, the insertion losses of any divider network are also increasing with the frequency of operation. A double balanced structure would need to split the LO power by four to drive, for example, the gates of a passive mixer. In case of a quadrature mixer with I/Q functionality an additional power split for the in-phase and the quadrature mixer would again lower the available power at the mixing devices. In many applications above 200 GHz , there is simply not enough LO power available to drive a double balanced mixer. On the other hand, a single-balanced mixer, which features a reasonable LO-RF isolation, might often be sufficient. An adequate LO-IF and RF-IF isolation could be easily achieved by low order filter structures since those frequencies are often separated by the factor 100.

2.2 Devices for Monolithic Integrated Mixers

Basically, mixing of different signals occurs in any nonlinear device. Reported mixers in the high mmW frequency regime are realized by either a nonlinear optical device [35, 38, 39], superconductor-insulator-superconductor (SIS) elements [40, 41], Schottky diodes [36], hetero junction bipolar transistors (HBTs), MOSFETs and HEMTs. The scope of this work is on monolithic integrated mmW mixers and therefore only integrated Schottky diodes and transistors are considered as mixing devices.

2.2.1 Diode Mixers

A single-ended diode mixer is simply realized by applying the LO as well as the RF or IF signal to the diode and use a subsequent filter to separate the wanted signal. In case of a down converting mixer, the LO and RF signal are added and applied to the diode as shown in figure 2.2. The down converted IF is separated using a low-pass filter (LP-filter). To simplify the analysis of the mixing operation, ideal voltage sources are used.

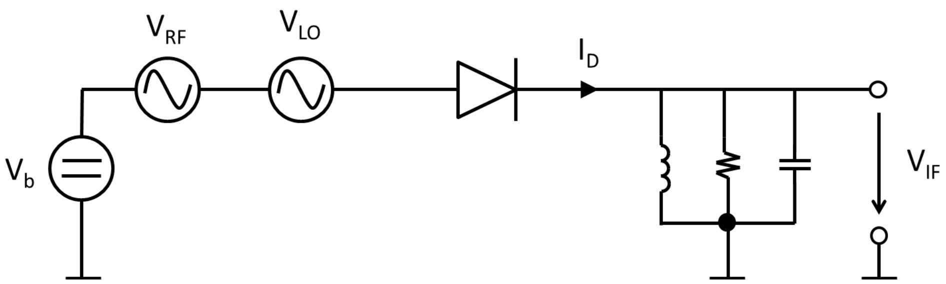

Fig. 2.2: Simplified schematic of a single diode down converting mixer.

The Taylor series up to the fifth degree of the current $I_D(V_D)$ through a diode equals:

$$I_D(V_D) = I_S(e^{\frac{V_{LO}+V_{RF}+V_b}{nV_T}} - 1) \tag{2.2}$$

$$I_D(V_D) \approx I_S(e^{\frac{V_b}{nV_T}} \cdot e^{\frac{V_{LO}}{nV_T}} \cdot e^{\frac{V_{RF}}{nV_T}}) \tag{2.3}$$

substituting $I_b = I_S \cdot e^{\frac{V_b}{nV_T}}$

$$I_D(V_D) \approx I_b \cdot [(1 + \frac{V_{LO}}{nV_T} + \frac{V_{LO}^2}{2(nV_T)^2} + \cdots) \cdot (1 + \frac{V_{RF}}{nV_T} + \frac{V_{RF}^2}{2(nV_T)^2} + \cdots)] \tag{2.4}$$

The mixing product occurs in the second order intermodulation product:

$$I_b \cdot \frac{V_{LO} \cdot V_{RF}}{(nV_T)^2} \tag{2.5}$$

For the down converting case, the RF and LO voltages are:

$$V_{RF} = A_{RF} \cdot cos(\omega_{RF} t) \tag{2.6}$$

$$V_{LO} = A_{LO} \cdot cos(\omega_{LO} t) \tag{2.7}$$

$$V_{RF} \cdot V_{LO} = A_{RF} A_{LO} \cdot cos(\omega_{RF} t) \cdot cos(\omega_{LO} t) \tag{2.8}$$

$$V_{RF} \cdot V_{LO} = \frac{A_{RF} A_{LO}}{2} [cos((\omega_{RF} - \omega_{LO})t) + cos((\omega_{RF} + \omega_{LO})t)] \tag{2.9}$$

Inserting the difference frequency term into equation 2.5:

$$I_{IF} = I_b \cdot \frac{A_{RF}A_{LO}}{2(nV_T)^2} \cdot cos((\omega_{RF} - \omega_{LO})t) \tag{2.10}$$

A current to voltage conversion by the filter network leads to the IF voltage:

$$V_{IF} \propto I_b \cdot \frac{A_{RF}A_{LO}}{2(nV_T)^2} \cdot cos((\omega_{RF} - \omega_{LO})t) \tag{2.11}$$

Although equation 2.11 implies that the IF voltage and hence the conversion gain increases linearly with the LO amplitude, there is a practical limit where the LO voltage is clamped by the diode. To achieve low conversion loss, the LO power level should be large to ensure proper switching of the diode.

Compared to diode mixers, FET mixers enable the design and realization of mixers which have conversion gain or lower noise figure. Basically, there are two types of FET mixers:

- Passive FET mixers
- Active FET mixers

Both types have their individual advantages and disadvantages which will be described in the following sections starting with the passive mixers.

2.2.2 Passive FET Mixers

Passive FET mixers do not provide power gain to the input signal but they may outperform active mixers in terms of linearity, bandwidth and, of course, power consumption. To realize a passive FET mixer, the LO signal is applied to the transistor's gate and modulates the channel resistance (see figure 2.3). Hence, this type of mixer is commonly referred to as "resistive mixer". To simplify the analysis, ideal voltage sources with zero source resistance have been used for the RF and LO signals in the following considerations.
The drain is biased at a DC voltage of 0 V to keep the FET in the linear region of operation. The RF signal is applied to the drain while the source is tied to ground. The resulting IF signal at the transistor's drain must be separated by an appropriate low pass filter. An advantage of the resistive mixer are the fewer spurious frequencies compared to other mixer types due to the linear channel resistance.

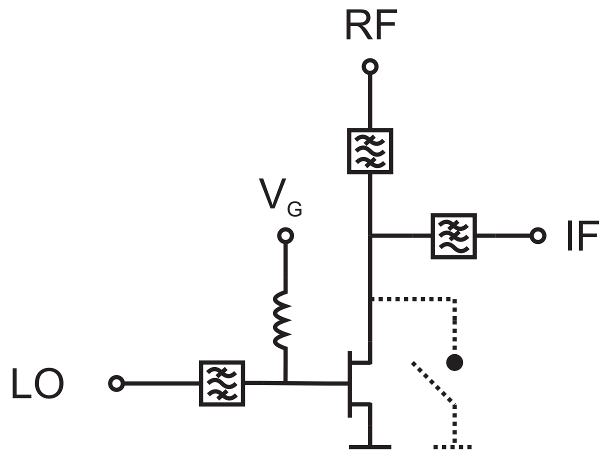

Fig. 2.3: Simplified diagram of a resistive FET mixer. At large LO power levels, the FET could be considered a switch

For large LO amplitudes the FET can be considered a switch, controlled by the LO signal. For the analytical description of such a mixer, the circuit schematic from figure 2.4 can be considered, where the RF signal is keyed by the LO signal.

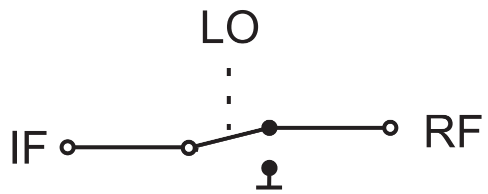

Fig. 2.4: A SPDT switch as a down converting mixer. The LO signal alters the IF terminal between 0 V and the RF signal

The corresponding waveforms are shown in figure 2.5 and 2.6. Figure 2.5a shows a cosine signal applied at the RF port of the switch. The pulse wave in figure 2.5b controls the switch with a duty cycle of 50%. The duty cycle d equals the ratio between the pulse length τ and the period T ($d = \frac{\tau}{T}$).

The Fourier series of a pulse train with an amplitude of one equals [42]:

$$f(t) = d + \sum_{n=1}^{\infty} \frac{2}{n\pi} sin\left(\pi nd\right) cos\left(\omega_{LO} nt - \pi nd\right) \tag{2.12}$$

For a 50% duty cycle ($d = \frac{1}{2}$) this results to:

$$f(t) = \frac{1}{2} + \sum_{n=1}^{\infty} \frac{2}{n\pi} sin\left(\frac{\pi n}{2}\right) cos\left(\omega_{LO} nt - \frac{\pi n}{2}\right) \tag{2.13}$$

For even n, the result becomes 0. If n is odd, the series equals:

$$f(t) = \frac{1}{2} + \frac{2}{\pi} sin(\omega_{LO} t) + \frac{2}{3\pi} sin(3\omega_{LO}) + \frac{2}{5\pi} sin(5\omega_{LO}) + ... \tag{2.14}$$

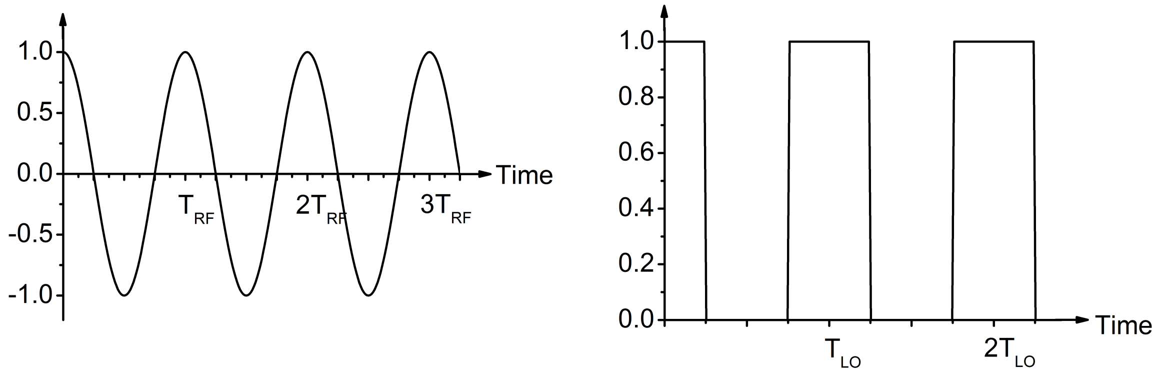

(a) **(b)**

Fig. 2.5: RF input signal with the frequency $\frac{1}{T_{RF}}$ (a) and pulse wave train (b) control signal with the frequency $\frac{1}{T_{LO}}$

Due to the symmetry, there are no even harmonics in the LO spectrum. When the LO switching signal is multiplied with a single tone RF signal $V_{RF}cos(\omega_{RF})$, the desired mixing products will be obtained:

$$V_{out}(t) = \frac{1V_{RF}}{2}cos(\omega_{RF}t) + \frac{2V_{RF}}{\pi}sin(\omega_{LO}t)cos(\omega_{RF}t) + ... \tag{2.15}$$

The desired output frequency $\omega_{RF} - \omega_{LO}$ results from the product $sin(\omega_{LO}t)cos(\omega_{RF}t)$. There are also higher order spurious signals by the odd harmonics of the LO frequency and a direct RF feed through to the output. These unwanted components need to be filtered from the output spectrum by a low pass filter.

The combination of the RF input signal and the LO pulse train is shown in figure 2.6. During the pulses, the output signal equals the RF input signal and is zero during the off cycle. Due to the difference in the frequency between the LO and RF signal, the resulting combination of both signals equals a sampled cosine signal with an envelope frequency of $\frac{1}{T_{IF}}$ (figure 2.6b).

Based on equation 2.15, the theoretical conversion gain of an ideal single FET resistive mixer can be calculated to:

$$V_{IF}(t) = \frac{2V_{RF}}{\pi}sin(\omega_{LO}t)cos(\omega_{RF}t) \tag{2.16}$$

$$V_{IF}(t) = \frac{2V_{RF}}{\pi}\frac{1}{2}\left[-sin((\omega_{RF} - \omega_{LO})t) + sin((\omega_{RF} + \omega_{LO})t)\right] \tag{2.17}$$

Since the sum of the LO and RF frequency $sin((\omega_{RF} + \omega_{LO})t)$ is out of band, the IF voltage and hence the conversion gain results to:

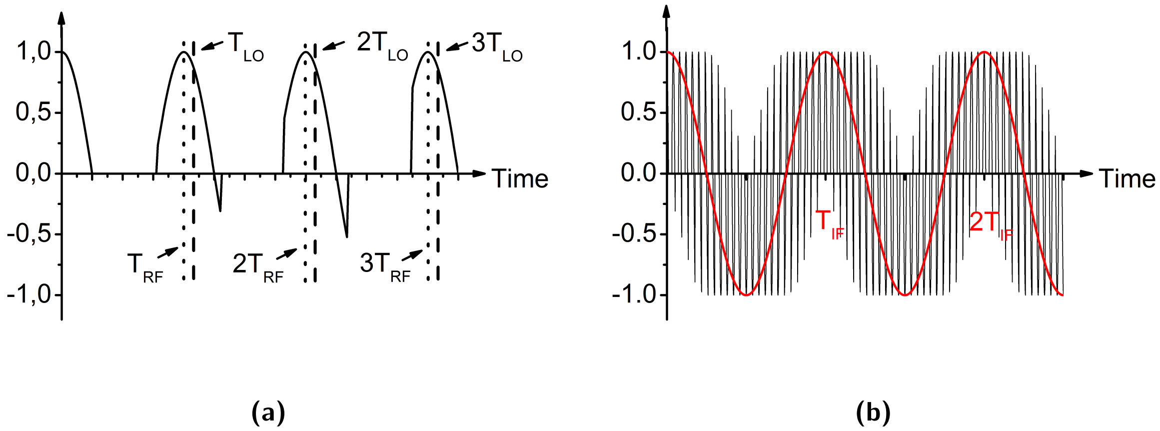

Fig. 2.6: Combination of the RF and LO signal (a) and the resulting output signal (b) with an envelope of the IF frequency.

$$V_{IF}(t) = -\frac{V_{RF}}{\pi} sin((\omega_{RF} - \omega_{LO})t) \tag{2.18}$$

$$CG = 20log\left(\frac{|V_{IF}|}{|V_{RF}|}\right) \tag{2.19}$$

$$CG = 20log\left(\frac{1}{\pi}\right) = -9.94dB \tag{2.20}$$

In case of a balanced down conversion, the voltage conversion gain rises by about 6 dB:

$$CG_{Bal} = 20log\left(\tfrac{2}{\pi}\right) = -3.92dB \tag{2.21}$$

The rise of the conversion gain for a balanced down conversion can be explained in two ways. While the LO signal in the single FET mixer is a pulse train with an amplitude between 0 and 1 to key the RF signal, the LO for the balanced down conversion is a square wave which commutates the RF signal between the IF terminals. This square wave has an amplitude of +1 and -1 which doubles the Fourier coefficient of the fundamental component. A more practical explanation is the comparison of the mixer to a rectifier. While the single FET mixer is only conducting during one half wave, the balanced resistive mixer utilizes, like a full-wave rectifier, both half waves of the RF signal resulting in a higher conversion efficiency.

These values represent the theoretical maximum for purely resistive mixing. In difference to the ideal switch, the channel resistance of a mHEMT versus the applied gate-source voltage is not an ideal step function but a nonlinear transition between the maximum channel resistance R_{max} and the on-state channel resistance R_{ON}. Based on transistor measurements, these values have been calculated for a 50 nm device with a geometry of 2×30 µm to be $R_{max} = 700\ k\Omega$ and $R_{ON} = 12\ \Omega$.
An exponential function as described in [43] is used to model the extrinsic channel resistance of the mHEMT, where a equals R_{ON} and b and c are fitting variables:

$$R_{ds}(V_{gs}) = a + b \cdot e^{-c \cdot V_{gs}} \tag{2.22}$$

The measured and simulated channel resistance for $a = 12$, $b = 10.1$ and $c = 12.8$ is shown in figure 2.7.

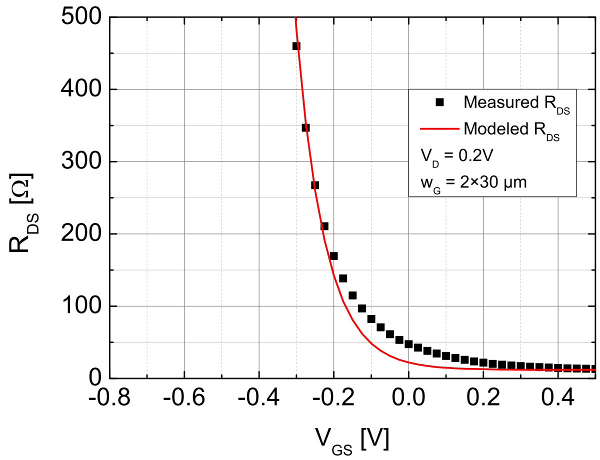

Fig. 2.7: Measured and simulated output resistance of a 50 nm mHEMT transistor versus the gate voltage. The marks represent the measured data points while the solid line shows the modeled channel resistance of a 2×30 µm device.

The output resistance for a cosine LO signal with the amplitude V is then:

$$R_{ds}(t) = a + b \cdot e^{-c \cdot V_{\omega_{LO} t}} \tag{2.23}$$

A resistive mixer based on a mHEMT transistor comes close to an ideal switch for large LO amplitudes. To determine the conversion gain and the output spectrum of a mixer based on a FET with a R_{ds} according to equation 2.22, model based simulations have been performed.
For the simulations, a Verilog-A model was used (see appendix 7.2). Figure 2.8 shows a simplified schematic of the employed circuit. The LO signal was modeled by a sine wave voltage source with an amplitude of 0.5 V applied to the transistor's gate while the RF signal was modeled by a sine wave source with an amplitude of 1 V and a source impedance of 50 Ω. Both signals will lead to mixing products at the drain of the transistor (net V_D) which will be examined.

Depending on the DC offset voltage of the LO source at the transistor's gate, the channel will conduct for a different amount of time. At higher offset voltages, the gate-source voltage stays longer above the threshold voltage V_{th} compared to lower offsets. This leads to a different duty cycle of the resulting pulse shape of the effective drain-source resistance. As could be seen from equation 2.12, the coefficient of the fundamental frequency component of the Fourier series of a pulse wave reaches its maximum of $\frac{2}{\pi}$ for a 50% duty cycle. Since the mixing operation is a multiplication of the pulse shaped channel resistance and the sinusoidal RF signal, the mixing product

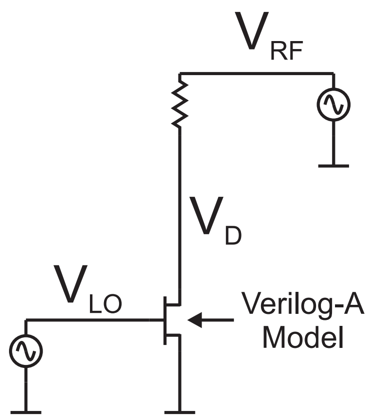

Fig. 2.8: Circuit diagram used to simulate the mixing performance of a resistive FET mixer.

and hence the conversion gain have also their maximum at a duty cycle of 50% (figure 2.9). It must be pointed out that this model and the calculations above do not take frequency dependent components into account in order to allow a frequency independent performance estimation and comparison to subharmonic resistive FET mixers in the next chapter. Frequency dependence and bandwidth limitations of resistive mixers are discussed in detail in section 2.2.2.1.

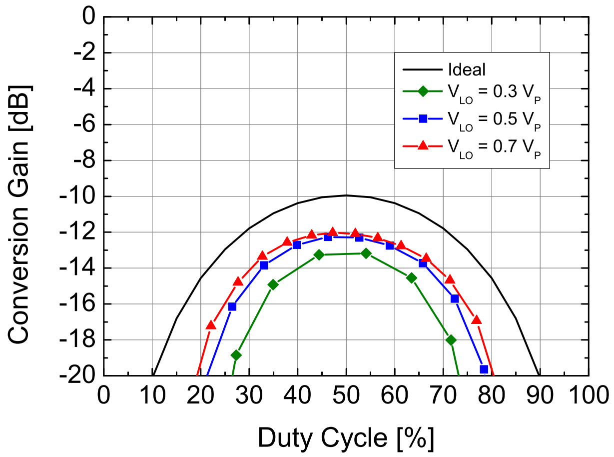

Fig. 2.9: Conversion gain of the fundamental resistive FET mixer as a function of the switching duty cycle. The curves with symbols represent different conversion gains for different LO amplitudes from 0.3 V_p to 0.7 V_p.

The simulations show only 2 dB less conversion gain for a LO peak voltage of 0.7 V using the Verilog-A model compared to the ideal switch. For large LO amplitudes the FET can be considered an ideal switch with a very high off-state impedance and an ideal short to the RF signal during the positive LO half wave. For smaller LO amplitudes, the FET differs more and more from an ideal switch and can be treated as a non-ideal switch with higher insertion loss during the on-state and less isolation when turned off. The associated pulse train of this lossy switch has therefore a smaller amplitude and smaller Fourier components. The Fourier coefficients of an ideal pulse train scale linearly with its amplitude. Figure 2.10 shows the linear relation between the conversion gain and the LO voltage for small LO peak voltages of the Verilog-A model in a double logarithmic plot. For LO peak voltages of more than 0.5 V the conversion gain saturates at a constant level of about -12 dB. At this LO level, the FET is switched between R_{max} and R_{ON} and higher LO levels will not lead to a higher or lower channel resistance. To achieve the maximum conversion gain of a resistive mixer, it is therefore necessary to apply a certain LO level.

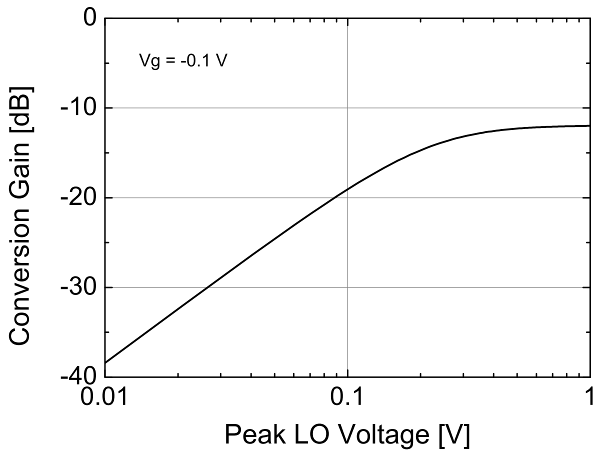

Fig. 2.10: Simulated conversion gain of the fundamental resistive FET mixer using the simplified Verilog-A model versus the applied LO peak voltage.

Subharmonic Resistive Mixer

Subharmonic mixers offer the advantage of requiring only half of the RF frequency as LO signal. This simplifies the generation of the LO signal significantly and becomes more important with increasing operation frequency. At high millimeter wave frequencies less and less power is available and it is becoming more difficult to generate the required LO levels to drive a resistive mixer into saturation.
The design of a resistive subharmonic mixer equals basically the design of a fundamental resistive mixer. The differences are the altered LO network to match the lower LO frequency and the gate bias needs to be shifted to a more negative voltage.
The relation between the harmonic components of the mixers output and the gate bias could be explained using the Fourier series expansion. As discussed above, the FET acts like a switch for large LO amplitudes. The resulting change in the channel's resistance could be considered a pulse wave (figure 2.11) with the duty cycle d.

The gate bias voltage modifies directly the duty cycle of the LO signal which affects the coefficients of the Fourier series. To realize a subharmonic resistive mixer, the second order component is of special interest. Depending on the duty cycle d, it varies from 0 ($d = \frac{1}{2}$) to $\frac{1}{\pi}$ ($d = \frac{1}{4}$). In contrast to the fundamental mixer, the conversion gain of the resistive subharmonic mixer has two peaks over the duty cycle. The second order Fourier coefficient of a pulse wave becomes $\frac{1}{\pi}$ for $d = \frac{1}{4}$ and $-\frac{1}{\pi}$ $d = \frac{3}{4}$. This is based on the fact that these wave forms are just inverted which does not affect the absolute values of

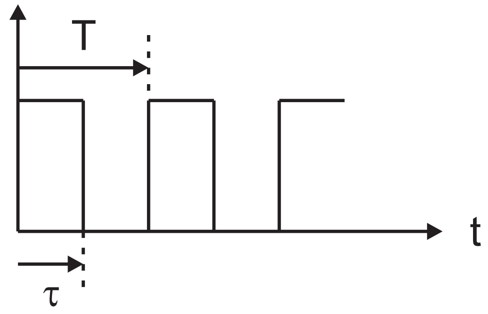

Fig. 2.11: The varying channel resistance of a FET can be considered a pulse wave form with the period T and the pulse length τ for large LO amplitudes. The pulse length is controlled by the gate bias voltage.

the Fourier coefficients but their polarity.

The theoretically achievable conversion gain of a subharmonic resistive mixer is about 6 dB less compared to the fundamental resistive mixer. Since the maximum of the second order Fourier coefficient is one half of the fundamental coefficient, the maximum conversion gain results to:

$$V_{IF}(t) = -\frac{V_{RF}}{2\pi} sin((\omega_{RF} - \omega_{LO})t) \tag{2.24}$$

$$CG = 20log\left(\frac{|V_{IF}|}{|V_{RF}|}\right) \tag{2.25}$$

$$CG = 20log\left(\frac{1}{2\pi}\right) = -15.96\ dB \tag{2.26}$$

Correspondingly for the balanced subharmonic resistive mixer:

$$CG = 20log\left(\frac{1}{\pi}\right) = -9.94\ dB \tag{2.27}$$

The simulated conversion gain of a purely resistive mixer based on equation 2.22 as a function of the duty cycle is shown in figure 2.12. As could be seen from the Fourier series (equation 2.12) there are two peaks for the conversion gain of a subharmonic mixer. In practice, only the 25% duty cycle could be used. To employ the peak at 75% duty cycle where the channel has only 25% of the time a high impedance, the gate has to be biased positively. Due to the inherent Schottky diode at the gate of a mHEMT, the LO signal will be partially clamped to the diode voltage and the mixer becomes impractical. For smaller LO amplitudes the FET cannot be treated as an ideal switch and the RF is no longer multiplied with an ideal pulse train. Therefore, the Fourier coefficients differ from equation 2.12 which explains the shift to higher/lower duty cycles for maximum conversion gain at smaller LO voltages. With increasing LO power levels, the mixer approaches the ideal curve and tends to the theoretical peak at a duty cycle of 25% and 75%.

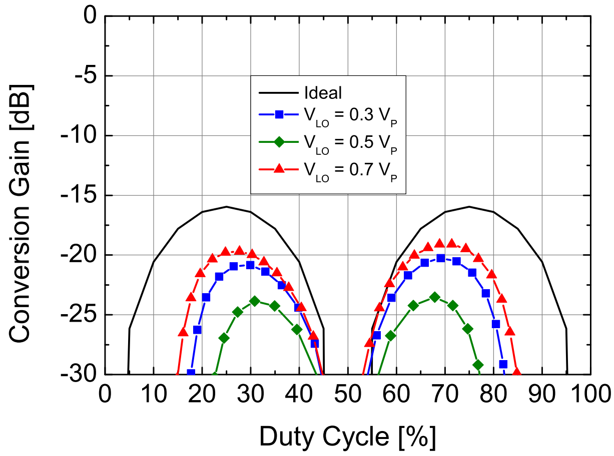

Fig. 2.12: Conversion gain of the subharmonic resistive FET mixer as a function of the switching duty cycle. The lines with symbols represent the conversion gain for different LO amplitudes from 0.3 V_p to 0.7 V_p.

As with the fundamental resistive mixer, the conversion gain is heavily depending on the applied LO power level. Figure 2.13 shows the simulated conversion gain versus the peak LO voltage at the gate. Compared to the fundamental resistive FET mixer, the conversion gain of the subharmonic mixer starts to decline after the peak around 0.7 V while it stays at a constant saturated value with the fundamental mixer. This is caused by a positive shift in the duty cycle for larger LO levels. Since the fundamental mixer is biased to have a 50% duty cycle, the duty cycle remains at 50% for larger LO amplitudes (symmetrical around the gate bias voltage). The subharmonic resistive FET mixer is biased at 25% duty cycle using a fixed gate bias voltage. With increasing LO amplitude, the duty cycle of the mixer increases when the gate bias voltage remains constant which decreases the conversion gain of the subharmonic mixer after the maximum has been reached.

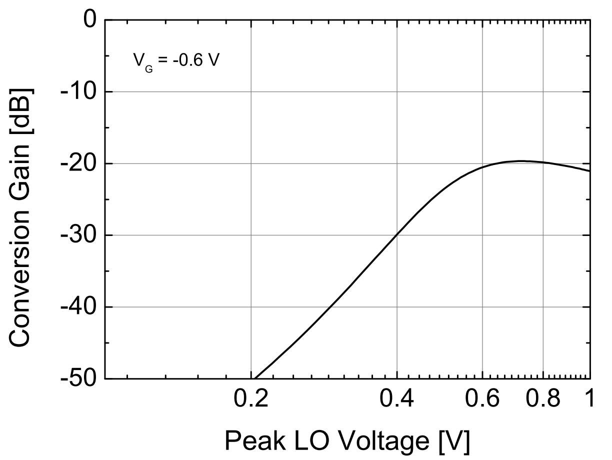

Fig. 2.13: Simulated conversion gain of the subharmonic resistive FET mixer versus the applied peak LO voltage.

Besides the conversion gain, which defines the efficiency of the mixer, the achievable bandwidth is of special interest in this work. A larger operational bandwidth increases the capacity of the wireless link but is not always easy to achieve. The theoretical limits for wideband matching of resistive mixers are therefore analyzed in the following chapter.

2.2.2.1 Bandwidth of Resistive Mixers

There are three possible band limiting factors when it comes to estimating the achievable bandwidth of a resistive FET mixer:

- The device cutoff frequencies.
- The achievable matching bandwidth.
- The bandwidth of passive circuit elements like baluns or hybrids.

In contrast to active mixers, passive mixers do not provide signal gain at the RF frequency. To obtain frequency conversion, it is only necessary to vary the channel resistance with respect to the LO voltage. This could be achieved even beyond the characteristic device cutoff frequencies f_t and f_{max} which are critical for amplifiers and active mixers. The frequency where the absolute value of the short circuit current gain of the transistor equals one is specified by the transit frequency f_t. For the design of amplifiers it is often more important where the power gain of the device equals unity. This frequency is defined as the maximum frequency of oscillation f_{max}. Although the device cutoff frequencies are also a limiting factor in passive mixers one may still use a resistive FET mixer above these frequencies at the cost of conversion gain.

Since the LO is fixed in the targeted communication scenario, the RF matching over a large bandwidth is the main challenge in designing broadband resistive mixers. In this work, virtually no single device mixer is examined since communication systems require usually balanced and/or quadrature mixers to achieve reasonable isolation and support complex modulation formats. With resistive mixers, the RF signal is applied to the transistor's drain terminal and the achievable bandwidth for a given matching can be estimated based on some simplifications regarding the parasitic FET elements and the matching network. A simplified small signal model of a resistive FET mixer as shown in figure 2.14 is used to underline that the bandwidth of a resistive mHEMT based mixers at mmW frequencies is usually limited by the passive RF baluns and hybrids and not the matching of the drain impedance.

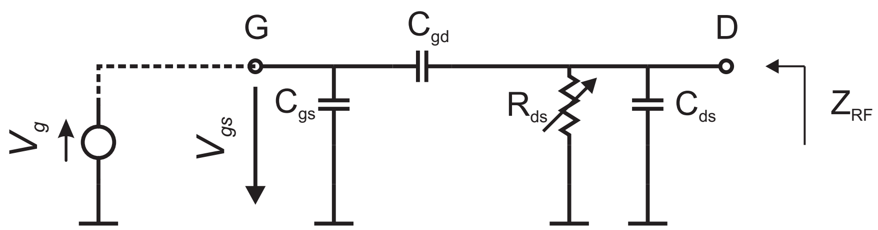

Fig. 2.14: Simplified equivalent circuit of a resistive FET mixer with no drain bias applied.

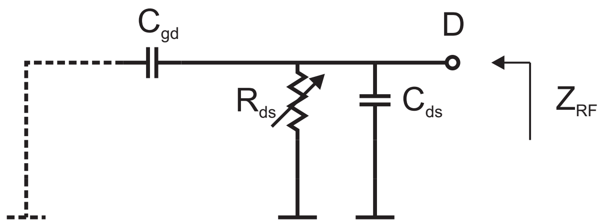

Fig. 2.15: Reduced equivalent circuit of the resistive FET mixer.

The voltage source at the gate terminal forms a RF short and reduces the circuit diagram as shown in figure 2.15.

The resulting input impedance is the parallel connection of the channel resistance $R_{ds}(V_{gs}(t))$ and the capacitances C_{gd} and C_{ds} which can be transformed to a single element C_r:

$$C_r = C_{gd} + C_{ds} \tag{2.28}$$

To achieve wideband RF matching, the RF input has to be matched to the impedance Z_{RF} formed by the parallel connection of $R_{ds}(V_{gs}(t))$ and C_r:

$$Z_{rf} = \frac{R_{ds}}{1 + j\omega C_r R_{ds}} \tag{2.29}$$

Assuming a lossless matching network, the Bode-Fano limit [44] describes the theoretically achievable bandwidth Δf over which a given R-C parallel connection can be matched to a resistive source with a reflection coefficient Γ:

$$\Delta f \leq \frac{1}{2 \cdot R_{ds} \cdot C_r \cdot ln\left(\frac{1}{|\Gamma|}\right)} \tag{2.30}$$

The reflection coefficient (Γ) is defined by the return loss specification of the mixer (e.g. >20 dB). For a first approximation, R_{ds} could be assumed to be the average channel resistance over time. This effective resistance is depending on the selected duty cycle and differs therefore between a fundamental and a subharmonic mixer as described in section 2.2.2. In practice, the IF filter at the transistor's drain will degrade the achievable RF matching bandwidth. Due to the limited chip area, first order low pass filters, realized by on chip capacitors, are commonly used with integrated mmW mixers to separate the IF from the RF. The IF capacitor is usually isolated from the RF by a short to open transformation. Since this simple transmission line transformation has a limited bandwidth, the IF matching increases the value of C_r and hence decreases the matching bandwidth Δf. To illustrate that the achievable RF matching bandwidth is not limited by the transistor's R_{ds} and the extrinsic parallel capacitance C_r these parameters have been extracted from large signal S-parameter (LSSP) simulations using a mHEMT from the Fraunhofer IAF technology with a gate length of 50 nm and a gate width of 2×20 µm.

For the fundamental resistive FET mixer, the values for R_{ds} and C_r have been calculated based on the simulated admittance parameters (Y-parameters). During the simulations,

a LO power level of 2 dBm and a gate bias voltage of -0.1 V have been applied to the transistor's gate. At 240 GHz, an extrinsic channel resistance R_{ds} of 17.7 Ω and a capacitance C_r of 4.5 fF have been simulated at the drain. Based on equation 2.30 the achievable bandwidth for a 20 dB matching would be more than 2 THz.
A subharmonic resistive mixer has a more negative gate voltage and a duty cycle of only 25% which leads to a higher channel resistance. The value for R_{ds} and C_r at 240 GHz with a LO power level of 5 dBm and a gate bias voltage of -0.7 V are namely 28.4 Ω and 9.4 fF. Although these values are higher compared to the fundamental mixer which would lead to a smaller Bode-Fano bandwidth, the achievable bandwidth is still greater than 800 GHz. The bandwidth of resistive mixers are therefore not limited by matching the transistor's drain to the RF frequency but by the passive networks like baluns and hybrids usually used in balanced and I/Q mixers.

2.2.3 Active FET Mixer

In an active FET mixer, the transistor is biased to provide transconductance which is the main difference between an active and a passive FET mixer. Depending on the circuit topology, active mixers are subdivided in:

- additive mixers
- multiplicative mixers

Active additive mixers are built similar to diode mixers by applying the two mixing signals to the transistor's gate. This topology is commonly referred to as gate mixer, since the LO is applied to the gate of the FET (see figure 2.16).

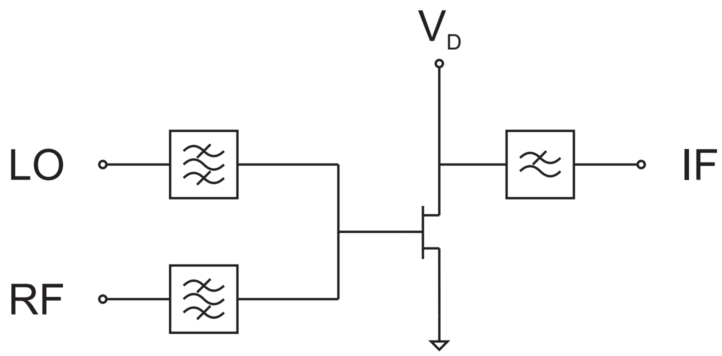

Fig. 2.16: Simplified topology of an additive down-converting FET mixer.

The FET is biased closed to its threshold voltage for maximum conversion gain at the fundamental frequency and stays saturated throughout the entire LO cycle. The mixing products are separated by a filter at the drain of the transistor. The drawbacks of additive mixing are the lower isolation and the many spectral components (LO/RF leakage, frequency difference and harmonics) at the IF output. To obtain LO to RF isolation, diplexer networks are necessary which require usually large chip area in integrated mixers. These are also the main reasons why only multiplicative active mixers are examined in the course of this work.

2.2.3.1 Multiplicative Mixing

In additive mixers, the frequency conversion occurs due to the incidental multiplication at the nonlinear transfer characteristic of the active device. A drawback of the incidental multiplication is the poor port isolation and a lot of unwanted intermodulation components [45]. Multiplicative mixers make use of a direct multiplication which leads to fewer spurious signals and higher port isolation since the LO and RF signals are fed into separate terminals of the FET. A drain mixer for example is realized by modulating the transconductance of the FET over the variation of V_{ds} by the large LO signal at the drain while the RF signal is applied to the gate. The IF signal is again separated by a filter at the drain terminal. An extension of this topology is the dual gate mixer, where two FETs are connected in a quasi-cascode configuration. The LO and RF signals are applied to the two individual gate terminals as shown in figure 2.17, which inherently increases the LO to RF isolation.

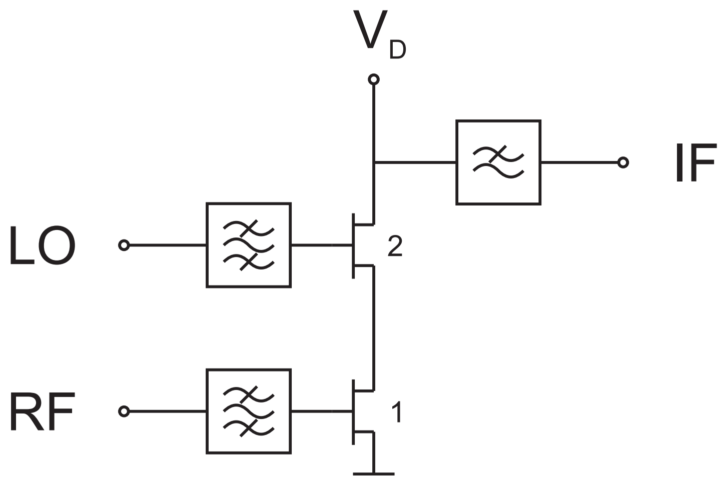

Fig. 2.17: Dual gate mixer block diagram.

Although the circuit is modeled as two transistors, dual gate mixers are often realized by a single device having two gate electrodes to control the overall channel individually. A scanning electron microscope (SEM) picture of a 4×45 µm dual gate mHEMT is shown in figure 2.18. In this configuration, the RF signal controls the FET in common source configuration while the LO signal is applied to the gate of FET 2.

To obtain frequency conversion, the circuit must be biased to keep FET 1 at the knee point between linear and saturated region, as shown in figure 2.19, while the FET 2 remains saturated. The mixing occurs through the variation of the drain voltage of FET 1 between almost zero and a point where the FET becomes saturated.

Hence, the mixing occurs mainly in FET 1 [46]. Due to the low transconductance of FET 1 in the linear region, the gain is lower compared to a single gate FET mixer, which remains in saturation during the entire LO cycle. Since FET 2 remains in saturation, it operates as a common gate amplifier to the IF signal from FET 1, similar to a cascode configuration. However, the gain is usually lowered by the mismatch between the common gate input impedance and the IF output impedance of FET 1. The maximum achievable conversion gain of a fundamental drain pumped mixer can be approximated by the maximum gain of FET 1 and the first Fourier coefficient. The maximum gain of FET 1 is

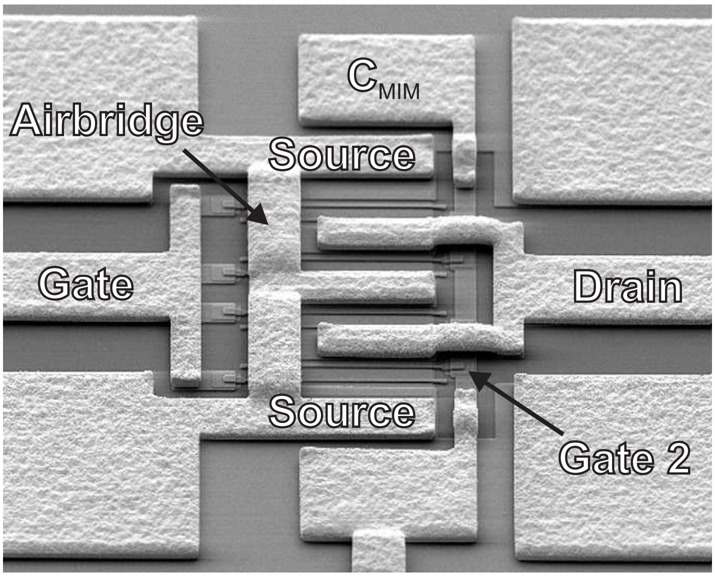

Fig. 2.18: A SEM picture of a four finger dual gate mHEMT. By courtesy of the Fraunhofer IAF.

defined by its maximum stable gain (MSG) which is proportional to the transconductance g_m of the device:

$$MSG \propto \frac{g_m}{\omega C_{gd}} \tag{2.31}$$

For a pulse shaped change in the transconductance the maximum value of the first Fourier coefficient becomes $\frac{2}{\pi}$ and hence the maximum conversion gain of the dual gate mixer:

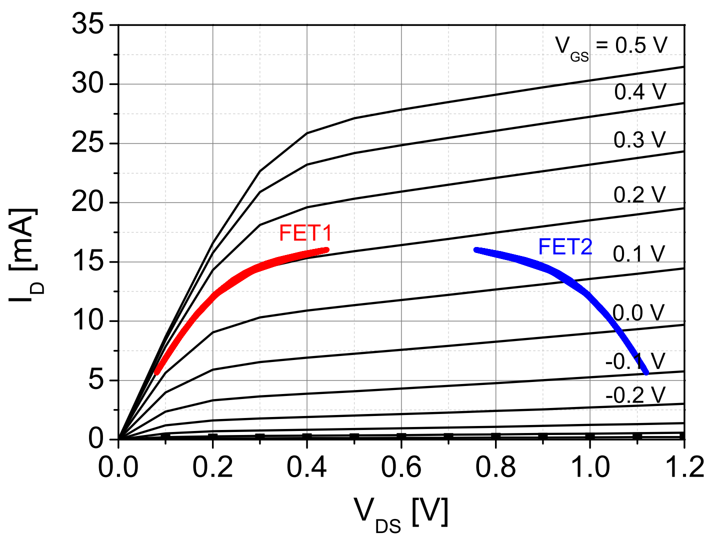

Fig. 2.19: Simulated output characteristics of a 2×30 μm transistor, fabricated in the 50 nm Fraunhofer IAF mHEMT technology. The colored lines, are the varying operating points of FET 1 and FET 2 when a sinusoidal LO with an amplitude of 0.316 V is applied.

$$CG_{max} \propto \frac{2}{\pi} \cdot MSG \tag{2.32}$$

The presented dual gate mixer is an unbalanced design and hence shows a poor port to port isolation. To increase the isolation and efficiency of the mixer, single balanced and double balanced structures are needed. A very famous implementation of a double balanced active mixer is the Gilbert cell mixer, named after its inventer Barrie Gilbert [47], which is described in the following section.

2.2.3.2 Gilbert Cell Mixer

The most advanced, versatile and popular multiplicative mixer is the Gilbert cell mixer which is basically a four-quadrant analog multiplier. To operate as a bilinear multiplier, the Gilbert cell multiplier must operate at frequencies where the transistors' capacitances are negligible [46]. Gilbert cell based mixers are usually realized to operational frequencies up to $\frac{f_t}{3}$. The basic mixer circuit is shown in figure 2.20 and equals two cross coupled differential amplifiers. It is similar to a double balanced dual gate FET mixer and operates in much the same manner [46]. The large LO signal is applied to the transistor pairs T1 and T2 which operate as commutating switches. The RF signal is applied to the differential amplifier formed by the transistor pair T3 and its output is modulated by the switching transistors. The current source is usually formed by a single transistor but is not essential, when the RF is applied differentially. This can be achieved by an active or passive balanced-to-unbalanced transfomer (balun). Usually, for on chip integration, active baluns are preferred since they require less chip area. With increasing operational frequencies passive baluns become smaller and smaller and may be a better choice with respect to stability, bandwidth and port matching compared to active baluns.
The design of a Gilbert cell mixer is simplified by the fact that the current source is a virtual ground to the RF transistors while the drains of the RF FETs are virtual grounds for the LO transistors. Therefore, they can be treated as simple common source stages during the design process [46].

2.2.3.3 Bandwidth of Active Mixers

The operational bandwidth of active mixers is mainly limited by three factors, input matching, IF matching and the characteristic frequencies f_t and f_{max} of the employed transistors. As with the passive mixers, achieving a reasonable good RF matching over the entire bandwidth is usually more challenging than achieving a good LO matching, since the LO is fixed in most communication scenarios. In contrast to passive mixers, the RF signal is fed into the gate of the transistor with active mixers instead of the drain with passive mixers.
Achieving broadband RF matching at the drain of the transistor is usually easier than at the gate since the drain impedance is closer to 50 Ω when the FET is conducting ($V_g > V_{th}$). Figure 2.21 shows the simulated gate and drain impedances from 1 to 200 GHz of a 2×20 μm device fabricated in the 50 nm mHEMT technology of the Fraunhofer IAF.

Apparently, the gate impedances lie at the edge of the Smith chart for all gate bias conditions and are therefore harder to match to 50 Ω compared to the drain impedances. In addition, the simulated gate impedance shows a distinct capacitive behavior with only a

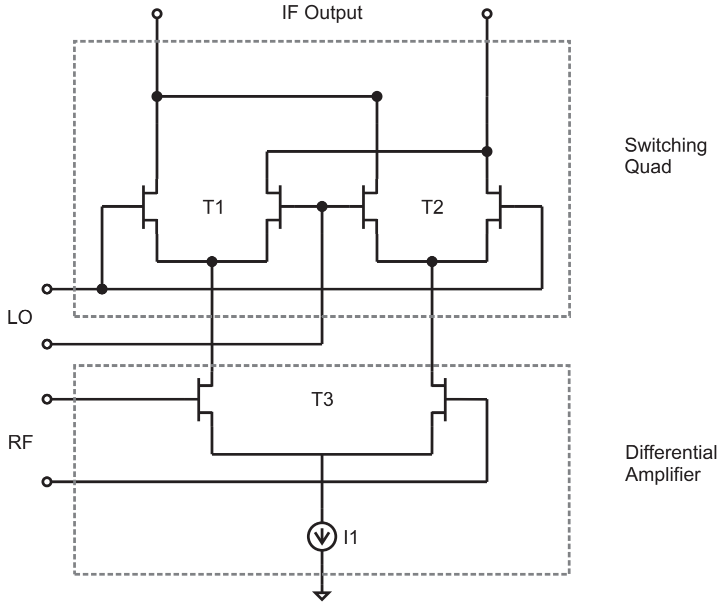

Fig. 2.20: Schematic of a Gilbert cell mixer. It consists of a differential RF amplifier and four commutation switches controlled by the LO signal.

small series resistance (turn into the Smith chart) and a very high parallel resistance R_{gs} (start at the open circuit point of the Smith chart). Regarding the Bode-Fano limit [44] for reactive matching as previously used with the passive mixer, the small gate-source capacitance C_{gs} is parallel to a very high impedance R_{gs}. The reflection coefficient (Γ) is in this case also defined by the mixer's return loss specification:

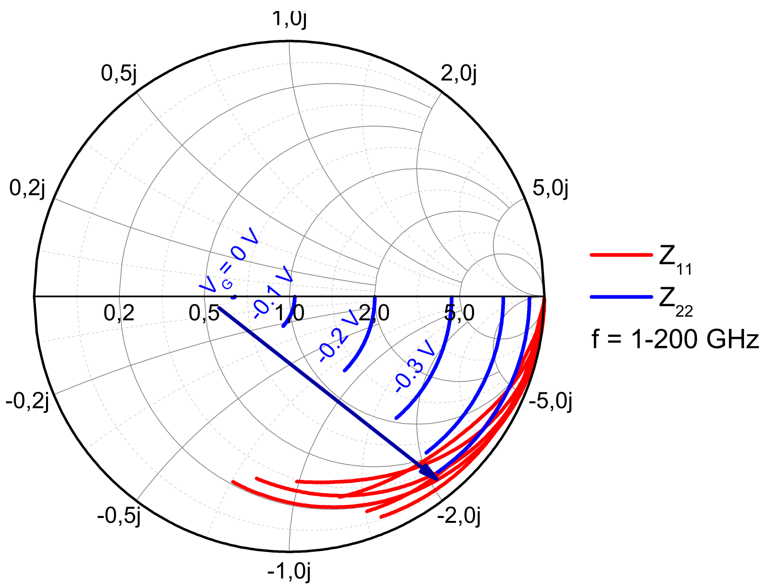

Fig. 2.21: Simulated gate (Z_{11}) and drain (Z_{22}) impedances of a 2×20 μm transistor with a gate length of 50 nm for different gate source voltages. The frequency is swept from 1 GHz to 200 GHz and the gate voltage is varied from 0 V to -0.5 V.

$$\Delta f \leq \frac{1}{2 \cdot R_{gs} \cdot C_{gs} \cdot ln\left(\frac{1}{|\Gamma|}\right)} \tag{2.33}$$

Based on simulation results, C_{gs} of a 2×20 µm device with a gate length of 50 nm can be calculated to be around 24 fF and the value of the parallel resistance R_{gs} is about 180 Ω at 240 GHz and a gate-source voltage of 0.2 V. Using these values, the achievable bandwidth for a return loss of 20 dB can be calculated according to equation 2.33:

$$\Delta f \leq \frac{1}{2 \cdot 180\ \Omega \cdot 24\ fF \cdot ln\left(\frac{1}{0.1}\right)} \tag{2.34}$$

$$\Delta f \leq 50.26\ GHz \tag{2.35}$$

which equals a relative bandwidth of 20.9%.

2.2.4 MMIC Technologies for mmW Mixers

There are different semiconductor technologies available to realize integrated broadband communication mixers, each one having its own advantages and disadvantages. The goal of this work is to realize broadband mixer cells for wireless communication scenarios in the upper mmW frequency range. Different MMIC technologies are therefore compared based on their capability to provide the necessary device performance with respect to cutoff frequencies, noise performance and conversion gain. Table 2.1 shows the reported cutoff frequencies and transconductances of the most prominent radio frequency integrated circuit (RFIC) technologies.

	CMOS	SiGe HBT [9]	InP HEMT [7]	mHEMT [8]
f_t [GHz]	445 [48]	300	600	660
f_{max} [GHz]	410 [49]	500	1200	N/A
g_m [mS/mm]	N/A	N/A	2400	2500

Table 2.1: Parameters of different RFIC technologies

The most mature semiconductor technology is, of course, silicon based CMOS which has improved the RF performance significantly in the last decade. Active MMICs fabricated in RF CMOS technologies currently reach operation frequencies up to the G-band (140-220 GHz)[50, 51]. A remarkable progress has been made in the past to drive the CMOS technology in the mmW frequency region. However, the active devices are still outperformed with respect to cutoff frequencies, noise performance and output power by compound semiconductors.
SiGe HBTs combine the advantages of an improved RF performance and the ability to be integrated together with CMOS technology. This enables the fabrication of low price, high volume integrated circuits with reasonable RF performance. Although SiGe HBT present a bipolar counterpart to HEMTs the latter are currently the fastest devices available.
InP based HEMTs are the first transistors featuring cutoff frequencies at and above one THz [7, 10]. They are best suited for high performance MMICs at mmW and sub-mmW

frequencies. The drawback of the InP technology is the high cost of fabrication due to the smaller wafer size. The Fraunhofer IAF metamorphic HEMT technology combines the advantages of InP like performance with low cost gallium-arsenide (GaAs) substrates.
An important figure of merit for integrated switches is the frequency described by [52]:

$$f_{SW} = \frac{1}{2\pi C_{OFF} R_{ON}} \tag{2.36}$$

where R_{ON} and C_{OFF} are the on-state resistance and off-state capacitance seen on the transistor's drain. Resistive mixers can be considered as switches for large LO amplitudes and this figure of merit can therefore also be applied to resistive mixer [53]. The on-state resistance of a transistor depends on the carrier mobility:

$$R_{ON} \propto \frac{1}{\mu} \tag{2.37}$$

Equation 2.36 and 2.37 imply that higher carrier mobility of the switching transistor leads to potentially higher switching and therefore mixing frequencies. A typical value for the electron mobility in Si at room temperature is $1400 cm^2/Vs$ while the electron mobility in the two-dimensional electron gas (2DEG) of the mHEMT is more than 8 times higher ($11800 cm^2/Vs$ [54]). For the design of passive mixers in the upper mmW frequency range, HEMTs are the best choice.

2.3 Fraunhofer IAF mHEMT Process

The Fraunhofer IAF mHEMT process is based on low priced high quality 4″ GaAs wafers. It features mHEMT devices in four different gate length technologies (100 nm, 50 nm, 35 nm and 20 nm), two front side metallization layers and a backside process with through substrate vias [8, 55, 56].

2.3.1 Front Side Process

To manufacture MMICs, a lot more devices and layers are necessary than only the active transistors. The Fraunhofer IAF mHEMT process features integrated resistors, capacitors, air-bridges and two metallization layers on the front side. A simplified diagram of the layers and structures of the Fraunhofer IAF mHEMT process is shown in figure 2.22.

For the transmission lines and interconnections, two gold metallization layers are available. The first metal (MET1) is an electron beam evaporated layer with a thickness of 0.3 µm. The top metal (METG) features an air-bridge technology and is plated with a thickness of 2.7 µm [57].
To realize the integrated thin film resistors, a nickel-chromium (NiCr) alloy with a resistance of 50-Ω/sq is used. The on-chip capacitors are realized as metal-insulator-metal (MIM) capacitors with a 250 nm thin silicon-nitride (SiN) as dielectric between

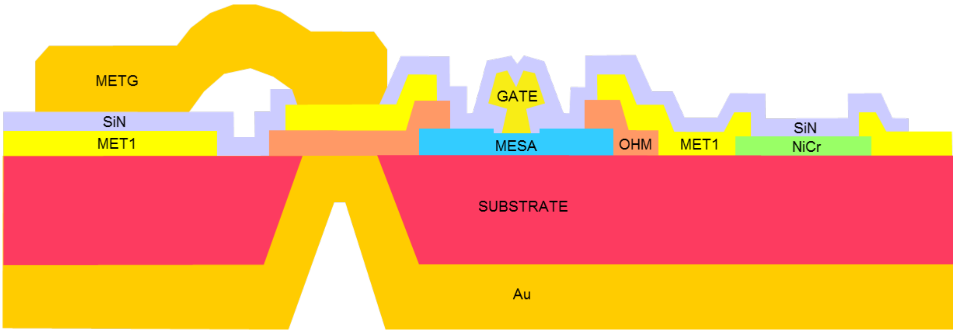

Fig. 2.22: Layer structure of the IAF mHEMT process by courtesy of the Fraunhofer IAF.

MET1 and METG and a capacitance of 0.225 fF/μm^2 [55]. The MIM capacitors can be placed on top of the substrate vias which enables the design of very small, highly integrated MMICs.

2.3.2 Back Side Process

Another important process step is the wafer thinning and etching of the through-substrate vias. The usage of coplanar waveguide (CPW) transmission lines on GaAs substrates at mmW frequencies may excite unwanted modes in the substrate [58]. To suppress any unwanted propagation of the electro-magnetic waves through the substrate, the wafers are thinned to a thickness of only 50 μm [8, 55, 59]. The backside of the wafer is gold plated and vias are introduced to connect the ground from the front side with the back side metallization. With more aggressive down scaling of the entire MMIC, the space for on chip DC blocking capacitors is becoming even smaller. For stability reasons it is virtually always necessary to place on-chip capacitors on the DC connections of the transistor. Usually, vias are placed beside the capacitors, but with smaller devices and transmission lines the available space between and beside capacitors is becoming smaller and smaller. The LNA (figure 4.51) in chapter 4.4 is a good example which illustrates this issue. The ability to place the through-substrate vias beneath a capacitor is therefore becoming essential for the design of MMICs at several hundred GHz. Otherwise missing vias would cause a degraded RF performance or poor DC blocking would lead to stability issues of the circuit.

2.3.3 Metamorphic HEMT

The mHEMT is a field effect transistor with an exceptionally high electron mobility and a Schottky contact as gate. The very high electron mobility is achieved by a special epitaxially grown heterostructure, in which a wide-energy-gap material is doped and carriers diffuse to the undoped narrow-bandgap layer at which heterointerface a 2DEG is formed. The benefit of this modulation doping is the spatial separation between the doped region and the channel carriers which results in a very high mobility due to the lack of impurity scattering [60]. Depending on the applied gate-to-source voltage, the concentration of the carriers in the channel is modulated which controls the drain to source current of the transistor.

As described in [54], different substrate materials like GaAs, Silicon or Germanium can be used for the growth of mHEMT heterostructures. The matching of the lattice constant is achieved either by a graded or a non-graded buffer layer. The Fraunhofer IAF employs for its mHEMT technology a molecular beam epitaxy (MBE) grown linear graded InGaAlAs buffer on 4″ semi insulating GaAs substrates. Beginning with an $Al_{0.52}Ga_{0.48}As$ layer, the Ga atoms are linearly exchanged against In within the 1 μm thick quaternary buffer layer. A scanning microscope picture of a cross section of a mHEMT device with a gate length of 100 nm is shown in figure 2.23. The metamorphic buffer layer is placed between the GaAs substrate at the bottom of the picture and the indium-gallium-arsenide (InGaAs) channel beneath the gate contact. The ohmic source and drain contacts are placed to the left and right of the gate.

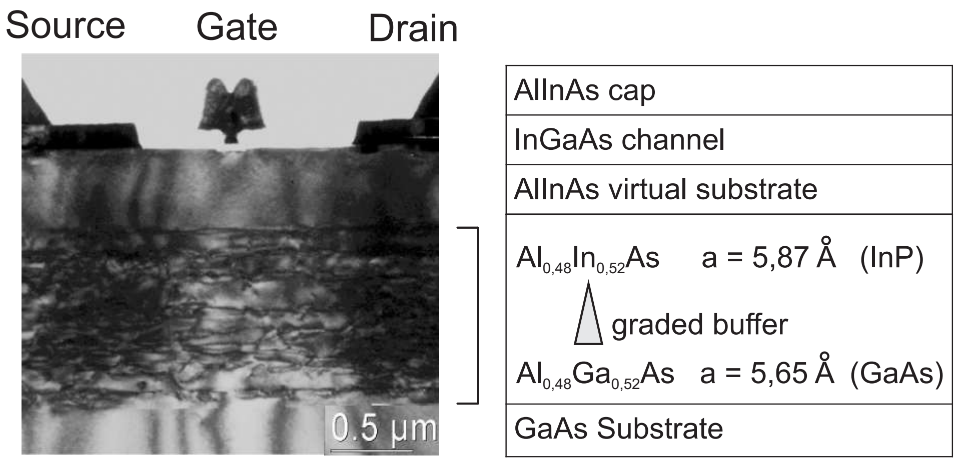

Fig. 2.23: SEM picture of a metamorphic HEMT, showing the T-shaped gate with a length of 100 nm and the metamorphic buffer layer. SEM picture by courtesy of the Fraunhofer IAF.

For the proper scaling of the device parameters with shrinking gate length the design of the heterostructure layer sequence is essential, as stated in [54]. The RF performance of ultra-short gate length devices is often limited by parasitic gate capacitances. An increase in the parasitics is caused by the dielectric passivation layer, which is needed to attain sufficient device lifetime. To suppress the RF degradation due to the parasitic gate capacitances the intrinsic C_{gs} must be increased by reducing the distance between the 2DEG and the gate which means reduced barrier and InGaAs channel thickness.
The process features currently transistors with 4 different gate lengths: 100 nm, 50 nm, 35 nm and 20 nm. The 100 nm and the 50 nm technologies are employing composite channels while smaller sized 35 nm and 20 nm technologies are using single layer channels [8, 56, 59, 61]. With the optimized MBE grown layer sequences channel mobilities as high as $\mu_e = 9800\ cm^2/Vs$ for the 35 nm and $\mu_e = 11800\ cm^2/Vs$ for the 50 nm mHEMT heterostructure were measured [54].

With shorter gate length and the parasitic reduction, the transit frequency f_t and the maximum oscillation frequency f_{max} increase (see figure 2.24). With shorter transistor channels, also the field intensity increases and requires a reduction of the drain to source voltage to prevent the transistor from break down. The voltage reduction lowers the

Technology	In Content	$I_{D,max}$ [mA/mm]	$g_{m,max}$ [mS]	f_t [GHz]
100 nm	65 %	900	1300	220
50 nm	80 %	1200	1800	375
35 nm	80 %	1600	2500	515
20 nm	80 %	1400	2500	660

Table 2.2: Parameters of different mHEMT technologies at room temperature

available output power of the device due to the smaller output headroom. There is always a trade off between output power and cutoff frequency. This plays a role in the design of up-conversion or Tx mixers where a linear behavior under large signal conditions is required. Depending on the desired operation frequency, the appropriate technology needs to be chosen. For resistive mixers up to 200 GHz the 100 nm technology is well suited. Although passive mixers do not require signal gain and do still operate beyond the cutoff frequencies of the device, the 50 nm or smaller technologies should be used to achieve efficient frequency conversion at higher frequencies. For active mixers the cutoff frequencies describe their limits since they demand signal gain for active operation.

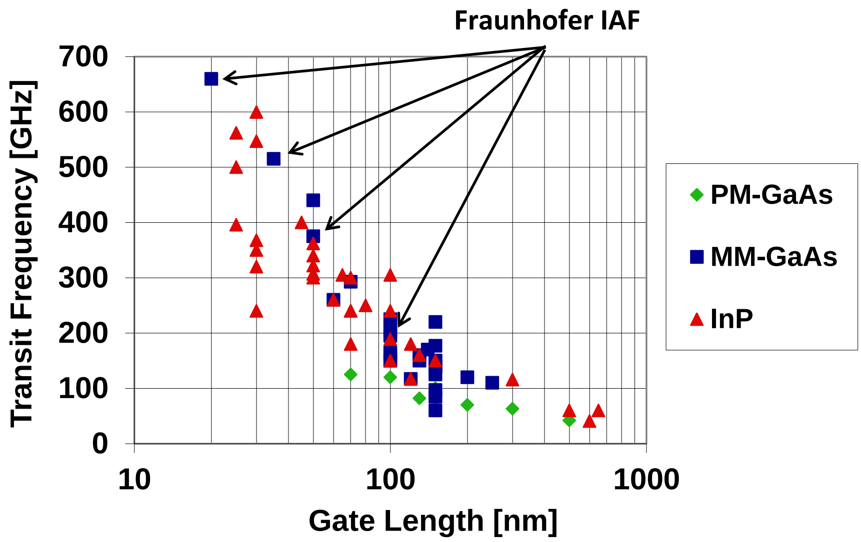

Fig. 2.24: Transit frequencies of different transistor technologies versus the gate length. Courtesy of Prof. G. Dambrine, IEMN.

2.3.4 Integrated Schottky Diodes

Virtually any microwave and millimeter wave diode mixer is based on Schottky barrier diodes. These diodes are typically created using n-type semiconductors. Due to the absence of minority carriers, there is no charge storage and hence almost no reverse recovery time. This results in higher switching speeds and there have been currently reported Schottky diode mixers with operating frequencies of up to several THz [62]. The mixing products in a diode are generated by its nonlinear I/V characteristic. The ideal diode transfer function is given by:

$$I_D(V_D) = I_S(e^{\frac{V_D}{V_T}} - 1) \tag{2.38}$$

Where V_D is the diode voltage and V_T is the temperature voltage ($V_T = qk_BT$).

In a real diode, the ideality factor n is introduced to match the slope of the current in a semi-log plot:

$$I_D(V_D) = I_S(e^{\frac{V_D}{nV_T}} - 1) \tag{2.39}$$

The Fraunhofer IAF mHEMT process features integrated Schottky diodes by using the metal-semiconductor contact formed at the gate electrode of the transistor. The gate contact is formed by a Pt-Ti-Pt-Au structure [61].

Figure 2.25 shows a measured I/V curve of a 2x30 μm gate diode of a 50 nm mHEMT transistor.

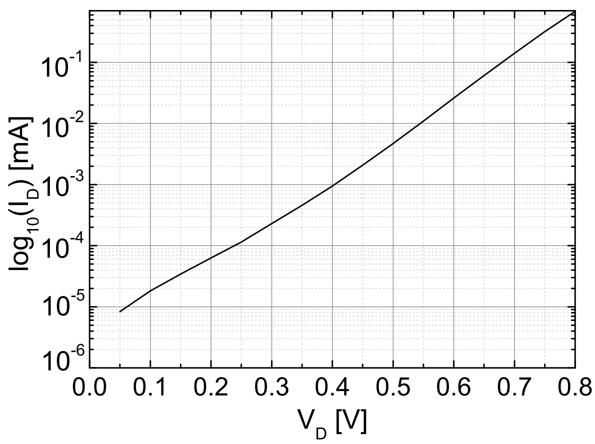

Fig. 2.25: Measured I/V curve of the Schottky diode of a 2x30 μm transistor with a gate length of 50 nm.

The ideality factor could then be calculated according to [63]:

$$n \equiv \frac{q}{k_BT}\frac{\partial V_D}{\partial(ln(I_D))} \tag{2.40}$$

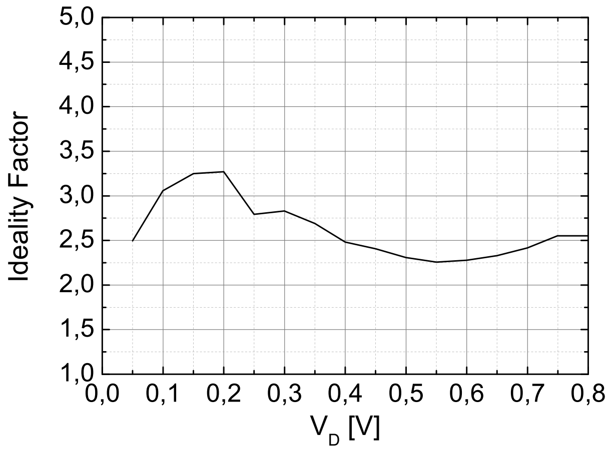

Fig. 2.26: Measured ideality factor versus the diode voltage of a 2×30 μm mHEMT gate diode.

The measured ideality factor versus the applied diode voltage is shown in figure 2.26. The best value of 2.25 is achieved at a diode voltage of 0.55 V.

Table 2.3 shows a comparison between the mHEMT diode and other reported Schottky diodes. There are technologies available which are optimized for Schottky diodes used in millimeter wave and THz mixers. The drawback of these high performance diode processes is the lack of active devices like HEMTs. This allows only a reduced scale of integration compared to a transistor process. On the other hand, the high ideality factor of the mHEMT gate diode makes is less suitable for mixer circuits since according to equation 2.11 the conversion loss increases with the square of the ideality factor. This is also the main reasons why the only FET based mixers are examined in this work and no mHEMT based diode mixers are investigated.

Technology	n	$R_S[Ohm]$	Reference
HEMT gate Schottky contact	2.25	23	This Work
Monolithic membrane diode	1.5	15-20	[62]
Air-bridged Schottky diode	1.172	10.68	[64]
Dot type Schottky diode	1.41	18.3	[65]

Table 2.3: Parameters of reported Schottky Diodes

2.4 Summary

The theory of passive and active mixers in the upper mmW frequency range has been presented in this chapter. The advantages and disadvantages of mixers based on diodes and FETs have been examined. Compared to active mixers, passive mixers are unable to amplify the input signal. On the other hand it can be shown that they are easier to match over a very large bandwidth. To realize very broadband mixers for communication applications, the signal gain maybe sacrificed for higher bandwidth as well as improved linearity and noise. Therefore mainly passive mixers are analyzed in this work.
Different semiconductor technologies and their cutoff frequencies and transconductances

have been presented. The mHEMT technology of the Fraunhofer IAF offers InP like performance on low cost GaAs substrates and has therefore been chosen as the manufacturing technology for the mixer circuits. However, the integrated Schottky diodes of this process show worse performance compared to dedicated RF diode processes which is the main reason why only FET based mixers have been realized.

To measure and characterize the realized RF circuits state of the art measurement techniques and equipment is needed. The employed measurement setups are described in the following chapter.

3 mmW Mixer Characterization

After design and fabrication, the MMICs are characterized using on-wafer measurement equipment. The main purpose of the characterization is the evaluation of the MMIC performance and also the wafer mapping to identify the working cells for shipment and packaging. During the circuit design, model based simulations were used to design the circuits according to the system specification. To determine whether the MMIC meets these specification or not different measurement setups are employed.
Linear circuits, active or passive are commonly measured using network analyzers to determine the S-parameters. Nonlinear circuits like mixers require a different measurement setup. Although modern network analyzers support the measurement of nonlinear devices, these features are usually limited to circuits below 100 GHz. This chapter covers the techniques and setups required to measure stand-alone mixers as well as transceiver circuits in the mmW frequency range.

3.1 On-Wafer S-Parameter Measurement of Mixers

Although mixers are nonlinear devices, S-parameter measurements are of particular interest. On the one hand, they are used to determine the characteristics of the linear passive components like couplers or baluns. And on the other hand, the port matching under small signal conditions (e.g. at the RF port) is important and determined using S-parameters.
S-parameter measurement is known for decades and has been becoming simpler through modern network analyzers which assist the user during calibration and measurement. At very high millimeter frequencies, higher effort is required since these measurements cannot be performed using the built-in signal sources. External frequency extension modules are required to expand the frequency range of the network analyzer towards several hundred GHz. The Fraunhofer IAF is one of the few organizations where S-parameter measurements up to 1 THz can be performed.
However, probe handling and on-wafer calibration are becoming more and more difficult with increasing frequency. The reduced size of the structures and circuits at millimeter wave and submillimeter wave frequencies introduces new effects and challenges which do not appear at lower frequencies. Coupling between the probes over the air or through the substrate are two effects which can possibly deteriorate the measurement results. To increase the calibration accuracy, new on-wafer calibration standards have been developed. Usually, on-wafer calibration is done using special calibration substrates. At higher frequencies, the difference between these standards and the on-wafer conditions increases and require on-wafer calibration structures to achieve the required accuracy.
For large signals (e.g. the LO), the small signal S-parameters may differ significantly from the values under large signal conditions. Figure 3.1 shows this effect for a L-matched

mHEMT in the 50 nm technology of the Fraunhofer IAF. The gate of the FET is matched under small signal conditions to a 50 Ω source at 120 GHz. A LSSP simulation with different LO levels from -20 to +7 dBm shows how the S_{11} moves to more capacitive values with increasing LO power. Measuring the matching at the LO port using small signals does therefore not give meaningful results. Unfortunately, there are no off-the-shelf frequency extension modules available to measure LSSP at 120 GHz or above using a vector network analyzer (VNA).

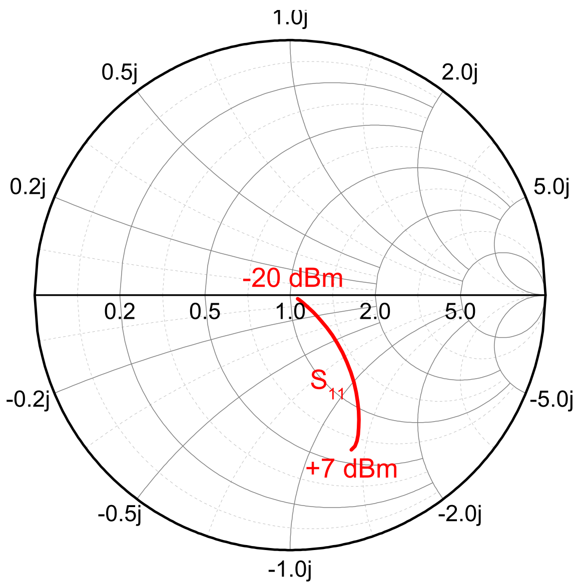

Fig. 3.1: Simulated S_{11} at 120 GHz of an L-matched mHEMT with a gate length of 50 nm and a width of 2×20 µm as a function of the LO power from -20 to 7 dBm.

3.2 Down-Conversion

In a down conversion scenario, the mixer is used to convert the RF signal to a lower frequency IF signal. Important figures of merit are the conversion gain of the mixer, the LO leakage and with I/Q mixers the I/Q channels' phase and amplitude imbalance.
To measure the conversion gain, a well-known RF power is applied at a specific frequency and the down converted IF signal is measured using a spectrum analyzer. The relation between the applied RF power (P_{RF}) and the measured IF power (P_{IF}) equals the scalar conversion gain of the mixer. This ratio is often expressed in dB for easier calculation:

$$CG[dB] = 10\, log_{10}\,(\frac{P_{IF}}{P_{RF}}) \tag{3.1}$$

A typical measurement setup is shown in figure 3.2. The LO and RF signals are generated using frequency synthesizers with subsequent frequency multipliers. To ensure the mixer operates linearly, the RF signal is attenuated to a power level <-20 dBm. After multiplication, the LO signal is amplified to drive the mixer into saturation. All power levels are calibrated to the on-wafer probe tips (P'_{RF} and P'_{LO}).

After biasing the chip with the corresponding DC voltages, the down converted IF signal is measured using a spectrum analyzer. The probe loss and the cable loss (L_{IF}) must be added to the measured IF power to correct the measured conversion gain for a given frequency. Typical power levels for a subharmonic mixer around 240 GHz are summarized in table 3.1.

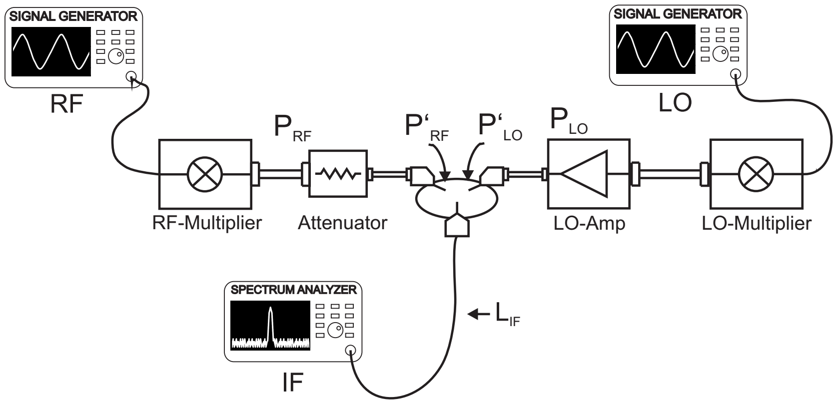

Fig. 3.2: Diagram of the down converter measurement setup.

P_{LO} [dBm]	P'_{LO} [dBm]	P_{RF} [dBm]	P'_{RF} [dBm]	P_{IF} [dBm]	L_{IF} [dB]
8.8	6	-24	-29	-55	6 at 40 GHz

Table 3.1: Typical power levels and cable loss during down converter measurements.

For wireless data transmission, both down and up-conversion mixers are needed. The up-conversion measurement setup employs basically the same equipment attached to different ports of the mixer.

3.3 Up-Conversion

In an up-conversion scenario, the mixer is used to convert a low frequency IF signal to the RF frequency. Important figures of merit are the conversion gain, carrier suppression, linearity and output power.
The measurement setup is shown in figure 3.3. The LO generation equals the down conversion measurement setup but the IF port is now used as an input. To measure the conversion gain, a signal with well-defined amplitude and frequency is fed into the IF port of the mixer using a frequency synthesizer.

Usually, one would like to analyze the frequency spectrum after up conversion. Since the up converted signals in this work are at frequencies up to 280 GHz, this requires a calibrated external mixer for the spectrum analyzer which currently only feature internal mixers up to 50 GHz. There are external mixers available for this frequency range, but they have a significant conversion loss (74 dB for OML M03HWD) and a ripple of more than 10 dB over the input frequency range. A power meter is therefore utilized to measure the absolute power levels of the up converted signal. This method yields to a sum of all

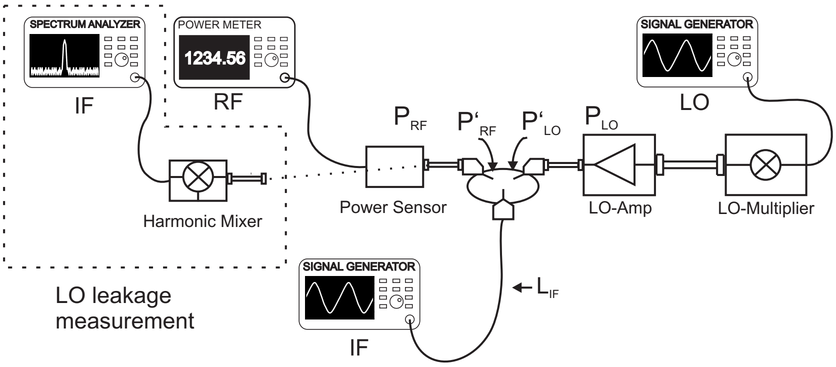

Fig. 3.3: Diagram of the up converter measurement setup.

signals in this frequency range including the LO and both converted sidebands (figure 3.4).

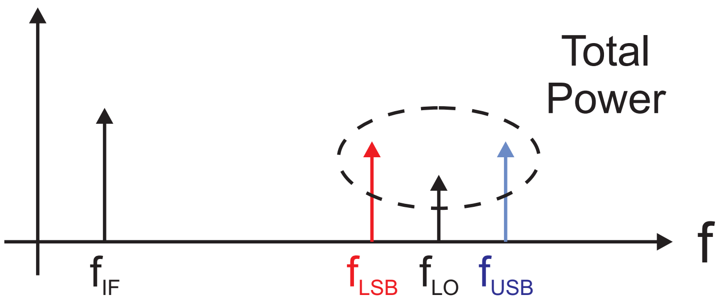

Fig. 3.4: Simplified transmitter output spectrum after up-conversion of an IF signal.

Although the external harmonic mixer is not suitable to measure the absolute power of the up converted signals it can be used to measure the carrier suppression. Due to the strong frequency response of the mixer, the IF has to be at a low frequency around 50 MHz to ensure a constant conversion loss across the LO frequency as well as the USB and LSB.

P_{LO} [dBm]	P'_{LO} [dBm]	P_{RF} [dBm]	P'_{RF} [dBm]	P_{IF} [dBm]	L_{IF} [dB]
8.8	6	-18	-23	0	6 at 40 GHz

Table 3.2: Typical power levels and cable loss during up converter measurements.

3.4 Receiver Noise Figure

Noise plays an important role in almost any millimeter wave system from astronomy over radiometers to communication systems. The signal-to-noise ratio (SNR), as one of the most critical system parameters, is directly defining the system's sensitivity and hence the channel capacity C of a wireless data transmission system [66]:

$$C = \Delta f[log_2(\text{SNR} + 1)] \tag{3.2}$$

Any stage in a receiver is decreasing the SNR of the received signal. To evaluate the noise performance of an amplifier, mixer or an entire receiver, the noise factor F is introduced. As long as the input noise is thermal noise at 290 K, it is defined as the ratio between the SNR at the input of a device under test (DUT) and the SNR at its output [67]:

$$F = \frac{SNR_{in}}{SNR_{out}} \tag{3.3}$$

A common nomenclature in engineering is to refer to the noise factor in decibel as the noise figure (NF):

$$\mathrm{NF} = 10\, log_{10}\,(F) \tag{3.4}$$

The overall noise of a millimeter wave system is determined by the performance of the individual building blocks as well as the system's architecture. Usually, the first stage in a receiver is a LNA. However, depending on the technology, at very high frequencies there are no LNAs available and it might be a good choice to use a down converting mixer as a first stage instead of a noisy, low gain amplifier. The noise figure of a multistage design could be calculated using Friis formula [68]:

$$F_{total} = F_1 + \frac{F_2 - 1}{G_1} + \frac{F_3 - 1}{G_1 G_2} \ldots \tag{3.5}$$

Where G_n is the available gain of the corresponding stage. Accordingly, the noise figure of the first stage defines a lower limit to the overall noise figure and the second stage noise contribution is divided by the gain of the first stage. In a receiver it is therefore recommended to use a high gain, low noise amplifier as a first stage to keep the total noise low.
A well-established noise figure measurement method is the so called "Y Method". The Y Method involves a switchable noise source attached to the input of a DUT. The Y factor is defined as the ratio between the output power of the DUT when the noise source is switched on (P_{Non}) and off (P_{Noff}).

$$Y = \frac{P_{Non}}{P_{Noff}} \tag{3.6}$$

The noise power P_N of a thermal noise source at a given temperature T within the bandwidth Δf is defined as:

$$P_N = k_B T \Delta f \tag{3.7}$$

This equals the power which an ideal resistor at the temperature T would emit. Since this power and the temperature have a linear relation, transposing 3.7 leads to:

$$T = \frac{P_N}{k_B \Delta f} \tag{3.8}$$

Which represents the noise temperature of a noise source. The Y factor can therefore be also expressed in equivalent noise temperatures, where T_h represents the "hot" temperature, when the noise source is switched on and T_c stands for the cold temperature, when the noise source is off:

$$Y = \frac{T_h}{T_c} \tag{3.9}$$

The Y factor is simply the gradient of the line which connects the two power levels when the noise source is switched on ($P_N(T_h)$) and off ($P_N(T_c)$) (see figure 3.5). Since only the ratio between the hot and cold output power counts, cable losses can be ignored as they are equal for both temperatures.

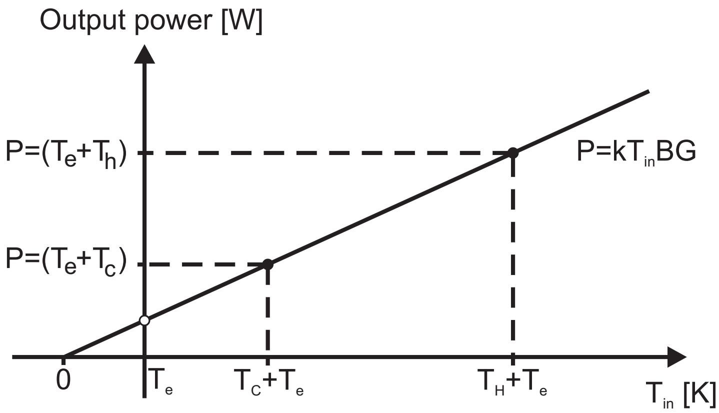

Fig. 3.5: Illustration of the Y-method for noise figure measurements where a noise source is periodically switched on (T_h) and off (T_c).

At lower frequencies, commercially available noise diodes are commonly used as noise sources. They can be directly controlled by a noise figure analyzer (NFA), which alters the diode between on and off. These diodes are delivered together with an excess noise ratio (ENR) table which holds the relative change in the output power of the noise diode, when it is switched on and off.

$$ENR = \frac{T_{on} - T_{off}}{T_0} \tag{3.10}$$

Or more commonly expressed in decibel [69]:

$$ENR_{dB} = 10\, log_{10} \left(\frac{T_{on} - T_{off}}{T_0} \right) \tag{3.11}$$

T_0 is the standardized reference temperature which is defined as 290 K. On the basis of the ENR table, the NFA is able to calculate the noise figure as well as the gain of the DUT. A typical measurement setup is shown in figure 3.6, where a receiver module is

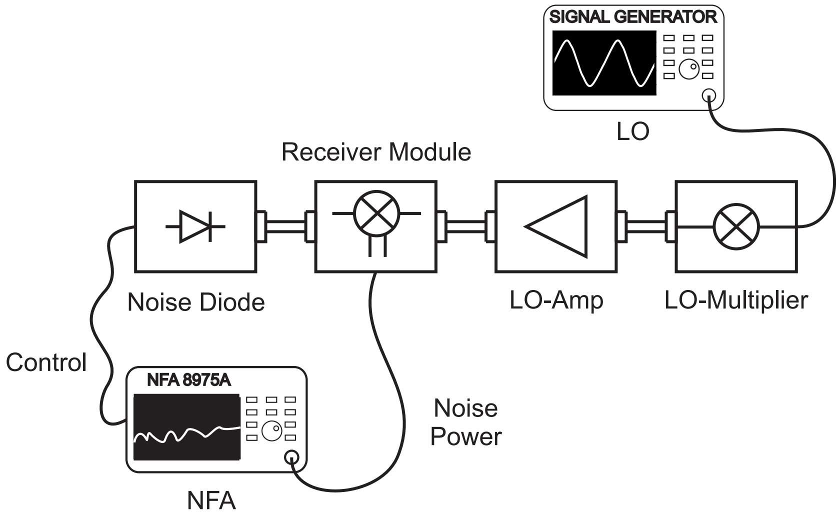

Fig. 3.6: Diagram of the noise measurement setup using a noise diode.

pumped with an amplified LO and connected to a noise diode. The NFA controls the noise diode and measures the IF power for P_{Non} and P_{Noff}. Based on the supplied ENR table it automatically calculates the receiver NF.

With increasing frequency, less commercial noise sources are available. At very high mmW frequencies only custom measurement setups are available to determine the receiver noise figure. To substitute the noise diode, a physically hot or cold source can be used. To measure the NF of the LNA and the entire receiver around 240 GHz in section 4.4 absorber material at the temperature of liquid nitrogen (77 K) and room temperature (297 K) was used as a noise source. The employed measurement setup is shown in figure 3.7. A horn antenna attached to the receiver module is pointing towards the hot and cold absorber while the output power at both IF channels is measured.

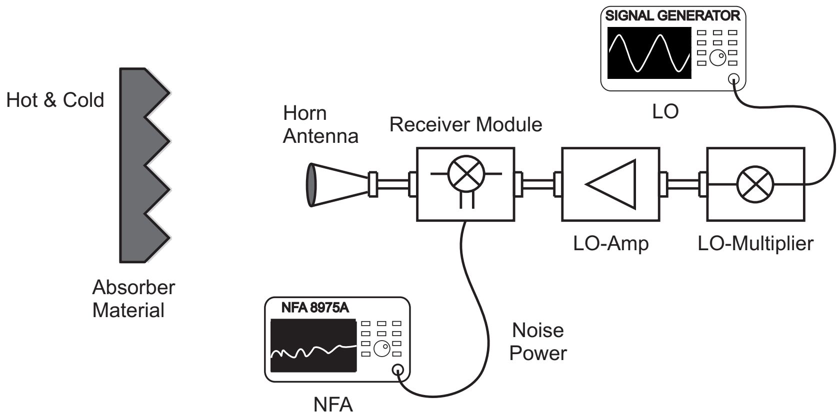

Fig. 3.7: Diagram of the custom hot/cold noise measurement setup.

The definition of the noise figure of a mixer or an entire receiver equals basically the definition of equation 3.4 which expresses a relation between the noise at the RF input and the IF output. In difference to an amplifier, a mixer has two input frequencies which generate the same IF frequency (upper sideband (USB) and lower sideband (LSB)) and contribute to the noise at the IF output. In case where only a single tone and no image frequency is present at the RF input, the measured noise figure is referred to as single sideband (SSB) NF while a double sideband (DSB) NF is measured when both RF frequencies contain information. The SSB noise figure is higher than the DSB noise figure since both contain the same IF noise, but the former has signal power only in one sideband. In case the conversion gain of the mixer is the same for both sidebands, the SSB NF will be 3 dB higher than the DSB NF [45].

After presenting the theory and the manufacturing technology in chapter 2 and the measurement setup in chapter 3, the next chapter will cover the design process of integrated passive circuit elements, as well as active and passive mixer cells. It will conclude with the design of a fully integrated Rx and Tx chipset for wireless communication around 240 GHz.

4 Broadband mmW Mixers

The requirements of most applications cannot be fulfilled by a single mixer cell. Specifications in a communication system demand a high port-to-port isolation and often quadrature mixers featuring I/Q IF terminals. The port-to-port isolation of an individual mixer cell is typically quite low. In addition, spectrum regulation or applications like single sideband modulation may require a suppression of the unwanted sideband. These design goals can only be achieved by more complex mixer designs combining individual mixer cells with additional passive coupler networks.

This chapter begins with the analysis and design of different passive couplers and hybrids for the on-chip integration at frequencies above 200 GHz including a Wilkinson power divider, 90° couplers[1] and a Marchand balun for the design of balanced and quadrature mixers. Afterwards, different mixer topologies using the Fraunhofer IAF mHEMT technologies are examined and evaluated with respect to their applicability in broadband transceiver circuits for wireless data transmission. For this comprehensive analysis, different mixer architectures (I/Q, balanced, active and passive) realized in different mHEMT technologies[2] are analyzed, designed and subsequently characterized. Based on the result from the coupler and mixer evaluations, the chapter concludes with the design, fabrication and characterization of the first integrated subharmonic multifunctional I/Q transceiver circuits in the frequency range between 200 and 280 GHz.

4.1 Passive Coupler Structures for Balanced and Quadrature Mixers

In this work, balanced mixers, I/Q mixers and their combination are analyzed. Balanced mixers can, for example, be realized by using either a 180° coupler or two 90° couplers. Figure 4.1 shows the block diagram of a balanced and an I/Q mixer design.

With increasing operational frequency, the dimension of the couplers are becoming smaller and smaller and allow the integration together with active circuitry on an MMIC. Basically, couplers and hybrids have been used for decades in high frequency circuits. However, using integrated couplers for mixers operating at frequencies between 200-300 GHz poses new problems and design challenges.

[1] branch-line coupler and a Lange coupler
[2] 100 nm, 50 nm and 35 nm gate length

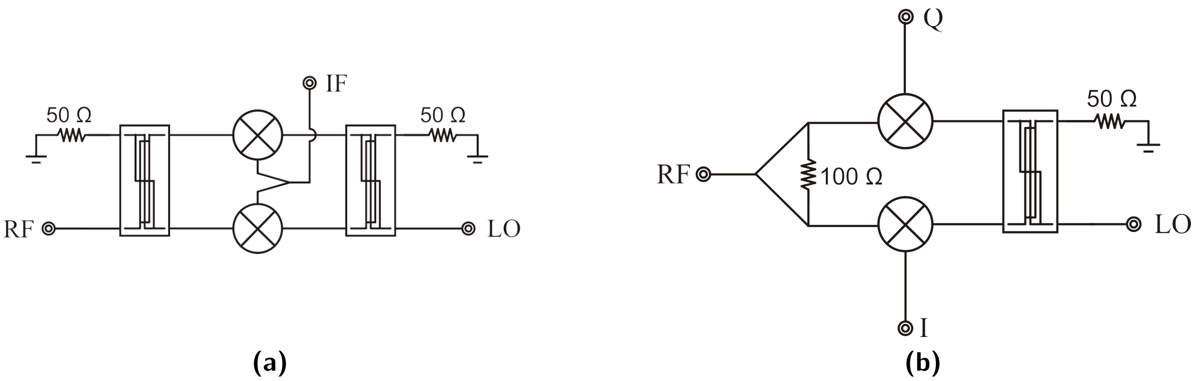

Fig. 4.1: Topology of a single-balanced mixer using 90°couplers (a) and an I/Q mixer (b).

4.1.1 Wilkinson Power Divider

The Wilkinson power divider allows the design of an ideal power splitter which is matched, reciprocal and also isolates both output ports from each other. It has been first introduced in 1960 by E. J. Wilkinson [70] for shielded coaxial transmission lines.
Different challenges arise when transferring this classical low frequency coaxial design to integrated millimeter wave circuits [71]. Coupling between the transmission lines plays an ever increasing role as the dimensions become smaller and smaller. In the classical approach, the isolation resistor could be assumed to be ideal while at millimeter wave frequencies, it must be treated as a lossy transmission line of a given length and width. The design of an integrated Wilkinson divider requires also the careful consideration of substrate modes.

The two main design parameters of an integrated Wilkinson divider are:

- The length of each arm of the Wilkinson divider ($\sim \frac{\lambda}{4}$).
- The distance between both arms and consequently the length of the isolation resistor and its connections.

The distance between both arms is in many cases inherently given by the layout of the remaining circuit. For example, the layout of an I/Q mixer circuit, consisting of a quadrature hybrid and a Wilkinson divider is much easier when the outputs of both have the same spacing, usually determined by the quadrature hybrid. Other layout constraints may also arise from the selected type of transmission line. For the design of the Wilkinson divider at 210 GHz, a CPWG has been chosen with a ground-to-ground spacing of 50 μm. In this configuration, each transmission line is guided by two ground planes which require additional space.
To calculate the S-parameters, an even and odd mode analysis is the method of choice [72]. A simplified schematic of the Wilkinson divider is shown in figure 4.2a. The S-parameters of port 2 and port 3 can be determined by utilizing the circuit's symmetry. Due to the symmetry of the Wilkinson divider, the analysis at port 2 and port 3 could be reduced by dividing the circuit in half along its line of symmetry. Figure 4.2b shows a diagram of the reduced circuit.

The return loss (S_{11}) does not depend on the isolation resistor when the ports 2 and 3 are terminated identically, and in this case the even mode simplifications can be used. The input impedance is then determined by the transformed impedance of the parallel connection of the feed line to the isolation resistor and the termination of port 2 and 3.

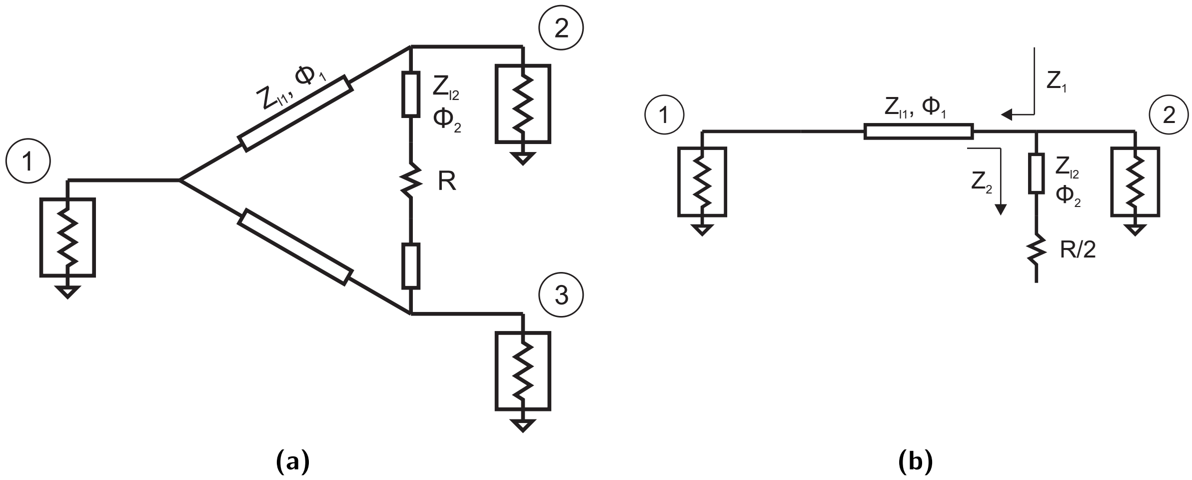

Fig. 4.2: Schematic of the Wilkinson power divider (a) and the simplified circuit (b).

Even-Mode Analysis

When the circuit is excited in even mode, a virtual open is created along its line of symmetry and the impedance of port 1 is doubled to twice the system impedance. The virtual open creates an open stub with the length ϕ_2 of the feed lines to the isolation resistor. The impedance at port 2 is the parallel connection of the transformed impedance of port 1 by the transmission line of length ϕ_1 and the open stub ϕ_2.

$$Z_{1e} = Z_{l1} \frac{Z_1 + jZ_{l1} tan(\phi_1)}{Z_{l1} + jZ_1 tan(\phi_1)} \tag{4.1}$$

$$Z_{2e} = -jZ_{l2} cot(\phi_2) \tag{4.2}$$

$$Z_e = Z_{1e} || Z_{2e} \tag{4.3}$$

Odd-Mode Analysis

In odd-mode excitation, a virtual ground is created along the line of symmetry, dividing the isolation resistor into two resistors with the value $R/2$. The terminal at port 1 is replaced by a short circuit and transformed by the transmission line l_1 with the length ϕ_1. The feed line l_2 with its characteristic impedance of Z_{l2} transforms the resistor of the value $R/2$ according to the transformer equation. The resulting odd-mode impedance is the parallel connection of these impedances:

$$Z_{1o} = -jZ_{l1}tan(\phi_1) \tag{4.4}$$

$$Z_{2o} = Z_{l2}\frac{R + jZ_{l2}tan(\phi_1)}{Z_{l2} + jRtan(\phi_1)} \tag{4.5}$$

$$Z_o = Z_{1o}||Z_{2o} \tag{4.6}$$

The reflection coefficients at the ports can be calculated using the even- and odd-mode impedances:

$$\Gamma_e = \frac{Z_e - 50}{Z_e + 50} \tag{4.7}$$

$$\Gamma_o = \frac{Z_o - 50}{Z_o + 50} \tag{4.8}$$

$$S_{22,33} = \frac{1}{2}(\Gamma_e + \Gamma_o) \tag{4.9}$$

The input return loss S_{11} equals the reflection coefficient of the input port 1. In case of a 50 Ω termination at port 2, an auxiliary variable $Z_{2'}$ is introduced to represent the parallel connection of the port termination and the impedance Z_2:

$$Z_{2'} = Z_2||50\ \Omega \tag{4.10}$$

$$Z_{in} = Z_{l1}\frac{Z_{2'} + jZ_{l1}tan(\phi_1)}{Z_{l1} + jZ_{2'}tan(\phi_1)} \tag{4.11}$$

$$\Gamma_{in} = \frac{Z_{in} - 50}{Z_{in} + 50} \tag{4.12}$$

$$S_{11} = \Gamma_{in} \tag{4.13}$$

The port matching as a function of the length $\phi_{1,2}$ of the transmission lines according to equations 4.9 and 4.13 is shown as a contour plot in figure 4.3. The dark blue region marks the perfectly matched condition and helps to estimate the length of the lines l_1 and l_2. It could be seen that all ports are matched for the conditions of the ideal Wilkinson divider ($\phi_1 = \frac{\lambda}{2}$ and $\phi_2 = 0$). In case of a non-zero length feed line ($\phi_2 > 0$) to the resistor, a trade off between input and output port matching must be made. To keep the input matched, ϕ_1 should increase with ϕ_2 while it should be decreased to keep the output ports matched. The realized integrated Wilkinson divider is based on the classical design and consists of two quarter-wavelength arms with an impedance of 70 Ω and an integrated 100 Ω NiCr isolation resistor. A SEM image of the test structure used to measure two port scattering parameters is shown in figure 4.4a. The unused port is terminated with an on-chip 50 Ω resistor for on-wafer measurements. The spacing between the output ports equals the spacing of the Lange coupler described in 4.1.2.2. The feed lines to the isolation resistor are 40 μm long (∼0.07 λ). Since the length ϕ_2 is determined by the

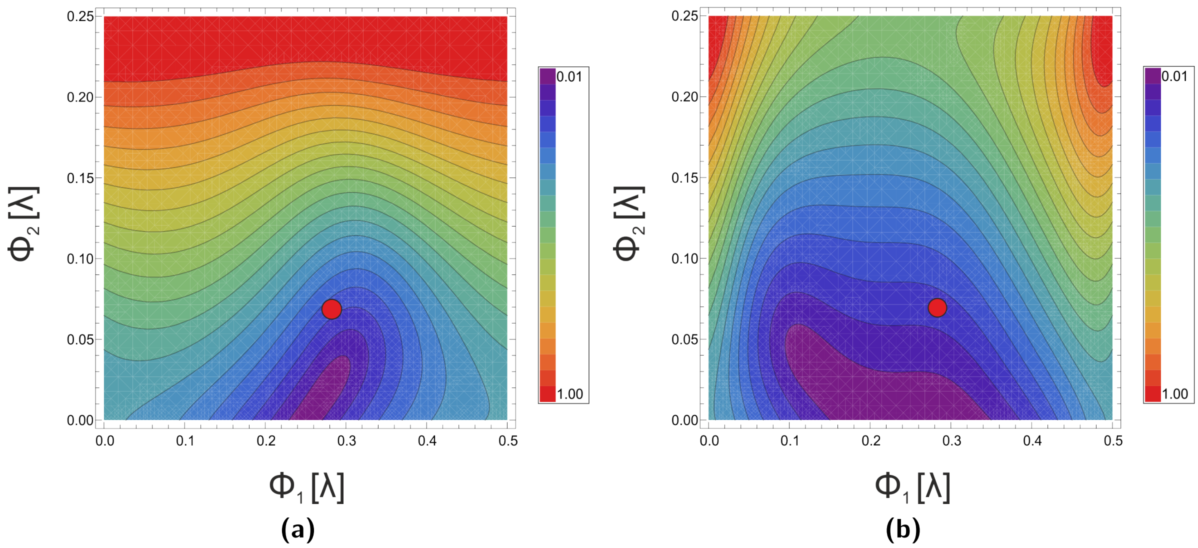

Fig. 4.3: Calculated S_{11} (a) and $S_{22,33}$ (b) depending on different lengths $phi_{1,2}$ of the transmission lines. The red dots mark the selected length of the transmission lines based on electromagnetic simulations.

spacing between the output ports to a length of about 0.07 λ, the length ϕ_1 has been chosen according to figure 4.3 to be approximately 0.29 λ to keep all ports matched. The final length has been evaluated using an electromagnetic (EM)-simulator and marked as red dots in figure 4.3. Each arm has a length of 160 µm and the inner conductor has a width of 7 µm. In combination with a 50 µm ground-to-ground spacing this equals an impedance of 70 Ω for the CPWG transmission lines. Through-substrate vias need to be placed around the coplanar transmission lines in a well-defined distance to prevent coupling through the substrate. Figure 4.4b shows a simulation of the electrical field using the high frequency structural simulator from Ansys Corp. (HFSS) where the blocking effect of the vias is clearly visible.

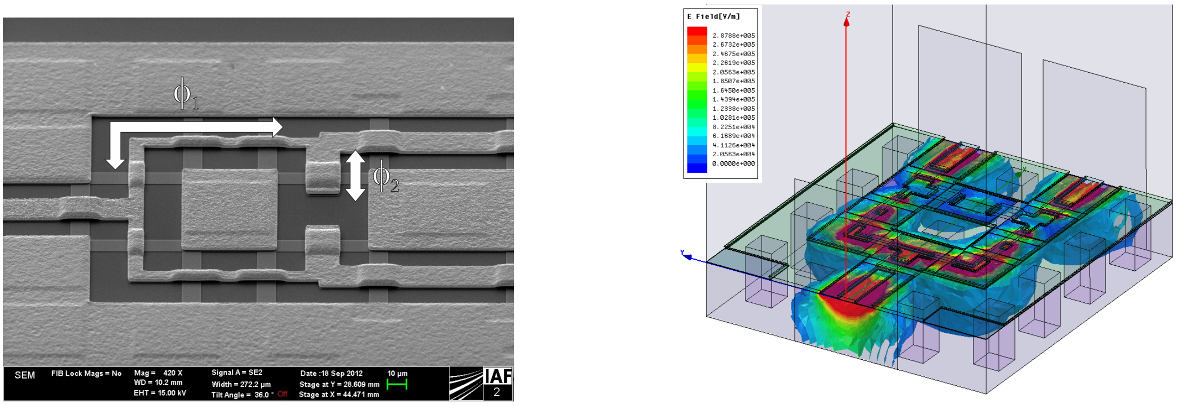

(a) **(b)**

Fig. 4.4: SEM picture (a) and simulated E-field (b) of the Wilkinson power divider. The arrows in the SEM picture mark the arm length ϕ_1 and the feed line ϕ_2 to the isolation resistor.

The measured and simulated S-parameters are shown in Figure 4.5. The measured transmission agrees well with the simulation results and stays around -3.8 dB in the entire G-Band (140-220 GHz). The port isolation reaches its maximum of 27.4 dB at 189 GHz which is slightly below the simulated results [100].

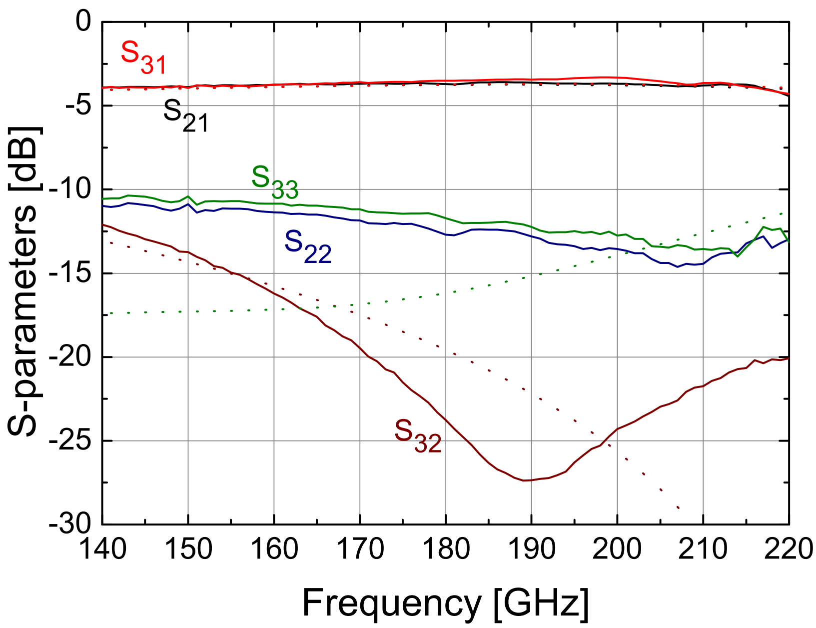

Fig. 4.5: Measured (solid) and simulated (dashed) S-parameters of the Wilkinson power divider.

To realize balanced and quadrature mixers, phase shifting couplers are needed. While balanced designs often employ baluns with a 180° phase relation, I/Q mixers require signals which are 90° out of phase. Such signals cannot be created by a Wilkinson power divider but by using directional couplers which are described in the next section.

4.1.2 Directional Couplers

In addition to an equal power split, the design of balanced and I/Q mixers requires also a phase shifting element. There are several well-known couplers offering a 90° or 180° phase shift for different applications. The following couplers are typically used in integrated microwave circuits:

- Coupled lines (90°/180°)
- Branch-line coupler (90°)
- Lange coupler (90°)
- Rat-race coupler (180°)
- Marchand Balun (180°)

The quadrature couplers have been of special interest in this work. They were used to design balanced mixers as well as fundamental and subharmonic I/Q mixers. A Marchand balun type coupler has been used to convert single-ended signals into balanced ones for the design of a Gilbert cell mixer.

4.1.2.1 210 GHz Branch-Line Coupler

Branch-line couplers are entirely planar structures and are therefore best suited for on-chip integration. However, they are generally larger than a coupled line hybrid [73].
Coupling of the branch-line coupler is achieved by the periodic interconnection of two transmission lines. The series and the shunt transmission lines are one quarter wavelength long. For a 3 dB coupler, the series transmission lines have a characteristic impedance of $\frac{R}{\sqrt{2}}$ while the impedances of the shunt arms are simply R. Compared to coupled line hybrids, the single-section branch-line hybrids have a narrow bandwidth of approximately 10% [46, 74]. The bandwidth could be extended by either using a multisection design [74] or by applying internal matching techniques [75].

The two main design parameters are therefore:

- The length of the transmission lines
- The number of branches

With increasing operating frequencies the transmission lines become shorter and cause a degradation of the coupler's performance due to the discontinuities introduced by the low impedance lines. The coupler becomes basically impractical when the arm lengths is in the order of the line width [46]. The coupler shown in figure 4.6 is designed for a center frequency of 210 GHz. In this case a quarter wavelength equals:

$$\frac{\lambda}{4} = \frac{\frac{1}{\sqrt{\epsilon_{re}}} \cdot c}{4f} \approx \frac{\frac{1}{\sqrt{6.95}} \cdot 3 \cdot 10^8 \frac{m}{s}}{4 \cdot 210 \cdot 10^9 \frac{1}{s}} \approx 135\mu m \tag{4.14}$$

Where ϵ_{re} is approximately the effective dielectric constant of a coplanar transmission line on GaAs. To achieve a 50 Ω port impedance, the series transmission lines need to have a characteristic impedance of 35 Ω. The inner conductor of a coplanar transmission line with a 50 μm ground-to-ground spacing on GaAs substrate has then to be around 32 μm wide which is only about a fourth of the line length. Figure 4.6 shows a SEM picture of the realized branch-line coupler. Although the MMIC process features two metallization layers, the entire coupler structure is realized in the first metal layer only. Besides the more precise manufacturing of the thinner first metal, the main reason for this approach was to keep the discontinuities as low as possible. Since the coupler is realized in the first metal layer, the second metal layer is used to connect the ground plane in the center of the coupler using air-bridges over the first metal layer (see figure 4.6). When both metal layers are used to form the coupler structure the only way to connect the center ground plane is to introduce air-bridges in the series transmission lines (as could be seen with the Wilkinson divider in figure 4.4a) which are additional discontinuities. On the other hand, the realization in the thin first metal layer leads to higher losses compared to the thick metallization.

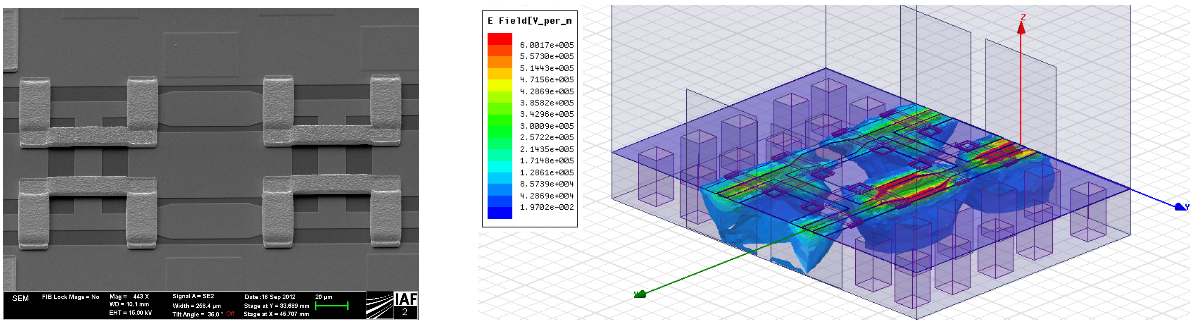

(a) (b)

Fig. 4.6: SEM picture (a) and simulated E-field (b) of the 210 GHz branch-line coupler.

The 3D EM-simulations of the coupler structure predict an insertion loss of 1.2 dB at 220 GHz while the coupler is about 0.5 dB under-coupled. The measured and simulated S-parameters are shown in figure 4.7. The simulation and the measurement show a good agreement up to 210 GHz. Beyond 210 GHz uncertainties of the measurement system are responsible for the large deviation between simulation and measurement. Nevertheless, the S_{21} parameter is already decreasing above 200 GHz when it should be rising to intercept the S_{31}. Instead, both S-parameters are falling above 200 GHz which is caused by the significant losses in the very thin first metal layer. The measured insertion loss at 210 GHz is 1.5 dB for S_{31} and 3.3 dB for S_{21}. The bandwidth is 30 GHz from 190 to 220 GHz which equals 14.6% of relative bandwidth.

The phase difference between port 2 and port 3 shows a good agreement with the simulation up to 210 GHz where the measurement uncertainties start to play a significant role. At 210 GHz, the phase difference is 89.95° which is very close to the ideal 90°. However, the large amplitude imbalance between port 2 and port 3 would decrease the isolation in a balanced mixer and lead to an I/Q imbalance with an I/Q mixer.
Another coupler which features a 3 dB power split with a 90° phase shift is the Lange

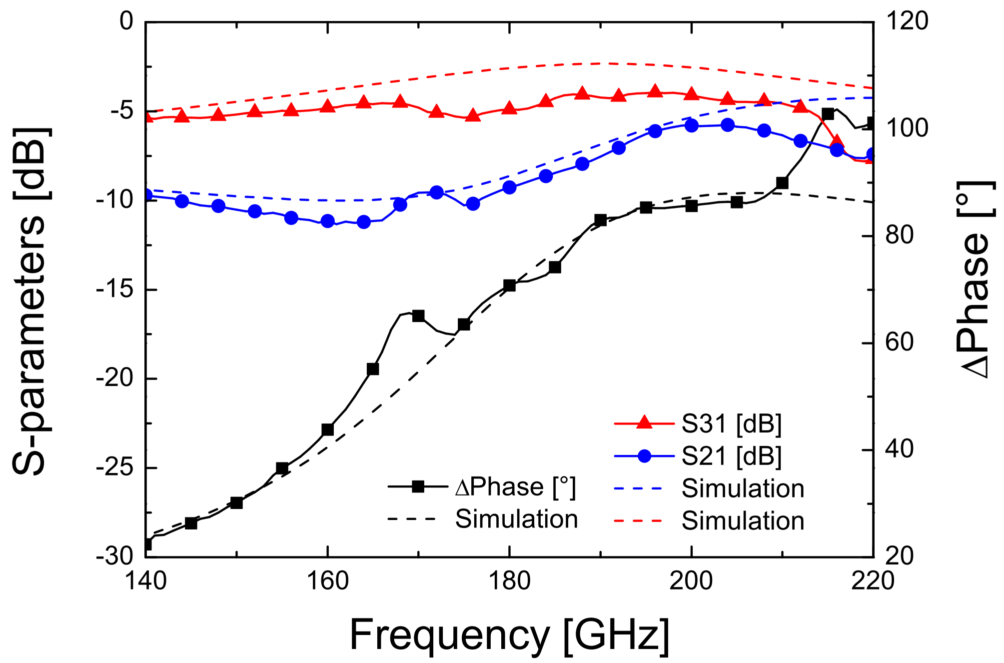

Fig. 4.7: Measured (solid) and simulated (dashed) S-parameters and phase difference of the branch-line coupler.

coupler. It requires typically a second wiring level and is therefore not an entirely planar structure like the branch-line coupler. However, many semiconductor processes feature multiple metal layers and are therefore able to manufacture integrated Lange couplers. Since they usually support a larger operational bandwidth than the branch-line coupler, they are analyzed in the next section.

4.1.2.2 210 GHz Lange Coupler

The Lange coupler is basically a coupled line hybrid and consists of multiple interdigitated coupled lines. Achieving a 3 dB power split in a 50 Ω system using edge coupled lines requires an even mode impedance of 120.7 Ω and an odd mode impedance of 20.7 ohm respectively [73]. Achieving this low odd mode impedance using simple edge coupling is only possible on high permittivity substrates like GaAs (ϵ_r = 12.9) and requires very narrow transmission lines. Figure 4.8 shows the calculated even and odd mode impedances of coupled microstrip lines realized using both metal layers, the thin first metal and the thicker top metallization on GaAs substrate (ϵ_r = 12.9). All calculations are based on the formulas from Kirschning and Jansen [76] which are also used by Agilent's LineCalc software [77]. The design parameters are the slot width (s) and line width (w) on a substrate of the given height (h). The red dot marks the required even and odd mode impedances to achieve a 50 Ω port impedance. However, the design rules of the manufacturing process using the thick metal allow only the realization of impedances within the hatched region.

Employing only the first metal layer relaxes the design rules and allows smaller gaps and more narrow line widths (figure 4.9). Unfortunately, the desired impedances are still

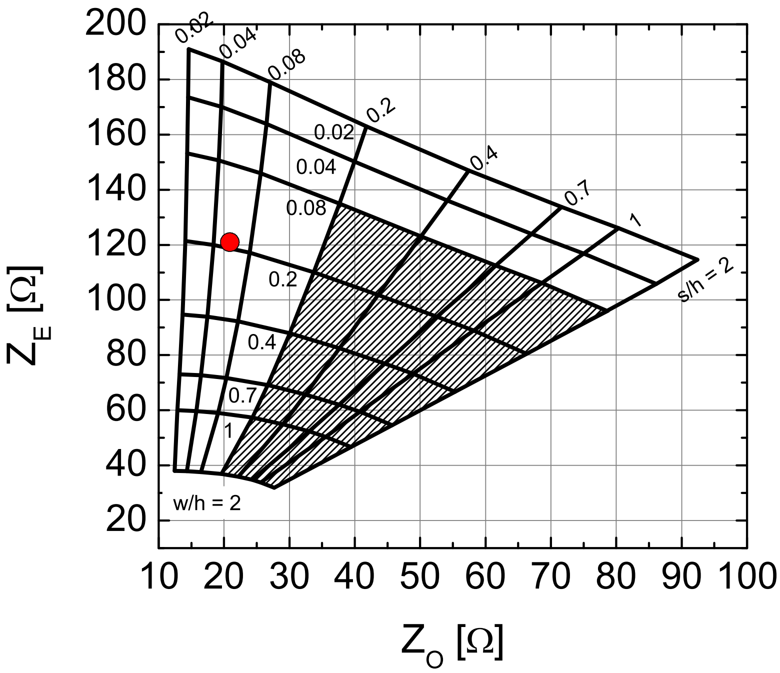

Fig. 4.8: Calculated even and odd mode impedances of coupled microstrip lines using both metal layers on GaAs substrate (ϵ_r=12.9). The design parameters are w/h and s/h. Regarding the design rules for the thick metallization, the hatched region marks the achievable impedances while the red dot marks the necessary even and odd mode impedances of coupled lines with a characteristic impedance of 50 Ω.

not achievable using coupled lines. The Lange coupler overcomes this problem by using several smaller lines which provide multiple couple edges.

The main design parameters of a Lange coupler are the line width, slot width and the line length which is approximately a quarter wavelength on the host substrate. For the 210 GHz Lange coupler, a four finger design has been chosen with a finger length of 124 µm. To determine the line width of the Lange coupler, a simple rule of thumb can be used for a first approximation. The total width of all strips should be equal to the width of a microstrip on the same substrate. A 50 Ω microstrip transmission line on 50 µm thick GaAs (ϵ_r = 12.9) has a width of about 38 µm which equals 9.5 µm per strip for a four finger design. EM-Simulations resulted in a line width of 5.5 µm for each finger to achieve good matching which is significantly lower than the approximated 9.5 µm. The main reason for this difference is the effect of the coplanar environment of the realized Lange coupler. As can be seen on the SEM picture in figure 4.10a, the outer strips of the Lange coupler face a ground plane which leads to a mixture of microstrip and coplanar transmission line behavior. The slot width determines mainly the coupling performance and has been chosen to 2 µm which is the smallest value allowed by the design rules.
Figure 4.10a shows a SEM picture of the test structure for S-parameter measurement. The coupler has been simulated prior to manufacturing using HFSS. A plot of the E-Field inside the coupler is shown in figure 4.10b. As already seen with the Wilkinson divider, the field is also propagating inside the GaAs substrate and the placement of the vias has a significant impact on the coupling and the port isolation.

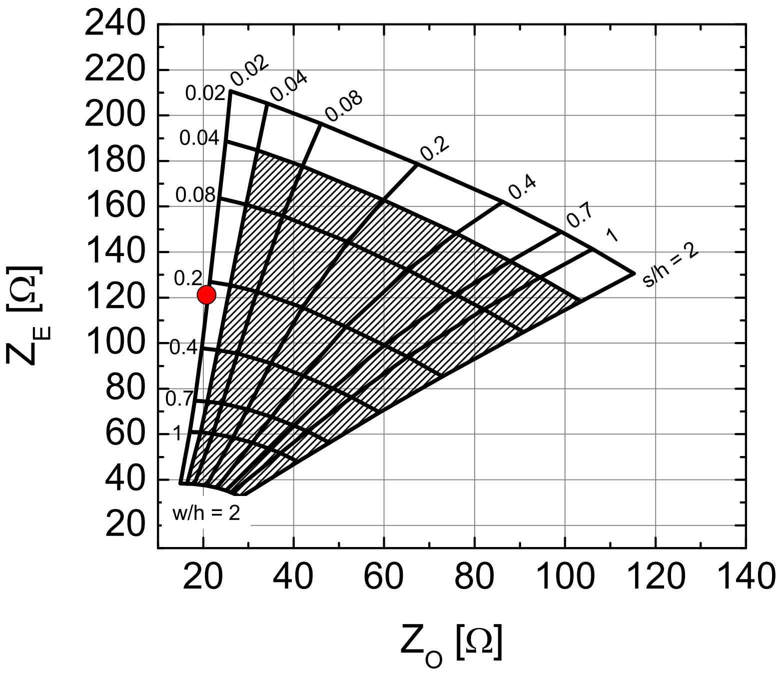

Fig. 4.9: Calculated even and odd mode impedances of coupled microstrip lines realized in the first metal layer only (ϵ_r=12.9). The design parameters are w/h and s/h. The more precise manufacturing allows smaller gaps and line width. The hatched region shows the achievable impedances. The required even and odd mode impedances of coupled lines with a characteristic impedance of 50 Ω (red dot) are outside of this region.

A on-wafer S-parameter measurement according to section 3.1 has been used to determine the performance of the coupler. The unconnected coupler ports were terminated by on-chip 50 Ω resistors. Figure 4.11 illustrates the measured S-parameter as a function of the frequency. The return loss of the coupler stays well above 9 dB in the entire measurement range while the insertion loss equals 1.4 dB at 210 GHz and the measured

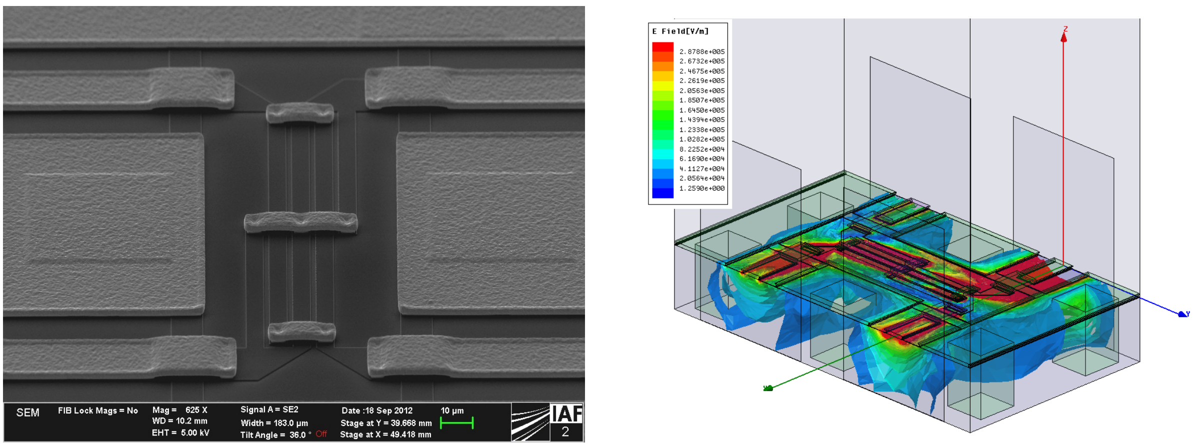

(a) **(b)**

Fig. 4.10: Chip photograph of the test structures (a) and the simulated E-field (b) of the Lange coupler.

isolation of the coupler is better than 21 dB at 210 GHz. The variation of the coupling parameters stays within ± 1.5 dB over the measured frequency range.

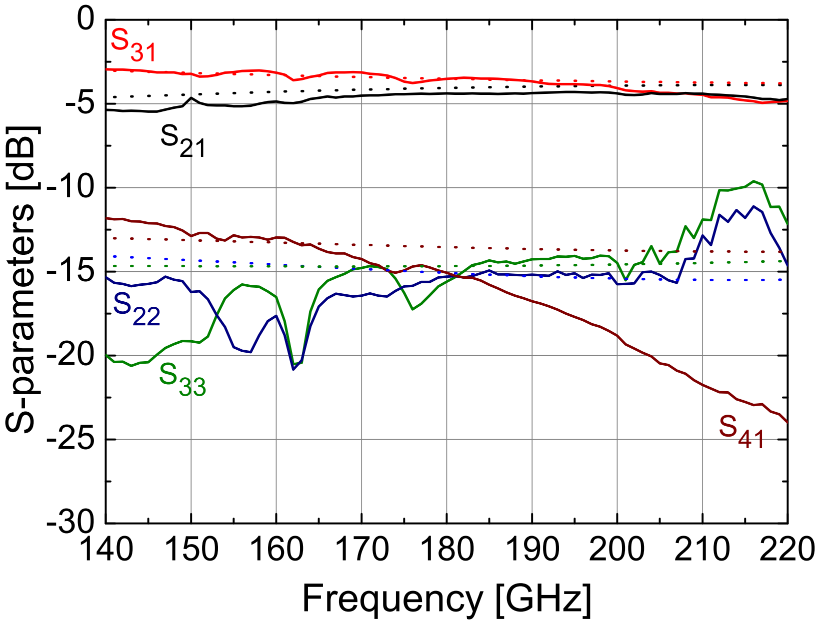

Fig. 4.11: Measured and simulated S-parameters of the Lange coupler.

The amplitude imbalance is of particular interest in balanced designs, where two components cancel each other and an amplitude imbalance would lead to a lower performance. The coupler achieves an extremely low amplitude imbalance of less than 0.1 dB at 210 GHz.
Besides the amplitude imbalance, the phase imbalance plays a major role in balanced and quadrature designs. The ideal Lange coupler would have an exact phase difference of 90° between the direct and the coupled port. Any deviation of this value will lead to a decreased performance in balanced and image rejection or single sideband mixers where the cancellation of the wave components relies on strict phase relations. The phase difference of the Lange coupler has been calculated based on the S_{21} and S_{31} measurements and equals 89.2° at 210 GHz.

4.1.2.3 240 GHz Lange Coupler

The center frequency of the 210 GHz Lange coupler is close to the edge of the WR-5 waveguide band (170 to 220 GHz). Hence, broadband applications are partially covering the WR-5 as well as the WR-3 (220 to 325 GHz) waveguide bands. To enable the design of broadband mixers, a Lange coupler with a center frequency of 240 GHz has been designed. The bandwidth of the coupler is completely covered by the WR-3 waveguide which works properly above 200 GHz.
The design of the 240 GHz Lange coupler is very similar to the 210 GHz Lange coupler. The coupler is also a four finger design with a reduced length of 110 µm but the same line width and slot width as used with the 210 GHz Lange coupler. Test structures have been manufactured to measure the S-parameters of the coupler using the measurement

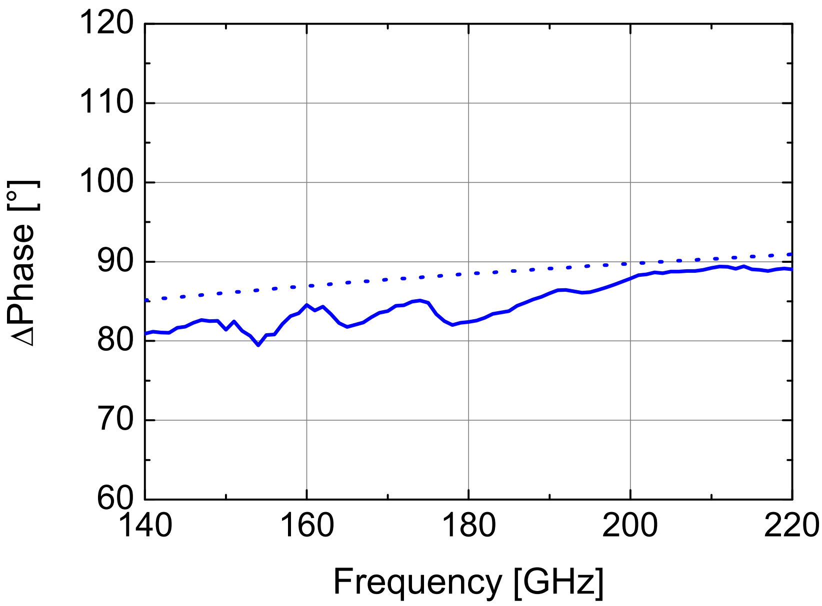

Fig. 4.12: Measured (solid) and simulated (dotted) phase difference of the 210 GHz Lange coupler.

setup described in section 3.1. Figure 4.13 illustrates the measured S-parameters versus the RF frequency of the 240 GHz Lange coupler. The insertion loss stays between 0.81 and 3.0 dB in the frequency range from 200 to 280 GHz while the return loss stays well above 10 dB on all ports. The measured 3 dB bandwidth of the coupler is 86 GHz, from 200 to 286 GHz.

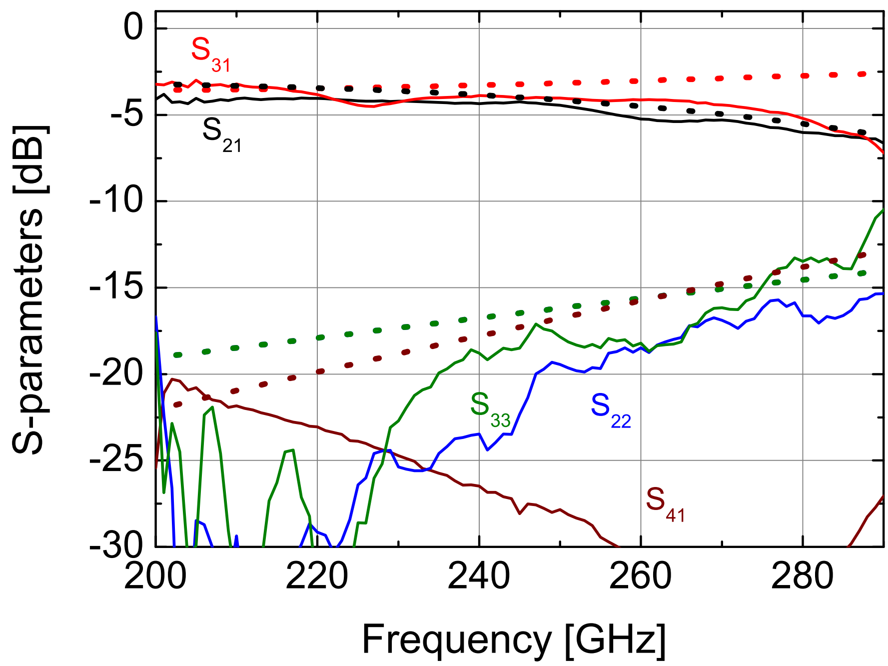

Fig. 4.13: Measured (solid) and simulated (dotted) S-parameters of the 240 GHz Lange coupler.

The phase difference has been calculated based on the S_{21} and S_{31} measurements. Figure 4.14 shows the measured phase difference between the ports 2 and 3 as a function of the frequency. The Δ phase stays between 88.7 and 106.8 degrees in the frequency range from 200 to 280 GHz and equals 90.6° at 240 GHz.

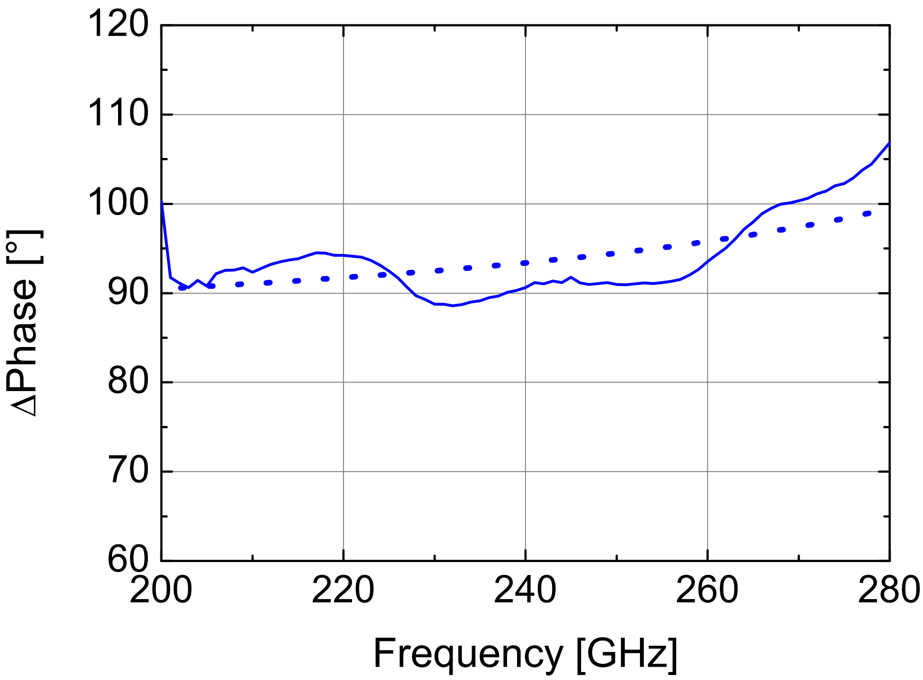

Fig. 4.14: Measured (solid) and simulated (dotted) phase difference of the 240 GHz Lange coupler.

4.1.2.4 94 GHz Marchand Balun

Balanced mixers require differential input signals and hence need a balun to perform the single ended to differential conversion. At lower frequencies, active baluns (e.g. differential amplifiers) are favored due to their small size [78]. With increasing operation frequency, passive baluns scale down with the shorter wavelength while active baluns are limited by the cutoff frequencies of their active devices. At high mmW frequencies the short wavelengths enable the planar integration of passive baluns together with active devices on a MMIC.

In section 4.2.2, a Gilbert cell mixer is presented which requires a balun for the RF and LO signals. The Fraunhofer IAF MMIC process, with two metallization layers, is best suited to realize planar hybrids. For wideband operation, most coupled line hybrids require a high ratio between the even mode and the odd mode impedances [79]. With integrated couplers, the even mode impedance is limited by the smallest manufacturable line width as well as the substrate height. A Marchand type balun is chosen in this work since it is more tolerant to lower even mode impedances [79]. The classical design of a Marchand Balun was proposed by Nathan Marchand in 1944 [80] for coaxial transmission lines. It consists of an open ended transmission line with a length of $\lambda/2$ and two shorted quarter-wavelength lines, coupled to the first transmission line which provide two output signals, ideally 180° out of phase. The realized planar balun is based on this circuit and realized in the first metal layer only (see figure 4.15). In contrast to the second, thicker galvanic metal, the first metal layer allows a very narrow line spacing of only 2 μm while it is 10 μm in the second metal layer.

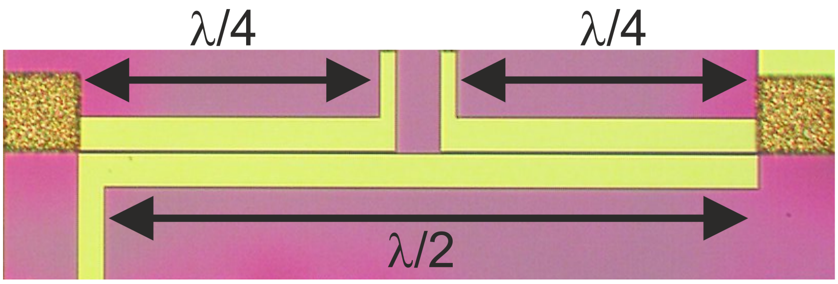

Fig. 4.15: Chip photograph of the 94 GHz Marchand balun. The $\lambda/2$ line has a length of 450 μm.

The design of the Marchand balun is aimed at balanced and broadband operation as well as low insertion loss around 94 GHz. These goals have to be achieved with respect to the MMIC technology and the according design rules. Since the length of the transmission lines are fixed at $\lambda/2$ and $\lambda/4$ by the circuit topology, the line width and the slot width are the two main design parameters.
The slot width should be as small as possible to achieve strong coupling between the lines for low insertion loss. According to [81], the coupling coefficient (k) equals:

$$k = \frac{r-1}{r+1} \tag{4.15}$$

where r represents the even mode and odd mode impedance ratio:

$$r = \frac{Z_e}{Z_o} \tag{4.16}$$

As a result, perfect coupling requires a large ratio between the even mode and the odd mode impedance. The calculated even and odd mode impedances for coupled microstrip lines in figure 4.9 would lead to a line width and slot width as small as possible (top left corner). On the other hand, the characteristic line impedance (Z_L) is related to the even mode and odd mode impedances as well [81]:

$$Z_L = \sqrt{Z_e \cdot Z_o} \tag{4.17}$$

Based on equation 4.17, there is a pair of even mode and odd mode impedances which match the line impedance to the 50 Ω input impedance. The line of corresponding even mode and odd mode impedance pairs is shown in figure 4.16. The design trade off is therefore coupling performance and impedance matching. The final dimensions have been evaluated using the Momentum simulator from Agilent and marked with a red dot in

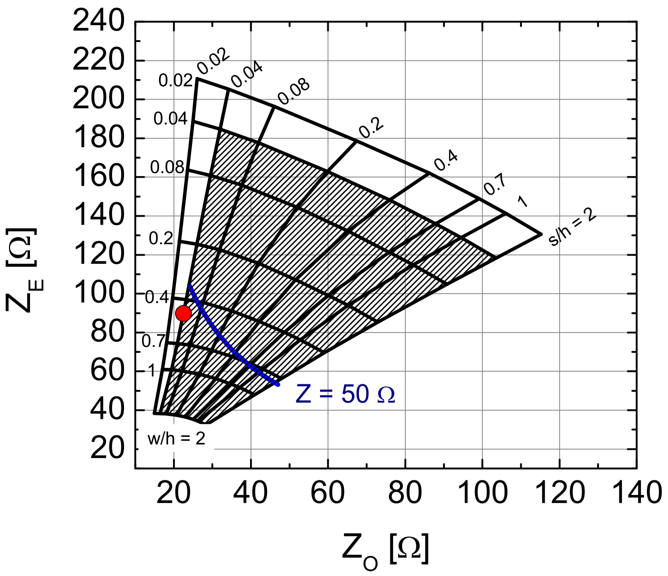

Fig. 4.16: Calculated even and odd mode impedances of coupled microstrip lines realized in the first metal layer only as shown in figure 4.9 and the pairs of even mode and odd mode impedances for a characteristic impedance of 50 Ω. The red dot indicates the final dimensions determined using electromagnetic field simulations.

figure 4.16. The lines are 22 µm wide and separated by a 2 µm slot which is the smallest gap allowed by the design rules.

Through substrate vias have been used to ground the ends of the quarter-wavelength lines. The simulated and measured S-parameters of the Marchand balun are shown in figure 4.17.

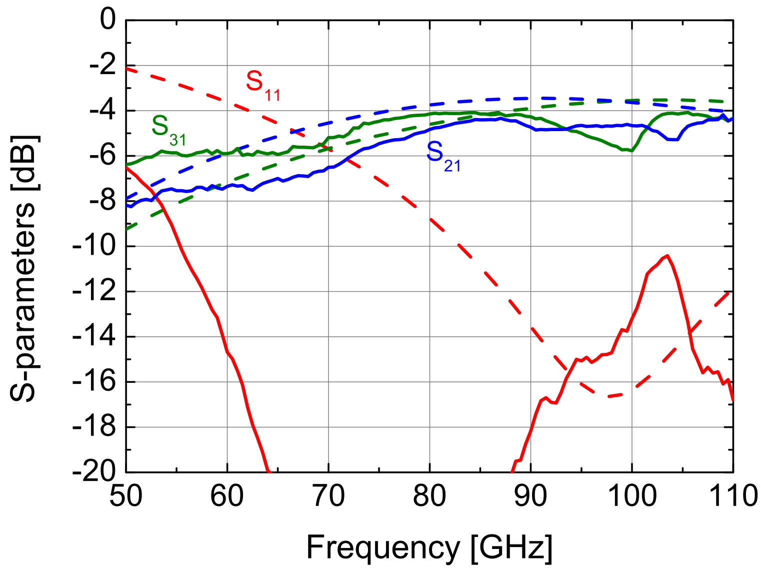

Fig. 4.17: Measured S-parameters of the Marchand balun.

Compared to the simulation, the measurement results show a down shift of the port coupling and especially the port matching to a center frequency of approximately 80 GHz. A possible reason for this frequency shift compared to the simulation could

be the insufficient modeling of the vias used to form a RF short at the end of the quarter-wavelength transmission lines. The via holes extend the electrical length of the transmission lines which would explain the frequency shift in the measurements.
Ideally, the output signals would be 180° out of phase but the phase difference of the Marchand balun is frequency dependent. The Δ phase between the output ports is therefore just as important as the coupling of the balun. Figure 4.18 shows the measured and simulated phase difference between the output ports of the Marchand balun as a function of the frequency. Compared to the simulation, the phase difference is slightly lower (about 5° at 80 GHz). The measured Δ phase stays between 170° and 165° in the frequency range from 68 GHz to 97 GHz and shows also a down shift towards 80 GHz.

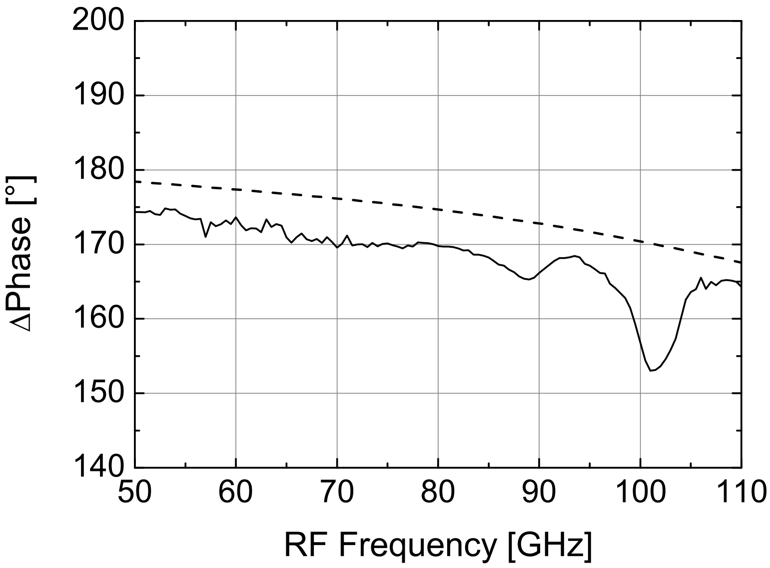

Fig. 4.18: Measured phase difference of the Marchand balun as a function of the input frequency.

4.1.3 Discussion

The design and manufacturing of integrated couplers and hybrids becomes a challenge at frequencies of several 100 GHz. Although the required chip area decreases, unwanted effects like modes in the semiconductor substrate play an increasing role and must be taken into account. The EM simulations of the presented Wilkinson divider and Lange coupler show the wave propagation through the GaAs substrate and emphasizes the important role of the through substrate vias. Beside the unwanted substrate modes, the increasing losses are a great challenge at higher frequencies. The smaller lines and the increasing losses are the limiting factor when it comes to mmW and sub-mmW coupling structures.
Table 4.1 summarizes the performance of the realized couplers and hybrids and proves the ability to realize integrated couplers even at high mmW frequencies using the Fraunhofer IAF mHEMT process. Compared to the Lange couplers, the branch-line coupler requires more chip area but is also outperformed with respect to insertion loss and, above all, operational bandwidth. The presented 240 GHz Lange coupler combines low

loss with wideband operation and phase accuracy and is best suited to realize balanced and I/Q mixers above 200 GHz.

f_c [GHz]	Type	Coupling Ratio [dB]	Insertion Loss [dB]	BW [GHz]	Rel. BW [%]	Ref.
170	Lange	3	0.7	70[1]	51.8	2009 [14, 15]
180	Branch-line	3	1	60	33.3	2006 [16]
210	Wilkinson	3	1	80	38.1	This work
210	Branch-line	3	3.3	30	14.3	This work
210	Lange	3	1.4	89.2	42.4	This work
220	Coupled line	3	0.6[2]	>80[2]	>36.4[2]	2012 [17]
240	Lange	3	0.87	90.6	37.7	This work
320	Tandem	3	1.2	100	37.03	2010 [18]

[1]based on S_{21} only
[2]simulated

Table 4.1: Comparison of the realized couplers and other reported mmW couplers above 100 GHz.

4.2 Active mmW Mixers

The advantage of active mixer circuits compared to passive mixers (e.g. resistive mixers) is the lower conversion loss or even gain. This is basically achieved by biasing the mixing transistor in a different operating point where the device possesses transconductance.
In the course of this work, different active mixer topologies have been examined:

- Subharmonically Pumped Active FET Mixer at 200 GHz.
- Gilbert Cell mixer at 77 GHz.

4.2.1 Subharmonically Pumped Active FET Mixer at 200 GHz

Subharmonic mixers which have their LO at half of the RF frequency are preferred in many applications due to the easier LO generation as well as the typically higher LO to RF isolation. An active subharmonic mixer combines the advantage of an easier LO generation with the low conversion loss of an active circuit. The subharmonically pumped active FET mixer is a mixture of a dual gate and a drain mixer topology, fabricated in the Fraunhofer IAF 50 nm technology.
A schematic of the circuit is shown in figure 4.19. Both input signals are applied to the gates of two cascaded FETs, usually called a dual gate approach. The difference in this work is that the IF is not tapped at the drain of the upper transistor but instead at the connection between the source and drain of the dual gate stage.

The RF and the LO signals are applied and matched to the transistors T2 and T1, respectively. A $\lambda/4$ transmission line makes a short to open transformation at the RF and LO frequencies to the gate bias. The transmission line TL1 at the drain of T1 makes a short to open transformation at $2\times f_{LO}$. The resistors R_1, R_2 and R_3 are used to protect

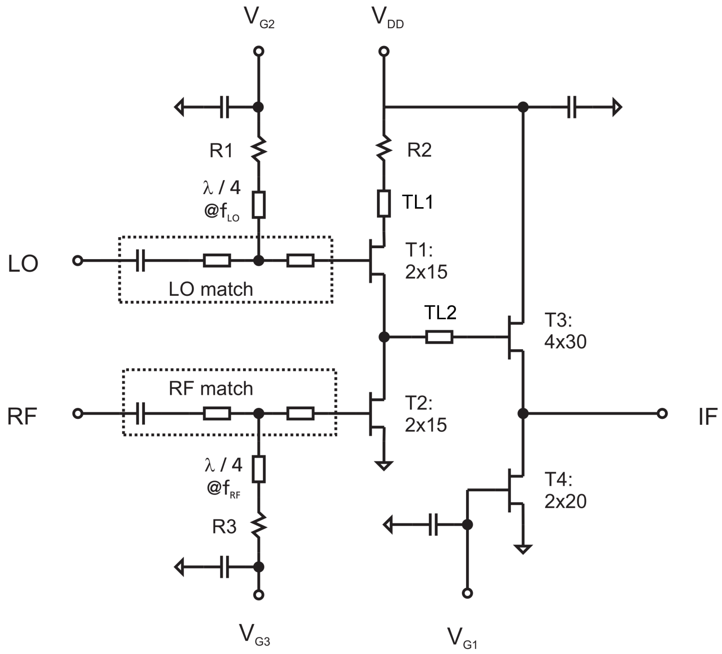

Fig. 4.19: Schematic of the active drain mixer.

the FETs from over currents in the drains and gates during circuit start up and have only small values of 10 Ω (R1, R3) and 5 Ω (R2).
The operating points of the transistors T1 and T2 are set according to the operating points of the dual gate mixer in section 2.2.3.1. Figure 4.20 shows the simulated dynamic I/V curves of the transistors for a LO amplitude of 2 dBm. Transistor T1 is biased in the active region and varies the current through transistor T2 depending on the LO voltage. To achieve the subharmonic operation, T1 needs to be operated in class B with a duty cycle of 25 %. As could be seen from the dynamic I/V curves, its quiescent current as well as the quiescent current through T2 is close to zero (class B). Transistor T2 operates as a drain mixer and performs the frequency conversion by altering between linear and saturated region. Since the frequency conversion occurs mainly in T2, the IF frequency can either be tapped directly at its drain or at the drain of T1. However, loading the drain of T2 directly with the IF impedance (typically 50 Ω) would lead to a significantly lower voltage swing across T2 and hence reduce the conversion gain. To overcome this problem, the source follower T3 acts as a buffer amplifier with a high input impedance and a low output resistance (approx. $1/g_m$ at the IF frequency).

In case the IF would be tapped at the drain of T1 as shown in [82], a current to voltage conversion must be made (e.g. using resistor R2) to generate the desired voltage swing at the input of the source follower. This requires the resistor R2 to be in the range of several hundred Ohms, depending on the current through T1/T2. Tapping the IF at the drain of T2 does not require an additional current to voltage conversion and may save the power loss in the resistor R2 by sacrificing the additional amplification of the IF signal in the common gate transistor T1.
Compared to [82], the achieved conversion gain is 3 dB higher and requires 10 dB less LO power which is probably mainly caused by the smaller gate length and higher cutoff

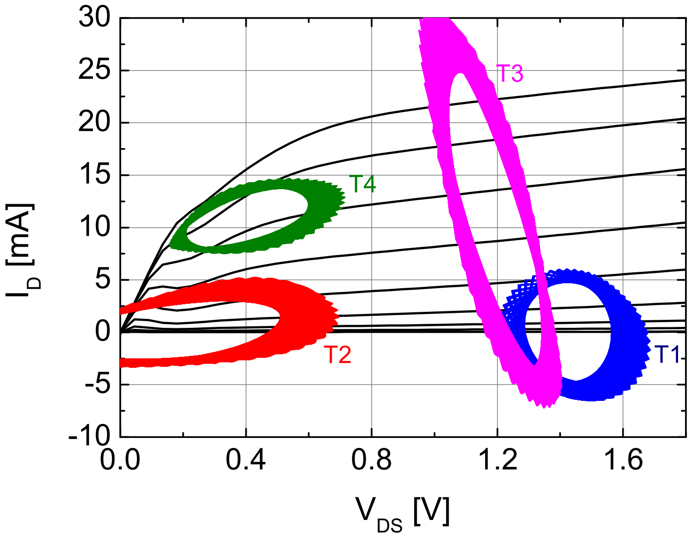

Fig. 4.20: Simulated I/V characteristics of the different transistors with a LO power level of 8 dBm and a RF input power of -25 dBm. For illustration, the output characteristic of a 2×15 µm transistor is plotted beneath the dynamic I/V curves.

frequencies of the employed 50 nm technology compared to the 100 nm technology used in [82]. Figure 4.21 shows a chip photograph of the realized subharmonically pumped active mixer.

All measurements have been performed in a down converter configuration. The LO has been generated using a W-band source module from HP and the RF signal has been supplied by an Oleson G-band source module. The mixer draws a drain current of 14 mA at a supply voltage of 1.6 V which leads to a DC power consumption of 22.4 mW. Figure 4.22 shows the measured conversion gain versus the applied LO power for a fixed

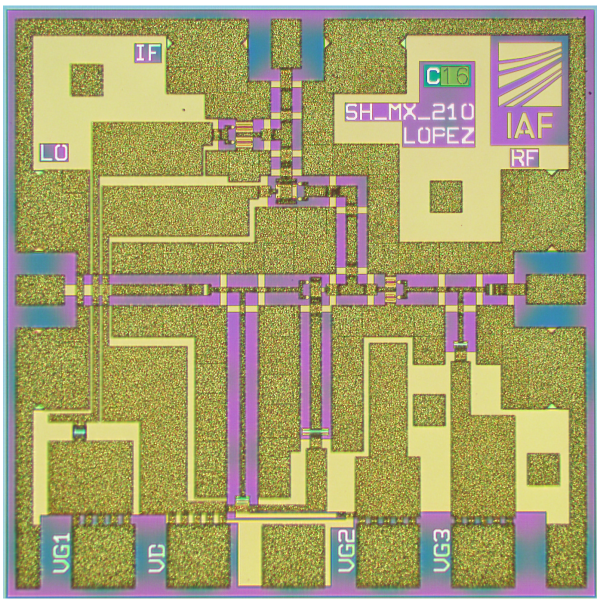

Fig. 4.21: Chip photograph of the subharmonically pumped active FET mixer with a chip size of 1×1 mm^2.

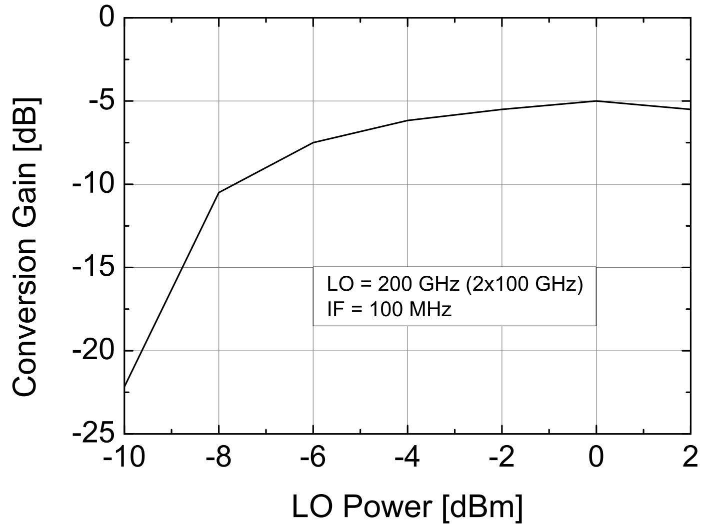

Fig. 4.22: Conversion gain vs. applied LO power of the active drain mixer. The bias conditions are: V_D=1.6 V, V_{G1}=0.1 V, V_{G2}=-0.1 V, V_{G3}=-0.25 V, I_D=14 mA.

IF frequency of 100 MHz. A minimum conversion loss of 5.3 dB is achieved with 0 dBm LO power.

In most communication systems, a fixed LO frequency is used in the receiver as well as the transmitter. The transmission of high data rate signals requires a large RF and IF bandwidth at a fixed LO frequency. Figure 4.23 shows the measured conversion gain of both, the upper and the lower side band of the mixer with a fixed LO at 100 GHz which is inherently doubled to 200 GHz in the mixer. The mixer achieves a 3 dB IF bandwidth of more than ±1 GHz at a LO power level of 2 dBm.

Figure 4.24 shows the measured conversion gain versus the RF frequency when the IF frequency is kept constantly at 100 MHz. In this configuration, the mixer features an RF bandwidth of approximately 8 GHz which is significantly more compared to the IF bandwidth with a fixed LO from figure 4.23. This is a strong indicator that the source

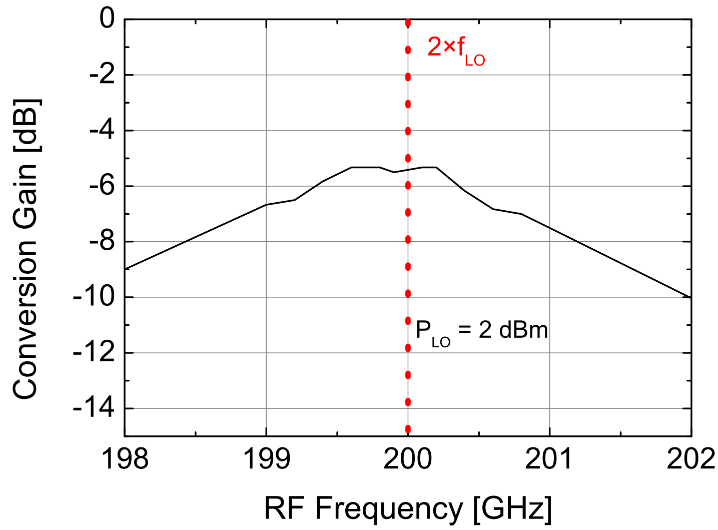

Fig. 4.23: Conversion gain of both sidebands around 200 GHz of the active drain mixer.

follower is not supporting a large IF bandwidth, although other possible reasons could be a narrow band matching at the RF or a interstage matching issue between the common gate and the common drain transistor. At least the former is very unlikely as this would also limit the bandwidth in the fixed IF scenario. The dip between 202 - 206 GHz is most likely caused by a on-chip resonance in the LO or RF path. The inductance of the transmission lines can form, together with the gate capacitances, a tank circuit with a resonance frequency in the range of the RF or LO frequencies. According to the used models, the inductance of the employed 70 Ω CPWG lines is for example, 62 pH/100 µm at 100 GHz. In a first approximation, it would therefore take about 40.8 fF of total parallel capacitance for a 100 µm long line to resonate at 100 GHz.

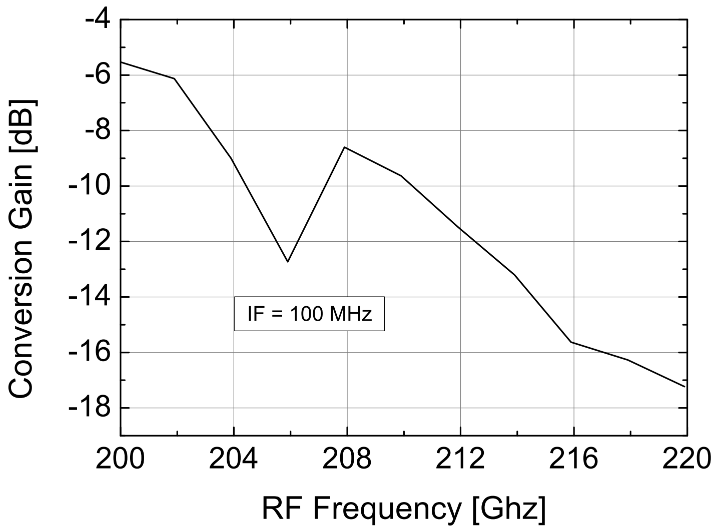

Fig. 4.24: Conversion gain of the active drain mixer vs. the RF frequency of the active drain mixer.

The active drain mixer is a subharmonic single-ended design. Double balanced active mixers show a superior port isolation and higher conversion gain compared to single-ended designs. As described in chapter 2.2.3, the Gilbert cell mixer is a very popular double balanced active mixer architecture which can be used up to frequencies in the range of $\frac{f_t}{3}$. A mHEMT based Gilbert cell mixer around 77 GHz is presented in the following section.

4.2.2 Gilbert Cell Mixer

In 2003, the Federal Communications Commission (FCC) issued a ruling that the E-band (71 to 76 GHz, 81 to 86 GHz and 92 to 95 GHz) is available for short range, high capacity communication [83]. Afterwards, the interest of industrial and scientific research groups increased to provide circuits and systems for mmW communication in this frequency range. The realized Gilbert cell mixer around 77 GHz operates in this frequency range and is based on the Gilbert cell described in section 2.2.3.2. A schematic of the realized circuit is shown in figure 4.25.

The outputs of the differential amplifiers are combined and the IF outputs are buffered by two source followers. The switching transistors have an equal size of 2×15 µm. In a classical differential amplifier, the transistor pair T3 would have two times the size of

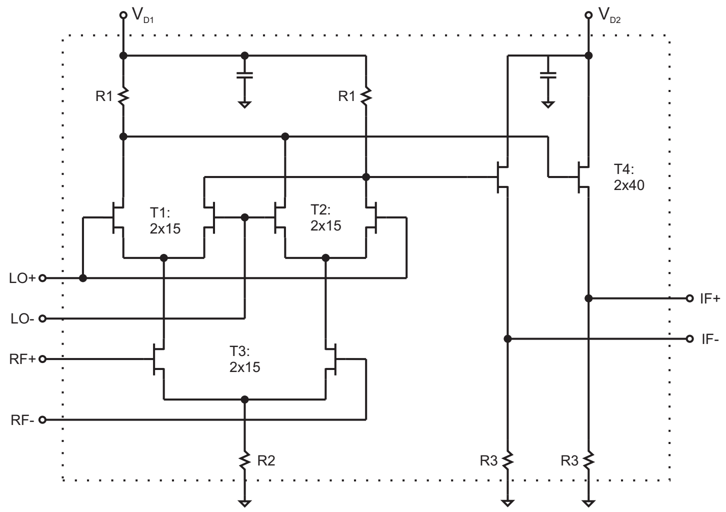

Fig. 4.25: Simplified schematic of the realized Gilbert cell mixer.

the transistor pairs T1 and T2 to handle twice the bias current. When the Gilbert cell is used as a frequency mixer, the large LO signal switches the current between the two transistors of pair T1 or pair T2. Since one transistor of the switch pairs T1 and T2 is always off, T3 can be of equal size as the transistors in T1 and T2.
A photograph of the 77 GHz Gilbert cell mixer, fabricated in the Fraunhofer IAF 100 nm technology, is shown in Figure 4.26. The baluns at the RF and LO ports are clearly visible and the mixer core has a size of only approximately 150×100 µm. This very compact layout allows the connections between the circuit elements to be significantly shorter than the wave length. The very short connections could so be treated as lumped elements and the operation frequency is mainly determined by the characteristics of the used baluns.

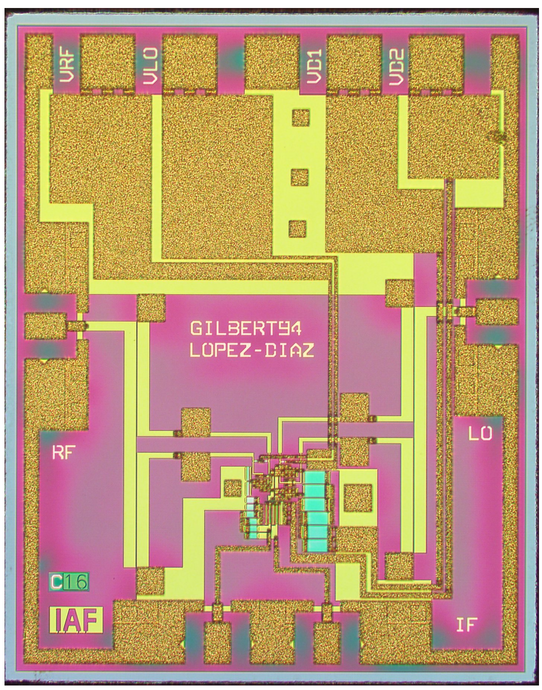

Fig. 4.26: Chip Photograph of the realized Gilbert cell mixer. Chip size is 1 × 1.25 mm^2.

Since all ports of the Gilbert cell require differential signals, baluns are needed to convert the single-ended LO and RF signals to differential ones. The planar Marchand balun, described in section 4.1.2.4, was designed for the on-chip integration with the Gilbert cell mixer. The differential IF signal can be converted to a single ended signal by an off-chip balun. To evaluate the performance of the mixer core, the baluns have to be excluded.

The conversion gain of the Gilbert cell mixer has been measured using a down conversion setup. An additional LO amplifier has been used after the W-Band source module to achieve on-wafer power levels of up to 10 dBm and ensure saturation of the mixer. Figure 4.27a shows the measured conversion gain of the Gilbert cell mixer as a function of the RF frequency at a fixed LO frequency. After subtraction of the losses in the balun, the de-embedded conversion gain is included as dashed line. The power loss in the balun over the RF frequency has been determined by a harmonic balance simulation based on the measured S-parameters of the Marchand balun. The balanced output signal has been combined by an ideal balun and terminated in a 50 Ω load. The difference of the input power and the output power at the termination resistor equals the power loss in the coupler for a 50 Ω load. Due to the lack of a broadband IF balun, the differential IF power has been calculated based on the individual power levels at the IF+ and IF- port. A maximum conversion gain of 8.2 dB was measured at an RF frequency of 76.1 GHz. After subtracting the power loss in the RF balun at 76 GHz (6.4 dB) the mixer core achieves a maximum conversion gain of 14.6 dB at 76 GHz.

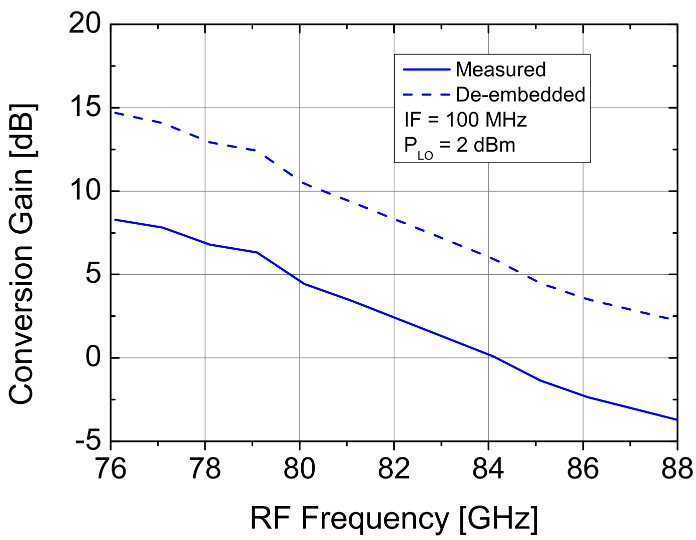

Fig. 4.27: Measured (solid) and de-embeeded (dashed) conversion Gain of the 77 GHz Gilbert cell mixer versus the RF frequency at 2 dBm LO power and 100 MHz IF frequency.

Due to the frequency shift, the measurement of the conversion gain versus the applied LO power was made at a fixed RF and LO frequency of 77.1 GHz and 77 GHz respectively (IF = 100 MHz). The Gilbert cell mixer achieves a maximum conversion gain of more than 12 dB for a LO power level of 8 dBm, see figure 4.28. After excluding the losses in the RF balun, the mixer core achieves a maximum conversion gain of 18.3 dB (dashed line).

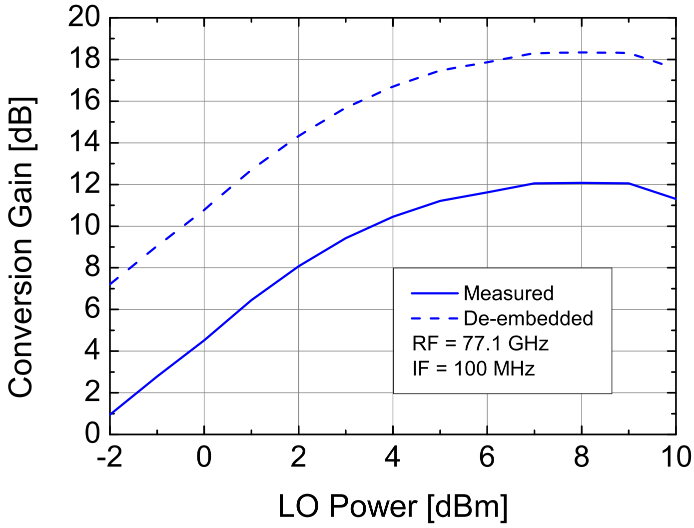

Fig. 4.28: Measured (solid) and de-embedded (dashed) conversion Gain of the 77 GHz Gilbert cell mixer versus the applied LO power at 77.1 GHz and a fixed IF frequency of 100 MHz.

The IF bandwidth of the mixer has been measured around 88 GHz which was the highest achievable frequency with the employed LO amplifier. A constant LO power level of 2 dBm was applied to the mixer while the RF frequency was swept from 88.01 GHz to 108 GHz (upper sideband). As shown in figure 4.29, the mixer features an IF bandwidth of 5 GHz.

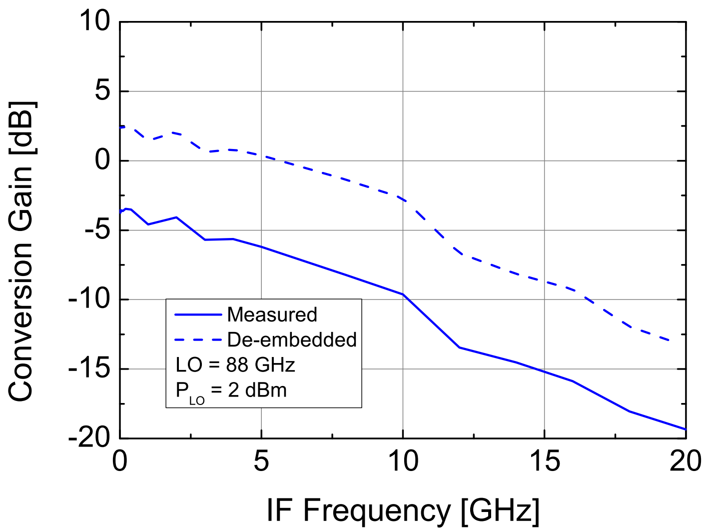

Fig. 4.29: Measured (solid) and de-embedded (dashed) conversion Gain of the 77 GHz Gilbert cell mixer versus the IF frequency at a fixed LO frequency of 88 GHz with an amplitude of 2 dBm.

Although the center frequency of the mixer is limited to frequencies around 80 GHz by the employed Marchand balun, it proves the ability of the Fraunhofer IAF mHEMT technology to realize differential circuits. Compared to lower frequencies, there are less reported active mixer circuits in the upper mmW frequency range. The following discussion summarizes the results of the presented active mixers and compares them to the reported state of the art.

4.2.3 Discussion

The main advantages of active mixers over passive mixers are the lower conversion loss or even conversion gain as well as the usually lower LO drive requirements. With respect to wireless data transmission, a mixer providing conversion gain may relax the requirements on the receive chain (e.g. LNA gain) significantly. However, this work is focused on ultra broadband wireless communication which requires wideband RF and IF performance.
Several active solid state mixers have been reported using different semiconductor technologies like CMOS [25, 84], SiGe [85, 86] or HEMTs [82, 87]. A comparison of the presented active mixers to other reported active mixers in this frequency range is shown in table 4.2. The presented results show the dominance of compound semiconductors in the upper mmW frequency range. But already at 77 GHz, standard CMOS technology shows remarkable performance [84]. For circuits around 150 GHz, silicon on insulator (SOI) technologies show reasonable results [25] but still lag behind those achieved with compound semiconductor technologies in this frequency range.
The two active mixers, presented in this chapter extend the state of the art in two ways. The subharmonically pumped active FET mixer at 200 GHz is the first dual gate mixer at 200 GHz which extracts the IF signal between the common source and the common gate and reduces the power consumption by 37 % compared to former reported dual gate mixers like [82].
The Gilbert cell mixer at 77 GHz is the first Gilbert cell mixer realized in a mHEMT technology which provides more than 12 dB conversion gain. In addition, it features a wide IF bandwidth of 8 GHz which equals more than 10 % relative bandwidth around 77 GHz.

Frequency [GHz]	f_{LO} [GHz]	Conversion Gain [dB]	IF-BW [GHz]	Technology	DC Power [mW]	Year and Ref
77	38	>8	-	65 nm CMOS	1	2013 [84]
77	77	>22	0.5	SiGe	300	2004 [85]
77	77	>11	-	SiGe	412.5	2006 [86]
77	77	>12	8	mHEMT	179.2	This Work
158.7	158.7	> -5	8	45 nm CMOS	9.9	2011 [25]
220	110	+2[1]	10	SiGe	72	2011 [21]
210	105	-8.5	2	mHEMT	36	2007 [82]
210	210	2.8	3	mHEMT	74	2008 [87]
210	105	-5	1	mHEMT	22.4	this Work

[1] Conversion gain of the entire receiver minus LNA gain.

Table 4.2: Comparison of reported active mixers in the mmW frequency range.

4.3 Resistive Mixer Cells for Broadband Applications above 200 GHz

As discussed in section 2.2.2.1, resistive mixers based on mHEMT devices are able to achieve very broadband operation when they are combined with broadband passive networks. Theoretically, they should be able to outperform active mixers with respect to the operational bandwidth. To evaluate the performance of different mixer topologies with respect to conversion gain and bandwidth, several resistive mixers have been designed and fabricated. Although the matching networks differ between the different realized circuits, the topology of the employed mixer cell is basically the one shown in figure 4.30. It consists of an mHEMT in common source configuration with the LO signal applied to the gate electrode. LO matching is achieved using the DC bias network on the gate. A serial capacitor and the transmission lines are used to transform the gate impedance to the 50 Ω input impedance at the LO port. The RF branch is matched in the same manner using a serial capacitor as well as transmission lines to and from the IF filter capacitor to transform the drain resistance into 50 Ω. Integration of an IF matching network on the MMIC is always a tradeoff between large IF bandwidth and port matching. At the low IF frequencies, transmission line transformations are hardly possible and the impedance is basically the effective channel resistance R_{ds} which heavily depends on the applied gate bias voltage and LO power. As shown in figure 2.21, the simulated drain impedance at 200 GHz has an absolute value of 47.6 Ω for a gate-source voltage of -0.1 V while it is already 99.6 Ω for -0.3 V. To increase the IF matching at lower frequencies, the capacitor at the IF port needs to be increased which limits the IF bandwidth at high frequencies.RF to IF isolation is achieved by a short to open transformation using the $\lambda/4$ transmission line to the IF capacitor.

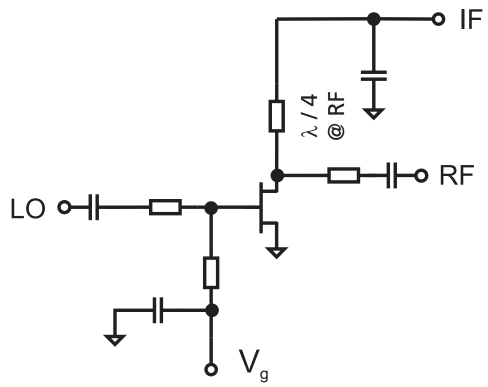

Fig. 4.30: Principal schematic of a resistive mixer cell.

4.3.1 Subharmonic I/Q Mixer at 210 GHz

To realize an I/Q mixer, the quadrature hybrids from section 4.1.2 have been used. The advantages and disadvantages of using either the presented Lange or branch-line coupler to realize a quadrature mixer are investigated. Two mixer circuits have been fabricated which employ either the Lange coupler or the branch-line coupler [101]. Both mixers are designed to operate around 210 GHz with a subharmonic LO at 105 GHz. The focus was set to the comparison of the difference between the Lange and the branch-line coupler with respect to conversion gain and I/Q imbalance. The IF bandwidth was, in this case, not of special interest. A standard pad, without a 50 Ω impedance, was used on both chips for the IF signal which limits the practical bandwidth to several GHz.

4.3.1.1 Branch-line Coupler I/Q Mixer

A chip photograph of the realized mixer employing the branch-line coupler is shown in figure 4.31. The branch-line coupler is visible on the right side of the chip. The open stubs are used to match the input impedance at the transistor's drain to the branch-line coupler.

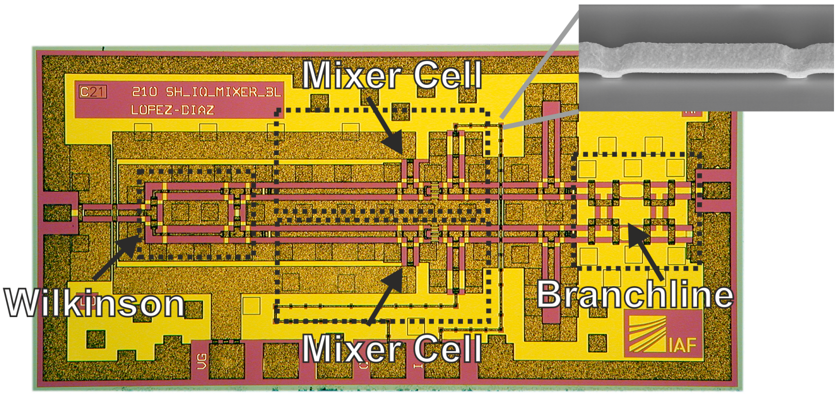

Fig. 4.31: Chip photograph of the I/Q mixer using a branch-line coupler. The chip size is 2×1 mm^2.

The IF signals are routed to the pads at the bottom of the chip by posted air microstrip type lines (see inlay in figure 4.31). Those microstrip lines are realized by using long air-bridges over the first metal layer which acts as a ground plane [88]. The air-bridges are supported by small insulated metal posts which appear as small dots on the I/Q transmission lines on the chip photograph. To achieve a characteristic impedance of 50 Ω, an air-bridge width of 5 μm for a height of 1.6 μm over the first metal has been calculated. The measured conversion gain at the IF-Q port versus the RF frequency is plotted in figure 4.32. A constant LO power of 2 dBm and a fixed IF frequency of 100 MHz have been used during the measurements. The operating frequency is centered around 194 GHz and the lowest conversion loss is achieved in the frequency range from 186 to 202 GHz. Although the coupling of the branch-line coupler is also decreasing above 200 GHz, it cannot explain the drop of the conversion gain above 202 GHz. This is most probably a combination of the coupler performance and a mismatch between the mixer and the coupler.

Figure 4.33 shows the measured conversion gain versus the applied LO power of the I/Q mixer at a constant RF frequency of 200 GHz. The large deviation between the I and Q ports is caused by the under-coupling of the branch-line coupler at 200 GHz (cf. figure 4.7).

The mixer achieves a maximum conversion gain of -19.3 dB at the IF-Q output with 2 dBm LO power. The I/Q amplitude imbalance gets larger with increasing LO power and reaches almost 5 dB at 2 dBm LO power. There are two reasons for this behavior.

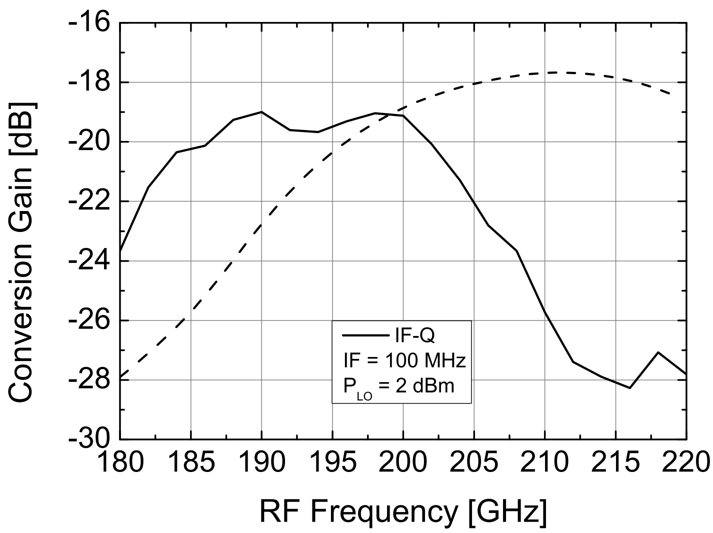

Fig. 4.32: Measured (solid) and simulated (dashed) conversion gain versus the RF frequency of the mixer with branch-line coupler.

The increasing LO power level entails a shift in the gate bias voltage of the mixing FET which leads to a different drain impedance seen by the branch-line coupler which could cause a greater imbalance between the two coupled ports. The simulated drain impedance at 210 GHz of the mixing FET over a power sweep of the LO from -10 to +2 dBm is shown in figure 4.34. For larger amplitudes of the LO, the drain impedance increases and might lead to an increased amplitude imbalance of the coupler. The other reason is a mismatch between the two mixing transistors which may have a different conversion gain as well as a different RF input impedance seen by the branch-line coupler which may also lead to a greater I/Q amplitude imbalance.

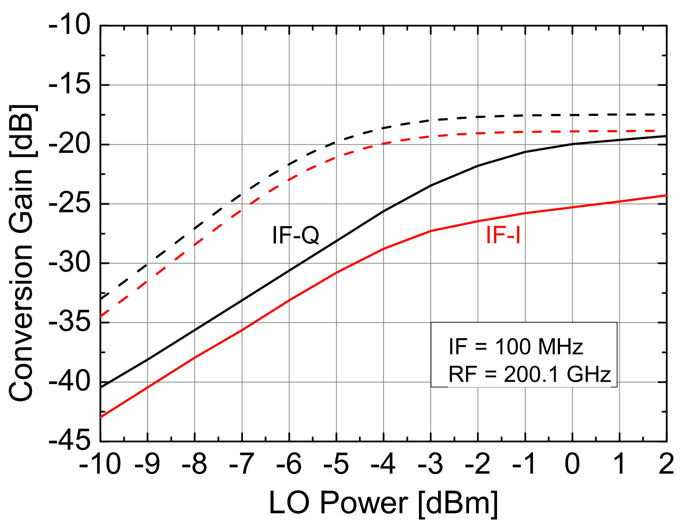

Fig. 4.33: Measured (solid) and simulated (dashed) conversion gain versus the applied LO power of the I/Q mixer with branch-line coupler.

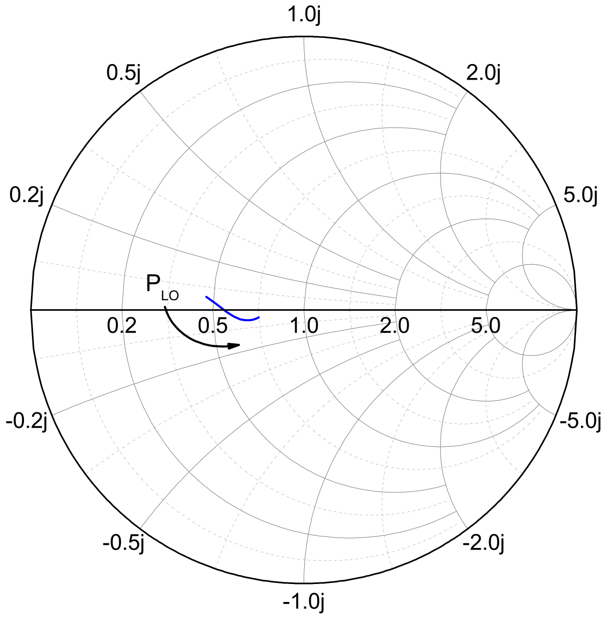

Fig. 4.34: Simulated impedance at the transistor's drain as a function of the LO power from -10 to 2 dBm at 210 GHz.

The port matching of the LO and RF port is plotted in figure 4.35. The RF port shows a return loss of more than 25 dB around 205 GHz. This significantly better matching of the RF port compared to the LO port is caused by the branch-line coupler at the RF terminal which is usually matched very well around its center frequency.

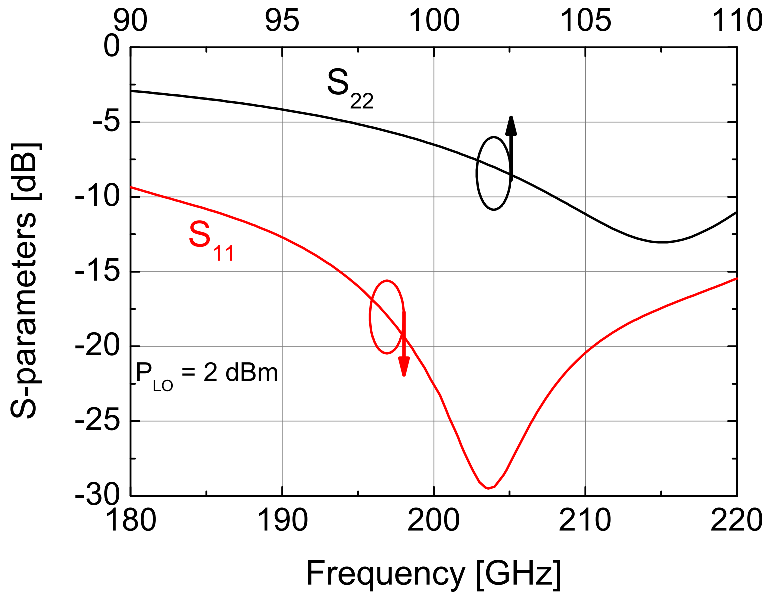

Fig. 4.35: Simulated S_{11} (RF port) and S_{22} (LO port) as a function of the LO and RF frequency for a LO power level of 2 dBm

One major advantage of the subharmonic approach is the improved LO to RF isolation due to the different signal frequencies. Table 4.3 summarizes the simulated port to port isolation. The subharmonic mixer achieves almost 24 dB LO to RF isolation at the doubled LO frequency although it is a single ended topology.

Port-Port	RF-LO	RF-IF	LO-RF	LO-RF$_{@2f_{LO}}$	LO-IF$_{@2f_{LO}}$
Isolation [dB]	25.8	43.6	30.6	23.6	57.7

Table 4.3: Simulated port isolation at 200.1 GHz (LO = 100 GHz) and 2 dBm LO power.

4.3.1.2 Lange Coupler I/Q Mixer

A second mixer has been fabricated using the Lange coupler instead of the branch-line coupler. Employing the Lange coupler promises a more broadband mixer design since the simulated and measured S-parameters of the Lange coupler (figure 4.11) show a larger coupling bandwidth compared to the branch-line coupler.
The basic mixer cell has not been changed compared to the design from section 4.3.1.1. Only the matching network at the RF port of the mixer has been slightly adapted to match the non-ideal 50 Ω impedance of the Lange coupler. Figure 4.36 shows a photograph of the MMIC with the Lange coupler at the RF port (right side of the chip).

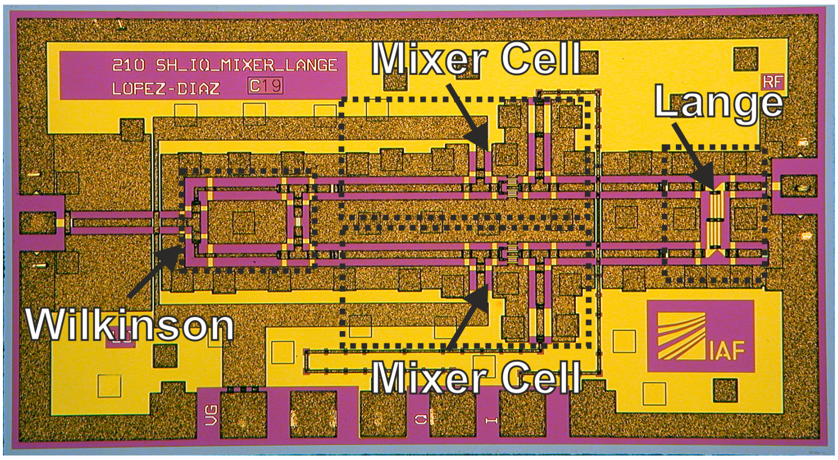

Fig. 4.36: Chip photograph of the realized balanced mixer. Chip size is 1.8 × 1 mm^2.

The measured conversion gain over the RF frequency with a fixed IF frequency of 100 MHz is shown in figure 4.37. Compared to the shape of the mixer using the branch-line coupler in figure 4.32, the mixer employing the Lange coupler is not shifted in the frequency and operates from 206 to 220 GHz. A minimum conversion loss of 18.4 dB is achieved at 214 GHz on the IF-Q port with a LO amplitude of 2 dBm.
Figure 4.38 shows the measured conversion gain of the subharmonic mixer comprising the Lange coupler over the applied LO power. The IF frequency was kept constant at 100 MHz during the measurement. Compared to the results using the branch-line coupler in figure 4.33, the I/Q imbalance is considerably lower. With 2 dBm LO power, the minimum conversion loss is 19.22 dB at the IF-Q port and 20.22 dB at the IF-I port.
The simulated port to port isolation of the subharmonic I/Q mixer using a Lange coupler are shown in table 4.4. The values are similar compared to the mixer using a branch-line coupler except the RF to LO isolation at the fundamental LO tone which is 12 dB higher

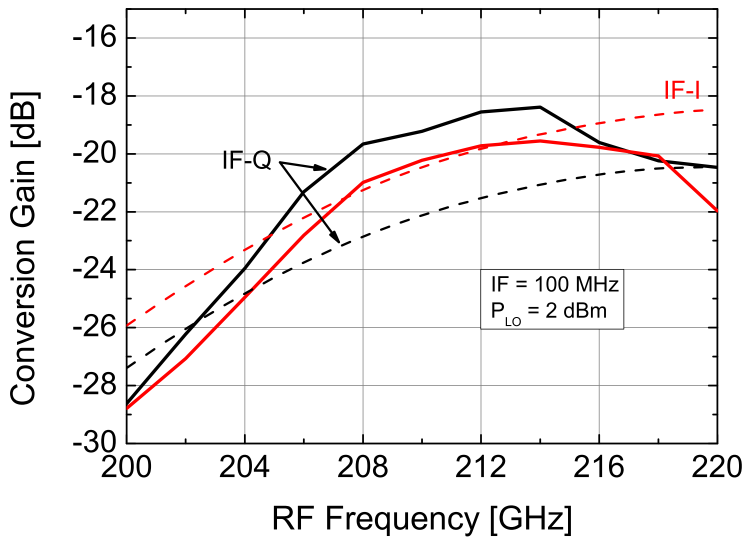

Fig. 4.37: Measured and simulated (dashed lines) conversion gain of the IF-I and IF-Q ports as a function of the RF frequency.

using the branch-line coupler. To increase the LO to RF isolation, a balanced architecture is needed. The following section covers the design of a single balanced resistive mixer at 210 GHz.

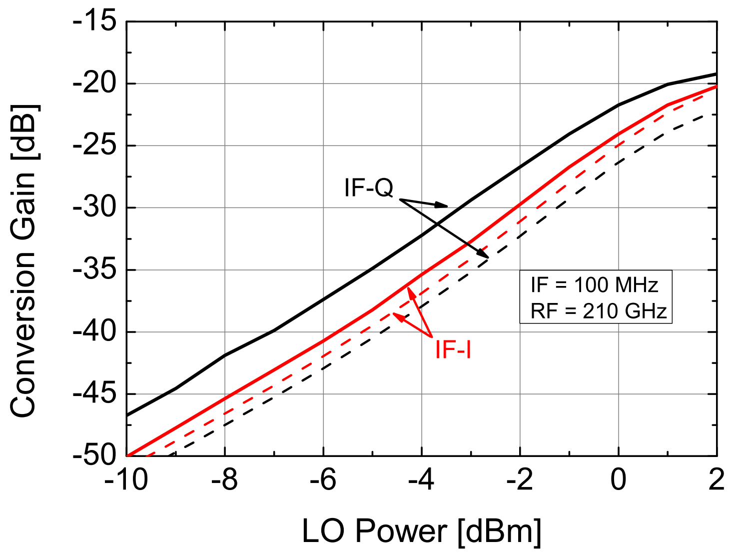

Fig. 4.38: Measured and simulated (dashed lines) conversion gain of the subharmonic I/Q mixer versus the applied LO power.

Port-Port	RF-LO	RF-IF	LO-RF	LO-RF$_{@2f_{LO}}$	LO-IF$_{@2f_{LO}}$
Isolation [dB]	20.2	47.8	18	24.7	56.1

Table 4.4: Simulated port isolation at 210 GHz (LO = 109.95 GHz) and 2 dBm LO power.

4.3.2 Balanced 210 GHz mixer with more than 50 GHz IF bandwidth

One major challenge in the design of mixers having a large IF bandwidth is the IF port matching over the entire frequency range. Bad matching causes standing waves and degrades the overall performance of the mixer. Usually, the IF port is matched using a low pass filter to separate the IF from the LO and the RF frequency. The low pass filter presents a virtual ground for the high RF and LO frequency while it provides matching at the lower IF frequency. When it comes to very high IF frequencies of several 10s of GHz, the filtering and matching becomes more and more difficult. Higher order filters would be a possible solution for this, but these filters require large area and are therefore not easy to integrate on a MMIC. Active filters using an IF amplifier could also be used but they are usually AC coupled and hence lose the information of the low frequency signals. Unfortunately, DC coupling is mandatory for some applications like Zero-IF mixers.
A possible solution to the matching problem is tapping the IF signal at the unused coupler port of a single balanced mixer architecture [102]. Figure 4.39 shows the simplified block diagram of the proposed architecture.
At lower IF frequencies, matching is achieved by the resistance of the transistor's channel at the specific gate bias voltage. As the IF frequency rises, the port matching of the coupler takes over and provides good matching up to several hundred GHz. Another advantage of this architecture is the inherent RF to IF isolation which equals the coupler's port isolation.

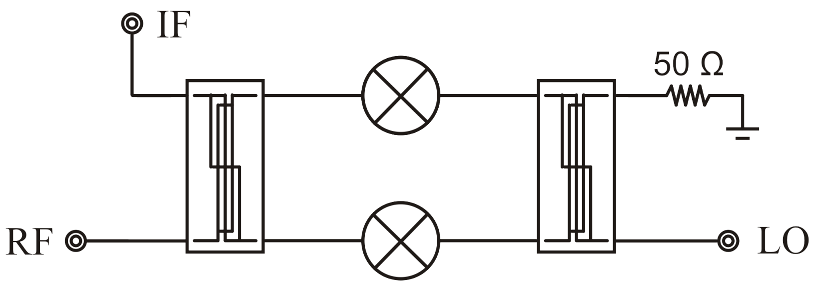

Fig. 4.39: Topology of the balanced mixer with the IF tap at the isolated coupler port.

A chip photograph of the realized mixer is shown in figure 4.40. The two Lange couplers at the RF and LO path are clearly distinguishable. The IF port is located at the top of the chip and connected to the isolated port of the Lange coupler.

The mixer has been characterized as a fundamental down-converter with a LO frequency located at 210 GHz. Figure 4.41 shows the measured conversion gain versus the IF frequency for different LO power levels. The RF frequency has been swept from 160 to 209.9 GHz while the LO frequency was constant at 210 GHz. A maximum conversion gain of -17 dB has been achieved at an IF frequency of 25 GHz and a LO power of 0 dBm. More LO power would certainly improve the conversion gain but there was no source available at 210 GHz which could deliver more than 2 dBm.

Some applications utilize DSB transmission and require therefore two times the IF bandwidth as RF bandwidth. To measure the conversion gain of the mixer for both

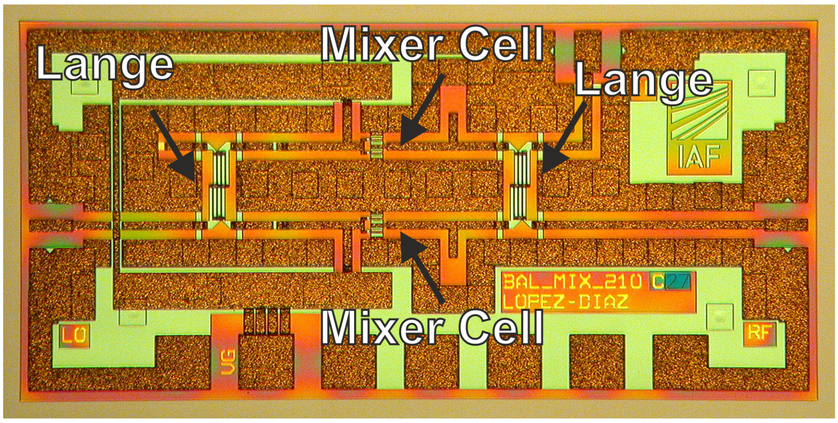

Fig. 4.40: Chip Photograph of the realized balanced mixer. Chip size is 1.5 × 0.75 mm^2

sidebands, the LO frequency was kept constant at 210 GHz while the RF frequency has been swept from 160 to 260 GHz using an Oleson G-Band Source Module for the LSB and a H-Band (220-325 GHz) extension module for the USB. The results with an LO power of 0 dBm are plotted in figure 4.42. The measured conversion gain stays within -16.4 and -21 dB in the entire frequency range.

To validate the IF port matching, the small signal S-parameter has been measured up to 50 GHz. The mixer has been biased and pumped with -2 dBm LO power during the measurement. Due to mechanical limitations at the probe station, the RF port was not driven by a RF source but terminated using a 50 Ω load.
Figure 4.43 shows the measured S_{11} at the IF port for different gate bias voltages. Apparently, the best matching is achieved with 0 V applied to the gate. The channel resistance is then close to 50 Ω which explains the good port matching.

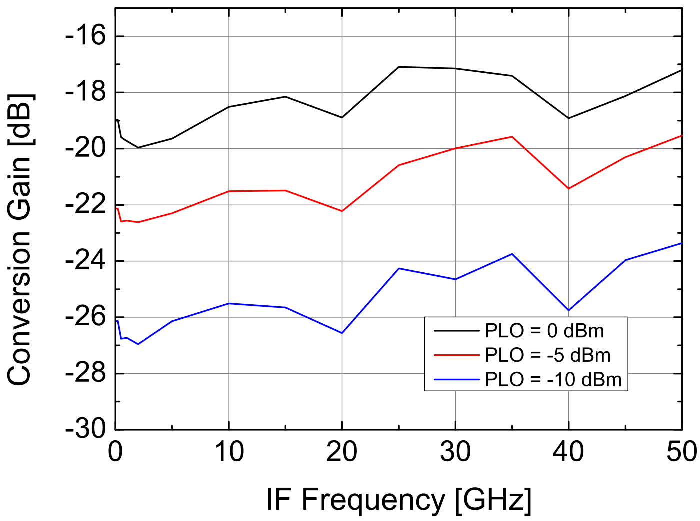

Fig. 4.41: Measured conversion gain of the balanced mixer versus the IF frequency of the LSB at three different LO amplitudes from -10 dBm to 0 dBm.

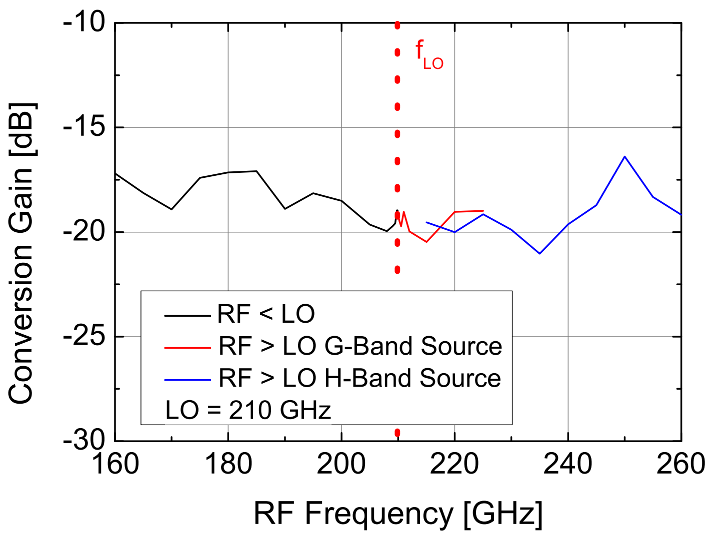

Fig. 4.42: Measured conversion gain of the balanced mixer versus the RF frequency using a fixed LO at 210 GHz.

The advantage of a single balanced mixer topology over a single-ended mixer is the higher LO-to-RF isolation which is heavily depending on the phase and amplitude matching of the employed coupler. Figure 4.44 shows the measured LO-to-RF isolation of the presented single-balanced mixer as a function of the LO frequency with a constant LO power level of 0 dBm. The isolation rises from 15 dB at 180 GHz to 26 dB at 218 GHz. The steep increase of the curve between 210 and 218 GHz is caused by the progression of the phase between the coupled ports of the employed Lange coupler (see figure 4.12) towards the ideal 90 degrees which is needed to cancel the LO signal at the RF port.

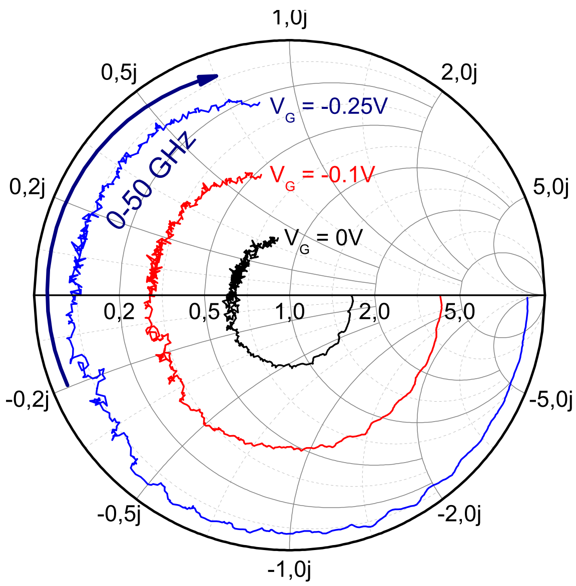

Fig. 4.43: S_{11} measured at the IF port of the balanced mixer for different gate voltages.

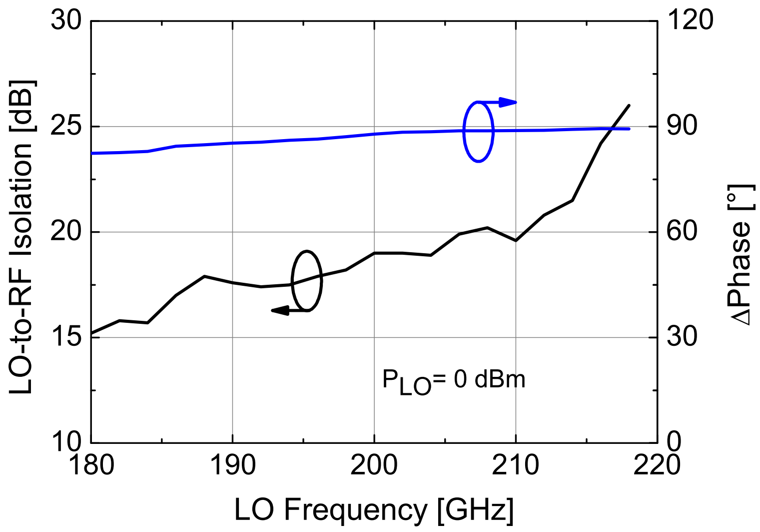

Fig. 4.44: Measured LO-to-RF isolation of the balanced mixer as a function of the LO frequency with a constant LO power level of 0 dBm.

4.3.3 Balanced Subharmonic Resistive Broadband Mixer

Superheterodyne receivers are widely used in modern radio architectures. But they reach their limits when it comes to transmit very broadband signals. In a superheterodyne receiver, the RF is converted to an IF and afterwards into baseband. To transmit a baseband signal of several tens of GHz, the IF conversion stage must have a correspondingly large bandwidth imposing stringent requirements on the separation of the RF, IF and baseband signals.

Direct conversion or zero-IF topologies are able to overcome this problem by using direct conversion from baseband to RF and vice versa. High millimeter-wave frequencies are able to provide very large absolute bandwidths (>100 GHz) which enable the transmission of very broadband baseband signals.

One major disadvantage of a direct conversion receiver is the signal leakage. Poor LO to RF isolation results in self-mixing at the mixer stage and a DC offset at the IF port which could possibly saturate the IF amplifier stages.

One advantage of subharmonic mixers is the inherent LO to RF isolation which exceeds the isolation of an unbalanced fundamental mixer. A superior LO isolation can be achieved by the combination of a subharmonic and a balanced design. Due to the fixed LO frequency in direct conversion scenarios, the balancing could be easily achieved by narrow band transmission line delays. Figure 4.45 illustrates the schematic of a resistive mixer cell, balanced using a delay line.

The chip photo of the realized balanced subharmonic resistive mixer is shown in figure 4.46. The coplanar delay line is clearly visible. The length of the delay line equals $\lambda/2$ at the fundamental LO frequency. The RF is mixed with the doubled LO frequency at the transistor's drain. To filter the IF from the RF and LO signal, an on-chip first order low pass filter is used. Due to the very large IF frequency of up to 40 GHz, the parallel capacitor has a relatively small value of a few pF. A drawback of this simple filtering is the bad matching at the IF port.

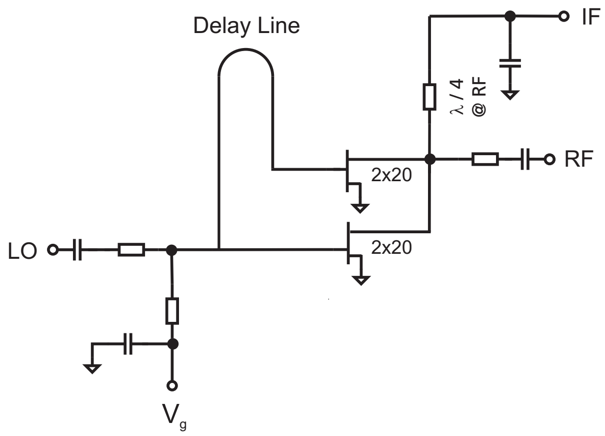

Fig. 4.45: Schematic of the subharmonic balanced mixer for 240 GHz.

To achieve good matching from DC up to 40 GHz, higher order filters have to be employed which require a lot of chip area. Off chip filter structures are able to improve the IF port matching but are not examined in this work.

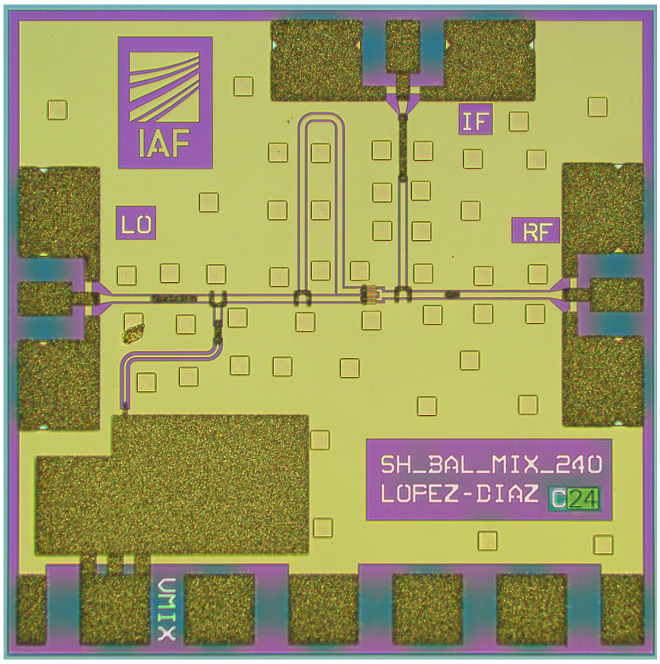

Fig. 4.46: Chip Photograph of the realized balanced mixer. Chip size is 1×1 mm^2.

The mixer is intended to be used in a up and down converter circuit and has been characterized in both modes of operation.

Down Converter

Figure 4.47 shows the measured conversion loss versus the applied LO power at a fixed IF frequency of 1 GHz and a LO frequency of 120 GHz, a minimum loss of 25.2 dB has been achieved for an LO power of 6 dBm.

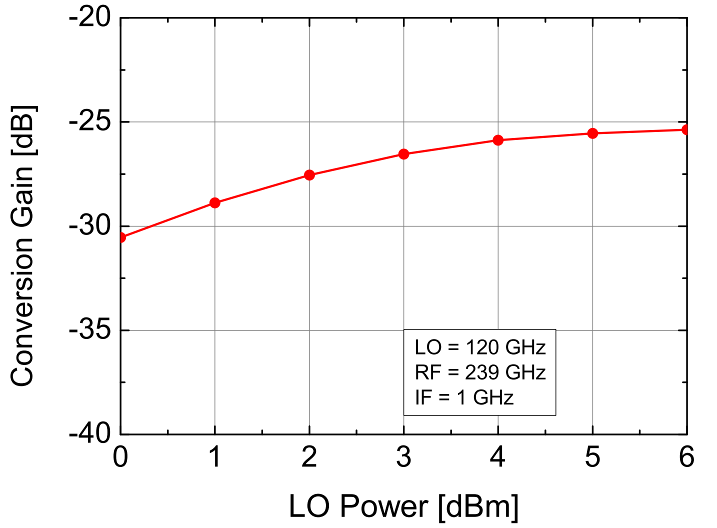

Fig. 4.47: Measured down-conversion gain versus the applied LO power.

Since broadband operation is a key design goal of this mixer, the frequency response with respect to the RF frequency for a fixed LO signal is of special interest. Figure 4.48 shows the measured down conversion gain as a function of the RF frequency from 200 to 280 GHz. The mixer allows a broadband operation with a 3 dB bandwidth from 212 to 276 GHz.

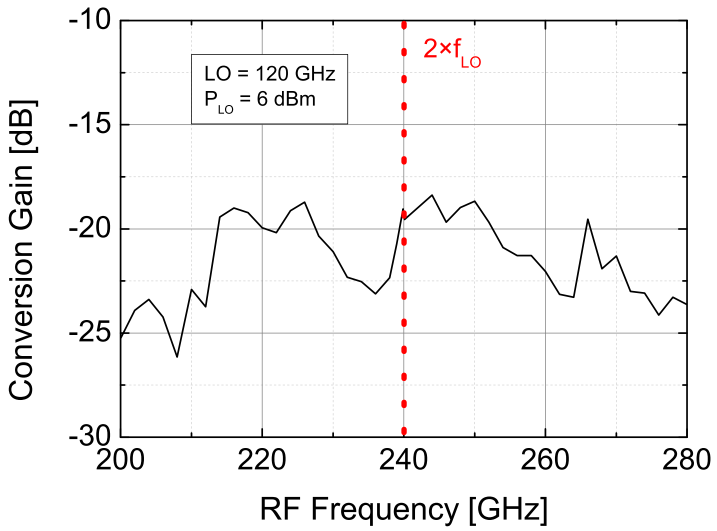

Fig. 4.48: Measured conversion gain over the RF frequency range in a down conversion configuration.

Up Converter

Due to the reciprocal nature of the resistive mixer, the balanced subharmonic mixer cell can also be used to convert a low IF frequency to the higher RF frequency.
The measured output power versus the applied IF input power to the mixer is shown in figure 4.49. The highest output power of -13.5 dBm is achieved for an IF power of 9 dBm. Compared to the measured conversion gain in down converter mode, it seems that the conversion gain for the up conversion is higher, since Pout/Pif equals -18.5 dB for 2 dBm IF power. This holds only true at first sight, because as described in 3.3 the output power of the up converter is measured using a power sensor which measures both sidebands as well as the leaking LO signal. This differs significantly from the single-tone measurement in down converter operation.

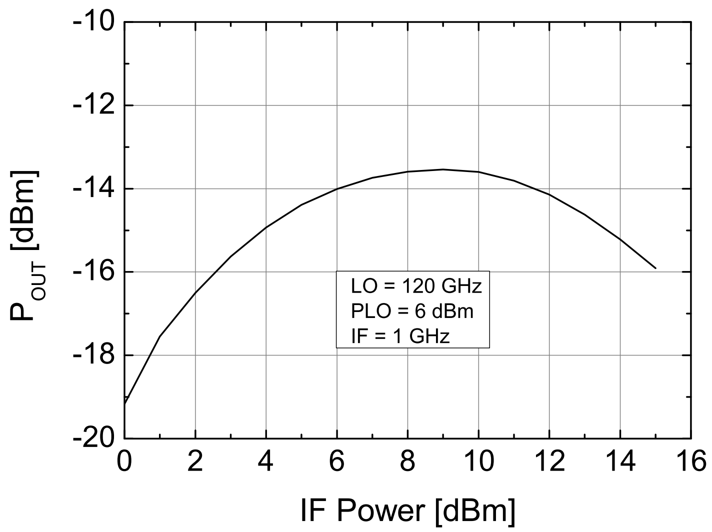

Fig. 4.49: Measured output power of the mixer versus the IF input power at 1 GHz and a LO at 120 GHz with 6 dBm.

The mixer is intended to be used in a data transmission application utilizing direct up and down conversion from and to baseband. To transmit high speed signals originating from an optical fiber, the mixer needs to feature an IF bandwidth of 40 GHz and an RF bandwidth of 80 GHz in a frequency range from 200-280 GHz. In the up-conversion configuration, the mixer achieves a 3 dB bandwidth of more than 40 GHz with a maximum output power of -16.3 dBm at an IF frequency of 3 GHz (see figure 4.50).

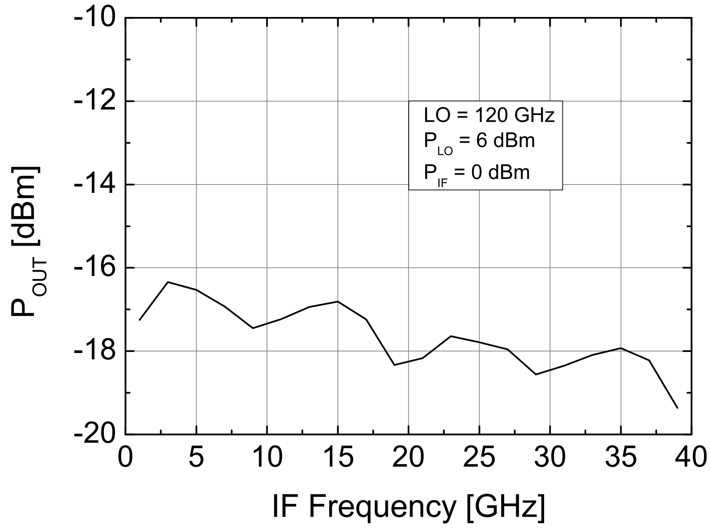

Fig. 4.50: Measured output power over the IF frequency.

4.3.4 Discussion

Broadband resistive mixers can be realized using different circuit topologies. Three different resistive mixers have been presented:

- I/Q mixer using either a branch-line or a Lange coupler.
- Fundamental single balanced mixer using two Lange couplers.
- Subharmonic single balanced mixer.

To achieve the goal of an integrated wideband mixer for wireless communication the combination of a subharmonic, balanced mixer with I/Q functionality would be ideal. The mixer must also support up and down conversion since it should be implemented in a receiver and a transmitter circuit. To realize an I/Q mixer, the Lange coupler showed a significantly better performance compared to the branch-line coupler with respect to bandwidth and I/Q imbalance. This is proven by the comparison of the I/Q mixers as well as the stand alone measurement of the couplers where the branch-line coupler showed 1.5 dB difference between the coupling parameters while the Lange coupler showed an amplitude imbalance of 0.1 dB.
The fundamental single balanced mixer achieves a good LO-to-RF isolation of 26 dB at 218 GHz and supports an IF bandwidth of more than 50 GHz. A drawback of the fundamental design is the LO signal generation above 200 GHz which becomes more challenging with increasing frequency. The design of an I/Q mixer based on this balanced architecture would require at least 3 dB more LO power since the signal is split between the I and Q channel mixer. Due to the two Lange couplers per mixer it would also require a large amount of chip area to realize such an I/Q mixer.
Table 4.5 shows a comparison of other reported resistive mixers in this frequency range and the ones presented in this work. The focus of this work is on integrated mixers which support large operational RF and IF bandwidth combined with quadrature operation to

f_c [GHz]	Type	Technology	CG [dB]	IF-BW[1] [GHz]	Rel. IF-BW [%]	Year and Ref.
300	fund. resistive	mHEMT	-20	N/A	N/A	2009 [95]
220	fund. resistive	mHEMT	-7.9	14	6.3	2008 [20]
200	fund. resistive	mHEMT	-8	>24	>11.4[2]	2011 [22]
200	single bal.	mHEMT	-12.2	>18	>9.8[3]	2011 [22]
200	fundamental	mHEMT	-11.7	N/A	N/A	2009 [23]
156.3	double bal	45 nm CMOS	-12	>26	>16.6	2011 [25]
240	sub-harm. balanced	mHEMT	-18.3	>30	>12.5	this work
210	fund. balanced	mHEMT	-17	>50	>23.8	this work
210	sub-harm. I/Q	mHEMT	-19.2	-	-	this work

[1] 3-dB bandwidth.
[2] f_{LO}=209 GHz
[3] f_{LO}=184 GHz

Table 4.5: Comparison of reported resistive integrated mmW mixers

form high speed receiver and transmitter MMICs. The state of the art is extended by this work with respect to the IF and RF bandwidth and the combination with I/Q functionality.

The subharmonic single balanced mixer requires less chip area and features a subharmonic LO which simplifies the generation of the LO signal. The broadband operation as up and down converter makes it the ideal choice to combine it with the presented Lange coupler to realize subharmonic receiver and transmitter MMICs with I/Q functionality which is presented in the next chapter.

4.4 Multi-Functional mmW Wave Receiver and Transmitter MMICs

A major advantage of the transistor-based integrated circuit technologies is the ability to create multifunctional MMICs based on active and passive building blocks. Extremely broadband single-chip receiver and transmitter MMICs can now be developed using the investigated coupler and mixer circuits described in chapter 4.1 and 4.3.

4.4.1 Motivation

The utilization of mmW frequencies above 200 GHz opens up new application areas of which in this work high speed wireless communication is of particular interest. Broadband short range and long range directional links (e.g. for last mile access or telecom backhauling) are, for example, two applications which benefit from the large absolute bandwidth available at these frequencies.
The tremendous growth in the number of mobile devices like smartphones and tablet computers demands new solutions for the wireless transfer of high quality media to and from those devices. WPANs, operating at mmW frequencies, are able to close this gap by the combination of high throughput based on the large available bandwidths and high frequency reuse factor due to the increased path loss in this frequency range.
When it comes to long range communication, wired high speed data transmission is, up to today, based on optical fiber communication which employs, e.g. OOK signals. The wireless transmission of such signals requires usually a change in the modulation format to increase the spectral efficiency of the radio signal. With increasing data rates the effort to change the modulation format in real time becomes more challenging and requires sophisticated signal processing. The large absolute bandwidths available around 240 GHz enable a new solution to this problem by the direct up- and down-conversion of the OOK signals without a change of the modulation format.
In this chapter, a fully integrated chipset is presented which operates at a center frequency of 240 GHz and is designed to perform a direct up and down conversion of signals coming from an optical fiber network [103].

4.4.2 Design Goals

The major design goals are derived from the intended application scenario, a bit-transparent wireless link around 240 GHz. The electrical spectrum of a 40 Gbit/s OOK signal has a bandwidth of 40 GHz. A double-sideband transmission of such a baseband signal requires the doubled IF bandwidth at the RF after up-conversion, in this case 80 GHz. Higher data rates could be achieved using more sophisticated modulation schemes like quadrature PSK (QPSK), QAM or orthogonal frequency-division multiplexing (OFDM). These higher order modulations have more demanding requirements on phase and amplitude imbalance as well as linearity.
To minimize the receiver noise figure and simultaneously increase the range of the wireless link, an LNA with high gain is used as a first stage to amplify the RF signal in the receiver.

Although the broadband subharmonic resistive mixer has a significant conversion loss in this frequency range, the entire receiver should be able to achieve a conversion gain without any IF post-amplification. The design parameters of the transmitter differ from those of the receiver since other power levels matter in the up-converter. The conversion gain, for example, plays a minor role compared to a down-converter since at the lower IF input frequencies sufficient power is usually available. The ability to handle large input signals and deliver sufficient output power helps to ease the power and gain budget in the transmitter.
Virtually any transmitter for wireless data transmission requires a post amplification stage to gain enough output power. Therefore the same LNA as with the receiver was employed in the transmitter with reversed input and output.

4.4.3 Integrated 240 GHz Low Noise Amplifier

The receiver and the transmitter employ a LNA to pre and post amplify the RF signal. The mixers in the up- and down-converter are preceded and succeeded, respectively by a 3-stage LNA which is designed to cover the entire frequency range from 200 to 280 GHz. The LNA has been taken from the Fraunhofer IAF IP portfolio and the design was not part of this work. Each amplification stage employs two 2×10 µm transistors in a cascode configuration. A single stage achieves about 10 dB small signal gain using the 35 nm mHEMT process.
To characterize the LNA, it has been manufactured individually and measured afterwards. Figure 4.51 shows a photograph of the stand-alone LNA. To contact and bias the LNA, RF pads and DC supply pads are added to the circuit which affect the behavior of the circuit at its very high operation frequency. To estimate the performance of the core amplifier when embedded in the complete Rx and Tx, the RF pads need to be de-embedded after the measurements.

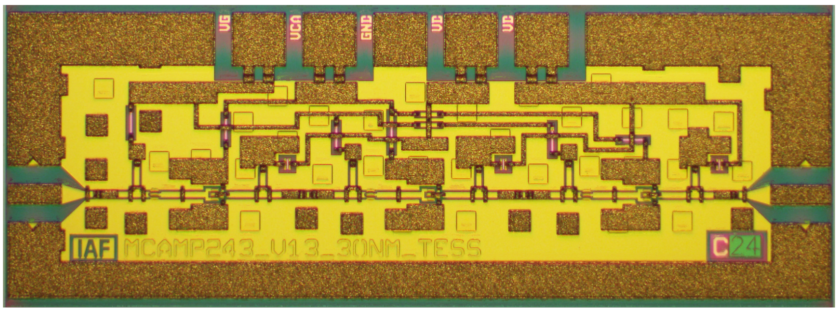

Fig. 4.51: Chip photograph of the stand-alone LNA with the input on the left side and the output on the right hand side. The chip dimensions are 1.2 × 0.5 mm^2.

The S-parameter measurements in figure 4.52 show a very flat gain shape of the amplifier from 210 to 280 GHz. The LNA achieves a small signal gain (S_{21}) of 26 to 30 dB while the input return loss stays well above 8 dB in the entire measurement range from 210 to 330 GHz. The isolation of the LNA is important in the receiver, since it ensures a good LO-to-RF isolation and prevents the LO leakage of the mixer stage from propagating through the antenna. In the individual LNA, the isolation is better than 37 dB in the measurement range. The de-embedding of the RF pads had only a small effect on the input and output return loss and did not affect the gain and isolation of the amplifier. The de-embedded S-parameters are therefore not plotted additionally in figure 4.52.

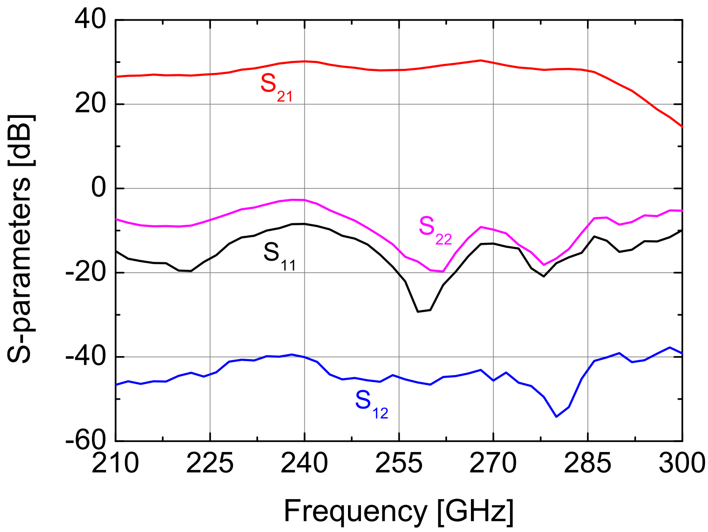

Fig. 4.52: Measured S-parameters of the 3 stage 240 GHz LNA.

Noise Performance

As the first stage in the receiver MMIC, the LNA has a significant impact on the noise performance of the overall front end. It mainly determines the noise figure of the entire receiver according to Friis' formula. To measure the noise figure of the LNA, the hot cold method from section 3.4 has been used. The LNA was packaged using a gold plated split block module with WR-3 waveguide connections. At the input a horn antenna was directly attached to the module while the output of the LNA was fed to a harmonic mixer to convert the signal to the measurement range of the following noise figure analyzer. The packaged LNA achieved a measured noise figure of only 5.8 dB at 240 GHz and stays below 6.7 dB up to 280 GHz (see figure 4.53).

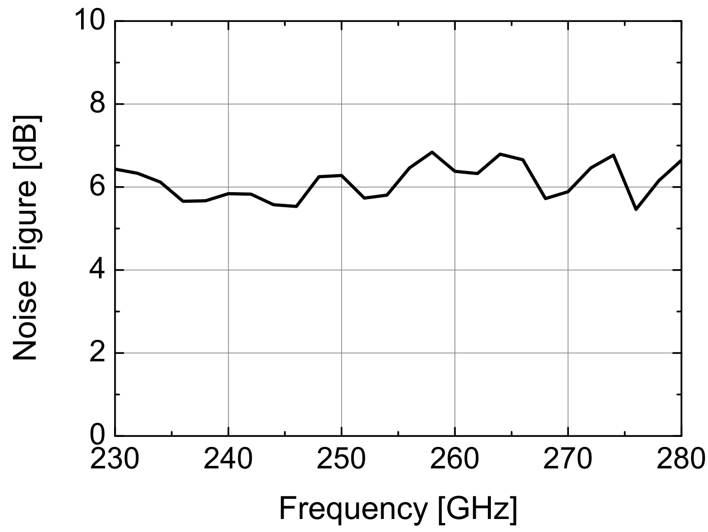

Fig. 4.53: Measured noise figure of a packaged LNA in the frequency range from 230 to 280 GHz.

4.4.4 Broadband Balanced Subharmonic I/Q Receiver

The receiver is based on the balanced subharmonic resistive mixer presented in section 4.3.3. The mixer has been chosen because of its balanced and yet small size design and its broadband operation. Figure 4.54 shows a block diagram of the receiver MMIC.
Since the receiver should feature I/Q IF terminals, two mixer cells are needed. The LO is split equally between the two mixers using a Wilkinson divider at 120 GHz and fed into the two balanced subharmonic mixer cells. The RF signal is amplified using the 3 stage LNA and split equally in amplitude but 90° out of phase using the Lange coupler at 240 GHz, described in section 4.1.2.3. Usually, the required 90° phase shift between the I- and Q-channel is done in the narrowband LO path. But due to the subharmonic approach, the LO phase shift would be doubled like the LO frequency. To overcome this problem, the Lange coupler has been placed in the RF path to generate the phase shift between the IF-I/Q ports.

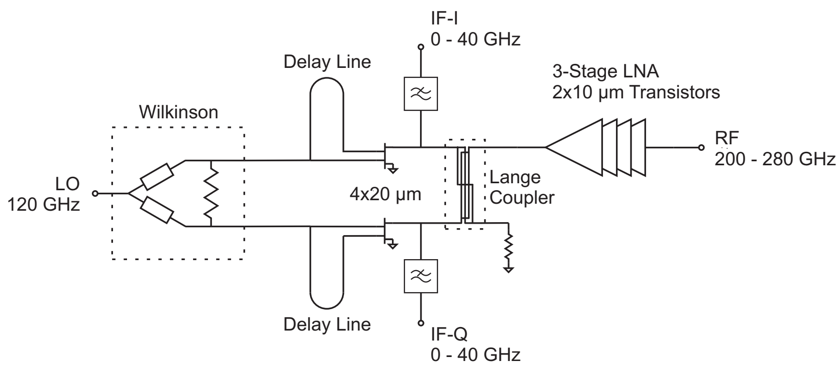

Fig. 4.54: Block diagram of the balanced subharmonic I/Q receiver MMIC.

Figure 4.55 shows a photograph of the receiver MMIC. The chip dimensions are 1×2.5 mm^2 and the two balanced subharmonic mixer cells with their delay lines are clearly recognizable on the chip. Due to the large RF and IF bandwidth, the IF signals need to be considered as high frequency signals and require to be routed using transmission lines and RF pads. The IF signals are connected on the top of the MMIC using coplanar GSGSG (G=Ground, S=Signal) pads while the LO uses a GSG pad with 100 µm pitch and the RF pad on the right hand side on the MMIC has a 60 µm pitch.

To measure the conversion gain of the MMIC on-wafer, the basic single-tone measurement setup from section 3.2 was used. The RF signal was generated by an OML V03VNA-T/R frequency extension module with a multiplication factor of 18. To ensure the power of the RF signal stays below -35 dBm, a manual WR-3 wave guide attenuator was used. Since the LNA in the receiver features up to 30 dB small signal gain, the receiver saturates at approximately -30 dBm of RF input power.
The LO signal was generated using a $\times 6$ frequency multiplier from Radiometer Physics GmbH (RPG) with a maximum output power of 7 dBm. Due to the additional losses in the RF-probes, an in-house W-Band amplifier was used to achieve an on-chip power level of 6 dBm at 120 GHz. The conversion gain as a function of the RF frequency has been measured for the IF-I and -Q ports and is shown in figure 4.56. The termination of the unconnected port had no discernible influence on the performance and the unconnected port was left open during the measurements. The MMIC achieves a 3 dB RF bandwidth of 30 GHz in the frequency range from 224 to 254 GHz.

Depending on the applied LO power, the gate voltage bias of the mixer for maximum conversion gain differs. With increasing LO power, the gate bias needs to be shifted to more negative voltages. This is based on the fact that the duty cycle of the subharmonic mixer should be around 25% as described in chapter 2.2.2 for maximum conversion gain. The gate voltage needs therefore to be shifted to more negative voltages with larger LO amplitudes to keep the duty cycle constant. Figure 4.57 shows the conversion gain as a function of the mixer bias voltage for three different power levels. The maximum conversion gain is achieved for the highest LO power of 6 dBm at a mixer bias voltage of -0.3 V. It is apparent that with the highest LO amplitude, the FET's channel alternates between pinch off and a very low R_{DS}. Besides higher conversion gain, the mixer gets also less sensitive to a bias voltage variation with higher LO power.

After characterization, the MMICs have been packaged by RPG in classical waveguide modules using a split block construction. The modules are made of brass with a gold plating. The MMIC is connected by wedge-wedge wire bonding, with the waveguide to chip transition realized by microstrip lines on 50 µm thick quartz substrates. A WR-

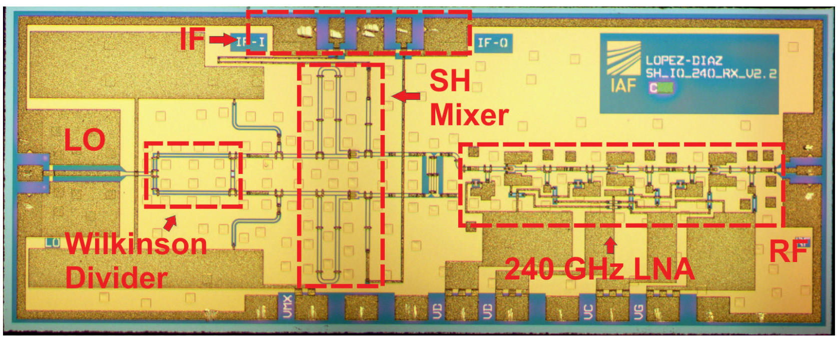

Fig. 4.55: Chip photograph of the balanced subharmonic I/Q receiver MMIC. Chip size is 2.5×1 mm^2.

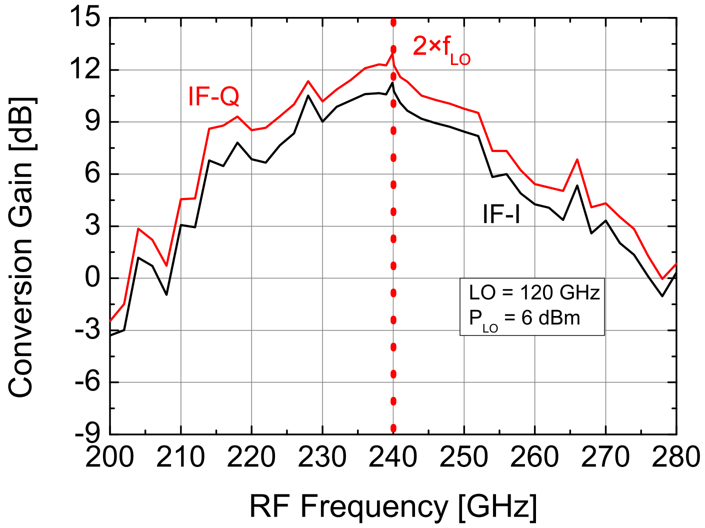

Fig. 4.56: Conversion gain of the MMIC versus the RF frequency with a fixed LO frequency of 120 GHz.

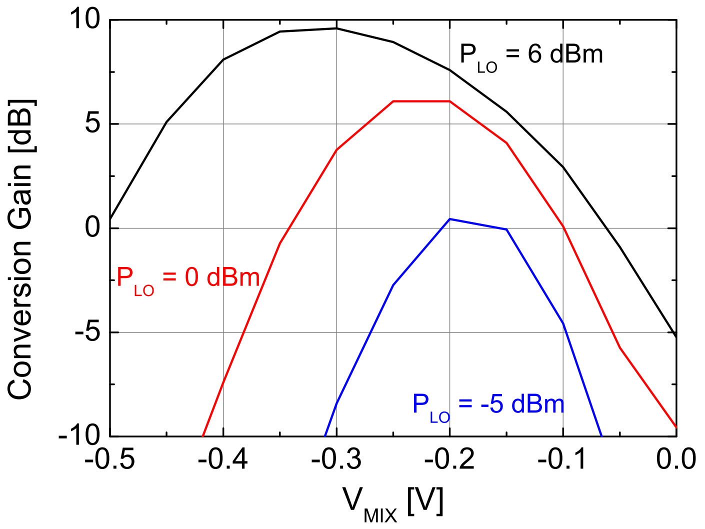

Fig. 4.57: Conversion gain of the Rx-MMIC as a function of the mixer gate voltage for different LO power levels at a fixed IF frequency of 1 GHz

8 waveguide is used to connect the LO signal to the module while a waveguide with 0.98×0.49 mm^2 dimension (slightly bigger than WR-3) is employed as RF connection with a center frequency of 240 GHz. The opened module with the MMIC is visible as an inlay in figure 4.58a. The IF connections on the left hand side of the pictures are routed using microstrip lines on a 75 µm thick alumina substrate. The partially visible printed circuit board (PCB) on the right side contains the DC voltage generation for different bias voltages of the MMIC with the wire connections to the DC pads of the chip. The IF signals are connected using female V connectors. The LO waveguide in figure 4.58b has obviously larger dimensions compared to the RF waveguide in figure 4.58a due to the lower LO frequency.

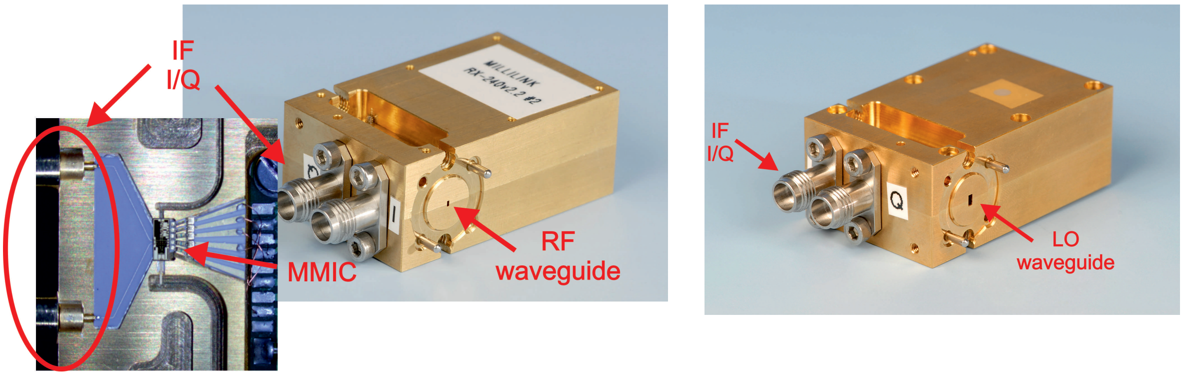

Fig. 4.58: Photograph of the receiver module and the opened split block module (inlay).

The module has been characterized using the same measurements as those used during the MMIC characterization. Calibration and measurement of the waveguide modules require less effort compared to on-wafer measurements since no wafer handling, probe placement and DC biasing is needed. All power levels are calibrated at the module's reference plane. During the on-wafer characterization, additional losses were introduced by the coplanar waveguide probes and their waveguide connections. For the module measurements, the output power of the frequency multipliers by 6 are sufficient and there is no need for post amplification of the 120 GHz LO signal.
The measured conversion gain as a function of the RF frequency of the receiver module is plotted in figure 4.59. The shape of the curve is similar to the measured conversion gain of the bare MMIC although the packaged chip is not exactly the one which has been fully characterized in this work. While the MMIC achieved a maximum conversion gain of 12.9 dB at the IF-Q channel, the module achieves only 3.8 dB on the IF-Q channel. The losses are mainly introduced by the waveguide to chip transition around 240 GHz and the bond wire.

Besides the conversion gain, the receiver noise figure is of special interest for a wireless data transmission system. The LNA features a noise figure of about 6 dB, as shown in section 4.4.3. Since the LNA is the first stage in the receiver, its noise figure defines the lower limit for the overall noise figure of the receiver. The additional noise of the mixer and the losses in the IF path add to the total receiver noise.
The noise figure of the module has been measured using the hot/cold measurement setup described in chapter 3.4. Figure 4.60 shows the measured noise figure of the receiver module for the IF-I and the IF-Q channel using a fixed LO at 120 GHz with an amplitude of 7 dBm. Due to the very low power levels of the hot/cold measurement and the serial measurement of the two IF channels, an uncertainty is introduced. The results from figure 4.60 are therefore considered as approximated values with a receiver noise figure of less than 9 dB at the IF-Q channel. According to equation 3.2 a higher SNR enables the transmission of higher data rates for a given bandwidth. A lower noise figure means therefore less degradation of the SNR and hence higher achievable data rates.

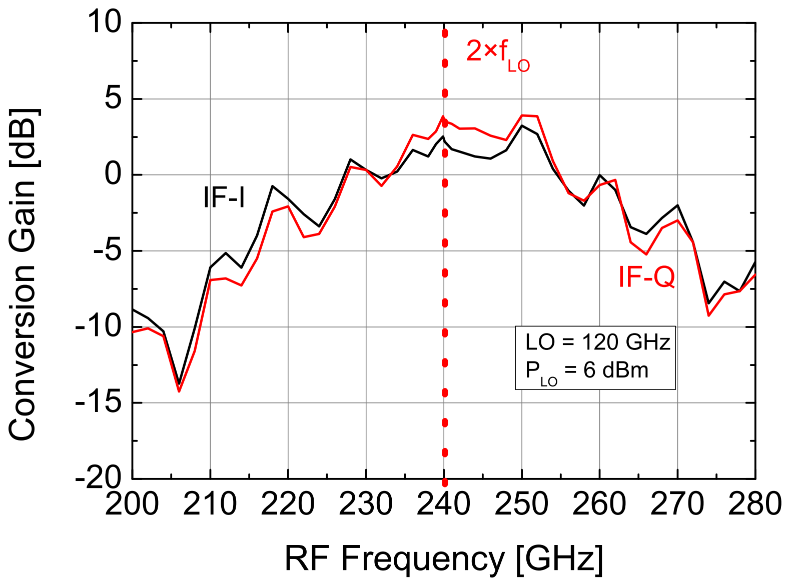

Fig. 4.59: Conversion gain of the Rx module versus the RF frequency with a fixed LO frequency of 120 GHz.

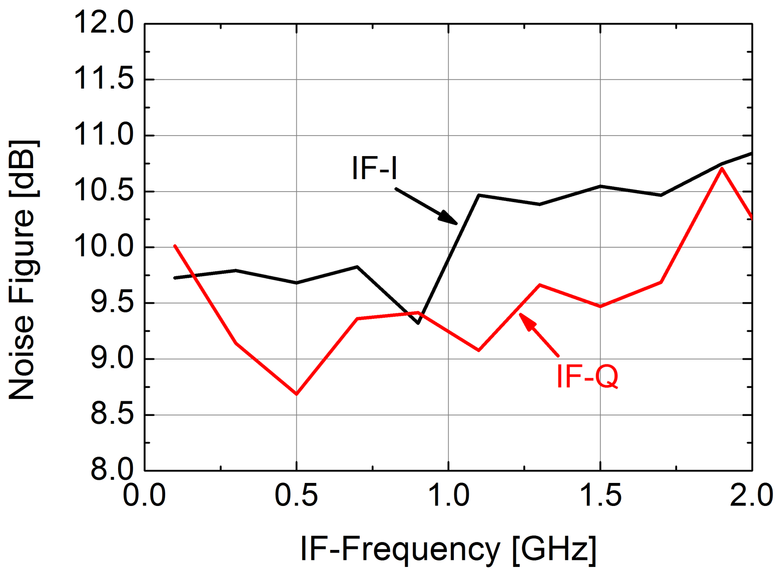

Fig. 4.60: Measured noise figure of the receiver module for both IF channels using a fixed LO at 120 GHz.

4.4.5 Broadband Balanced Subharmonic I/Q Transmitter

The transmitter employs the same building blocks as the receiver MMIC. It consists of two balanced subharmonic mixer cells, and the 3-stage LNA from section 4.4.3 to post amplify the up-converted RF signals. A Wilkinson divider and a Lange coupler are used to split the LO and combine the RF signals of the mixer cells. In contrast to the receiver, the LNA in the transmitter is used as a medium power amplifier. The transmit amplifier is the same design used as LNA in the receiver with reversed input and output. Figure 4.61 shows a block diagram of the transmitter to illustrate this configuration.

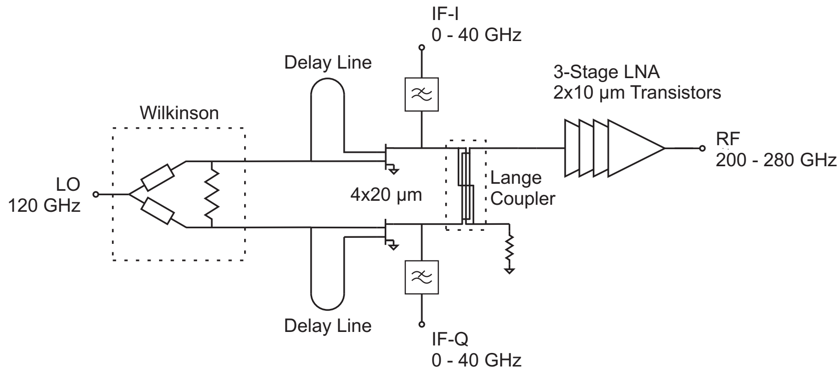

Fig. 4.61: Block diagram of the broadband balanced subharmonic I/Q transmitter MMIC.

The small 2×10 µm transistors in the amplifier are able to deliver up to +3 dBm of saturated output power. More saturated output power would be desirable to increase the linearity of the transmitter and bridge longer distances. However, the design of unconditionally stable power amplifiers supporting this very broad frequency range is extremely challenging. In addition, the available power decreases at higher frequencies and only a few technologies are able to deliver power above 200 GHz. Figure 4.62 shows the saturated output power as a function of the frequency of published solid state power amplifiers. Up till now, the highest operation frequency of 650 GHz is achieved by an InP HEMT based amplifier featuring a saturated output power of 4.8 dBm [89].

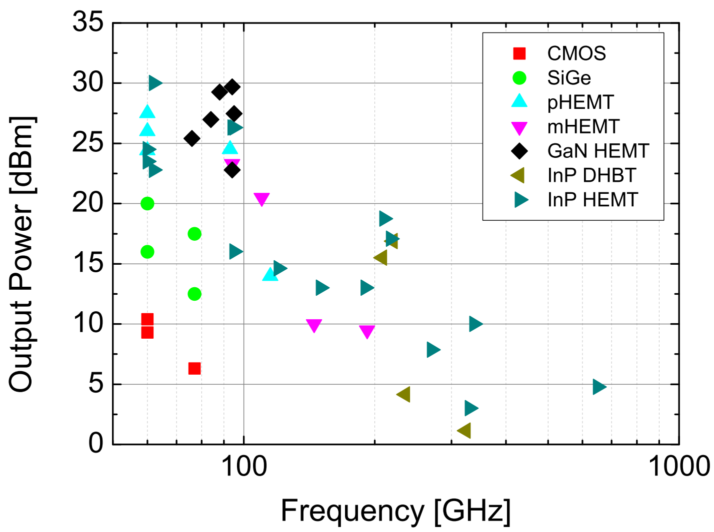

Fig. 4.62: Saturated output power of different solid state power amplifier MMICs as a function of their center frequency.

A chip photograph of the transmitter MMIC is shown in figure 4.63. The balanced approach is particularly important in the transmitter to achieve sufficient carrier suppression. An unbalanced fundamental resistive mixer has an increased LO leakage since the LO is pumped with high power and lies within the RF frequency range. Even if the mixer features e.g. 10 dB isolation between the LO and RF port, the leaking signal has still a power level of -10 dBm when an amplitude of 0 dBm is applied to the LO input. In case of only 10 dB conversion loss the carrier will be 3 dB above both side bands if 0 dBm IF power is applied (-13 dBm at LO±IF).

The balanced and subharmonic design of the realized mixer is best suited to ensure sufficient carrier suppression. Due to the subharmonic LO, the fundamental component is inherently filtered by the on-chip high pass filter as well as the waveguide cutoff which is in this case:

$$f_c(TE_{10}) = \frac{c}{2 \cdot a} = \frac{3 \cdot 10^8}{2 \cdot 0.98 \cdot 10^{-3}} \approx 153\ GHz. \tag{4.18}$$

The 120 GHz LO is thereby considerably lower than the cutoff frequency of the waveguide. The LO balancing adds additional suppression through destructive interference. The transmitter has been characterized in terms of output power and carrier suppression. Figure 4.64 shows the measured double sideband output power as a function of the IF frequency. The transmitter MMIC achieves a maximum DSB output power of -0.7 dBm at an IF frequency of 1 GHz at the IF-I port and a 3 dB IF bandwidth of 28 GHz between 12 and 40 GHz.

To measure the output power an Erickson power meter has been used as described in section 3.3. Since this instrument measures the delivered power in the entire measurement range this method is not suitable to determine the carrier suppression of the transmitter. To measure the carrier suppression, an uncalibrated harmonic mixer has been used to compare the strength of the carrier signal to the power in both side bands.

The conversion loss of the commercial harmonic mixer is heavily dependent on the selected frequency. Due to the significant conversion loss of approximately 74 dB, it is virtually impossible to perform an accurate calibration of the mixer using the available frequency source modules. The available source modules are only able to deliver an output power between -38 and -22 dBm in this frequency range. Together with the high conversion loss of the mixer, the power levels are at the sensitivity limit of the employed spectrum analyzer. To overcome this problem, only a low IF of 50 MHz has been used to ensure no significant change in the conversion loss between the carrier at 240 GHz and both side bands. The MMIC achieved a minimum carrier suppression of more than 9 dB at 240 GHz with an IF power of -10 dBm and a LO power level of 6 dBm. The power of both side bands increases with more IF power which leads to an improved carrier suppression at higher IF power levels.

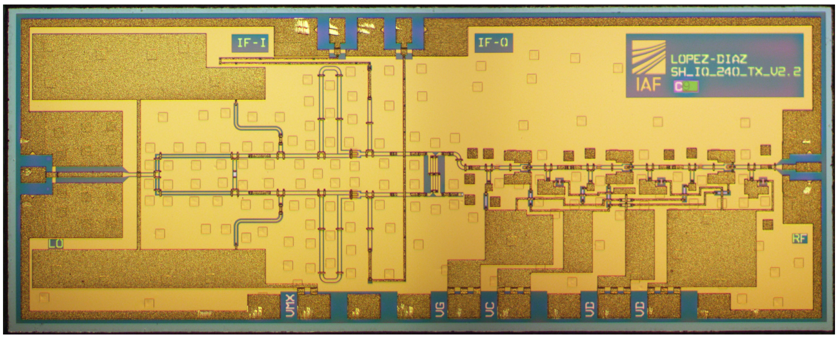

Fig. 4.63: Chip photograph of the balanced subharmonic I/Q transmitter MMIC. Chip size is 2.5×1 mm^2.

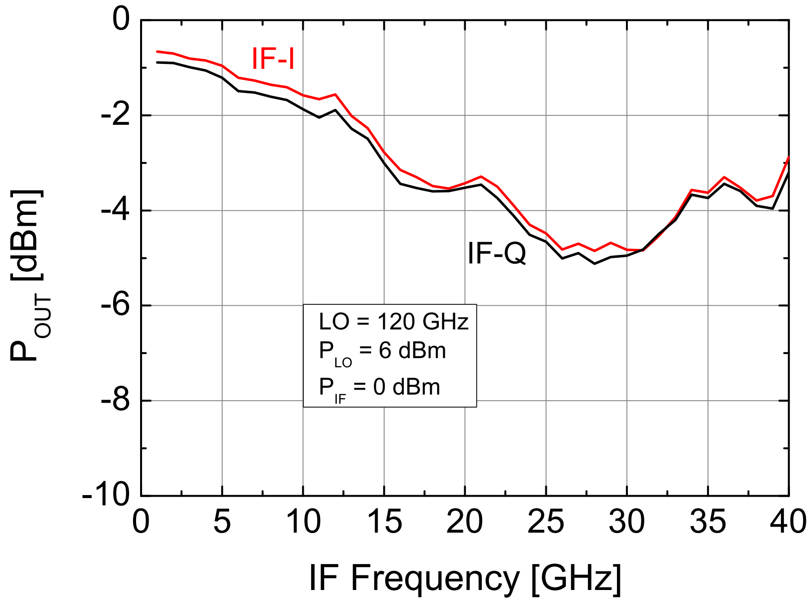

Fig. 4.64: Measured total output power (LSB, $2\times f_{LO}$, USB) of the MMIC versus the applied IF power for a fixed LO power of 6 dBm.

Due to the pad compatibility of the Rx and Tx MMICs, the same split block module was used for the packaging of the Tx MMIC as has been used for the Rx [104]. The packaging was also performed by RPG.
To measure the performance of the packaged MMIC, the output power of the module has been measured using the same set up as with the on-wafer measurements except for the coplanar waveguide probes and DC supply. The measured output power as a function of the IF frequency is shown in figure 4.65. It should be noted that the on-wafer measurements from figure 4.64 do not correspond to the exact same MMIC packaged in the module. The module achieves a maximum DSB output power of -3.6 dBm at an IF frequency of 2 GHz. Compared to the MMIC, the module achieves about 3 dB less output power, which is caused by the additional losses in the waveguide transition. The 3 dB bandwidth of the module equals 34 GHz which is similar to the MMIC (28 GHz).

The carrier suppression of the packaged MMIC is better than 11 dB with a LO power level of 7 dBm and an IF input power of -10 dBm. This is 2 dB more compared to the bare MMIC, which is mainly caused by the lower on-chip LO power level due to the losses in the waveguide to coplanar transitions.
The leaking LO signal is also limiting the dynamic of the transmitter. The output power of an ideal transmitter would rise and fall in a linear relation to the IF input signal. In a real transmitter, the upper limit of the output power is determined by the saturated output power which could be delivered by the power amplifier and the lower limit is defined by the LO leakage which presents a constant power signal, even if no signal is applied to the IF terminals.

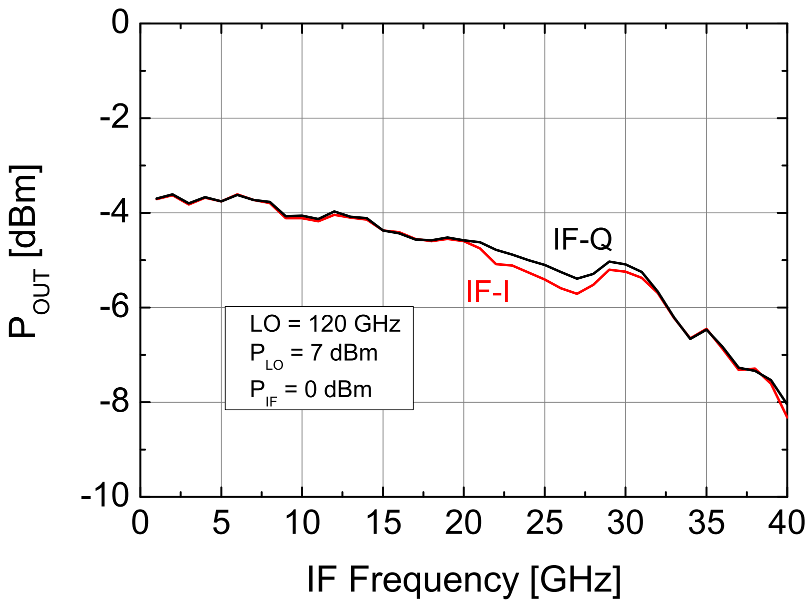

Fig. 4.65: Measured output power of the Tx-module with a fixed LO frequency of 120 GHz.

4.5 Summary

In this chapter the necessary building blocks to create entire multifunctional receiver and transmitter MMICs for high data rate communication at mmW frequencies have been examined and subsequently integrated on a 240 GHz receiver and transmitter MMIC. This includes passive structures like power dividers and hybrids, active and passive mixer circuits.

The analysis and design of the passive coupler structures prove that a Lange type coupler can still be realized at frequencies around 240 GHz showing broadband coupling and phase relation. The main design challenges are the high center frequency where all parasitics like air-bridges have an increased impact. The design in the grounded coplanar technology results in mixed coplanar and microstrip modes and the performance is also depending on the via hole placement. The only way to ensure a working design is to perform full 3D electro magnetic simulations during the design phase.

The comparison of different active and passive mixers including a dual gate, Gilbert cell and resistive FET mixer, all manufactured in the Fraunhofer IAF mHEMT technology, showed the advantage of passive mixers over active topologies for broadband circuits. Although, the passive mixers exhibit a higher conversion loss compared to active mixers, they are easier to match over a wide frequency range (cp. section 2.2.2.1). In direct conversion applications, a leaking LO may block the desired signal [90] and requires balanced topologies to achieve a high LO-to-RF isolation. The presented balanced subharmonic resistive broadband mixer combines the advantage of wideband operation and high LO-to-RF isolation. The integration together with an LNA and the Lange coupler made the realization of the first subharmonic 240 GHz quadrature receiver and transmitter MMIC possible.

The 240 GHz receiver MMIC achieves high conversion gain combined with very broadband quadrature IF terminals compared to other reported integrated receiver circuits (see table 4.6).

f_c [GHz]	f_{LO} [GHz]	Technology	CG [dB]	NF [dB]	IF-BW[1] [GHz]	Rel. IF-BW [%]	Year and Ref.
320	17.7	SiGe	-14	36	8	2.5	2012 [27]
300	100	mHEMT	13.7	N/A	N/A	N/A	2011 [28]
220	110	SiGe	16	15	10	4.5	2011 [21]
220	110	mHEMT	2	8.4	4.5	2.0	2008 [29]
220	55	mHEMT	3.5	7.4	6	2.7	2011 [30]
200	100	mHEMT	7	6.9	N/A	N/A	2009 [23]
240	120	mHEMT	12.9	11.5	16	6.6	This Work

[1] 3-dB bandwidth

Table 4.6: Reported monolithically integrated mmW receiver circuits

The realized quadrature transmitter MMIC around 240 GHz showed excellent broadband performance combined with a low conversion loss and high output power and excels other reported integrated transmitters in this frequency range (table 4.7).

f_c [GHz]	f_{LO} [GHz]	Technology	IF-BW[1] [GHz]	CG [dB]	P_{Out} [dBm]	Year and Ref.
630	210[2]	InP HBT	15	-24	-30	2012 [31]
245	-[3]	SiGe	-	-	1.4	2012 [32]
220	110	mHEMT	20	-3.6	1.4	2011 [96]
220	55	mHEMT	10	-8	-6	2011 [30]
240	120	mHEMT	28	-0.6	-0.6	This Work

[1] 3-dB bandwidth.
[2] On-Chip PLL with external 21 GHz reference oscillator.
[3] On-Chip VCO

Table 4.7: Reported integrated mmW transmitter circuits

5 High Speed Wireless Data Transmission

The design of the presented receiver and transmitter MMICs is focused on the wireless data transmission application. Besides the characterization of the MMICs, the evaluation within a real data transmission scenario is therefore mandatory to determine the performance of the mixers and the entire wireless link.

Radio communication uses different modulation formats from simple amplitude modulation to more sophisticated multi carrier modulations. The focus of this work is the direct up and down conversion of signals from a fiber optic network ("Fiber over Radio") using the modulation scheme of the optical fiber network. Optical communication systems often employ simple OOK modulation but current research is also dealing with complex modulated signals on optical fibers. A direct up and down conversion of such broadband signals is made possible by the large absolute bandwidth around 240 GHz and simplifies the processing effort in the baseband significantly.

Only a few technologies are able to operate in the millimeter wave frequency range. Transmitters above 200 GHz are currently realized either using photonic generation [33, 35, 37] or compound semiconductors, namely SiGe [32], GaAs [30, 34], [99] and InP [31]. On the receiver side, InP based HEMT devices offer lowest noise and provide sufficient gain to realize broadband wireless links. The Fraunhofer IAF mHEMT technology offers InP like performance combined with low cost GaAs substrates. The realized receiver and transmitter modules are the first available chipset offering broadband operation combined with I/Q functionality.

Different modulation formats make distinct demands on the RF front-end with respect to bandwidth, linearity and I/Q balance. To characterize the RF front-end consisting of the packaged receiver and transmitter MMICs from chapter 4.4 various measurements with different modulation formats have been performed. All measurements were carried out either at the Fraunhofer IAF or at the Karlsruhe Institute of Technology (KIT) in collaboration with the staff from the Institute of Photonics and Quantum Electronics (IPQ) and Institut für Hochfrequenztechnik und Elektronik (IHE).

First, a VNA based S-parameter measurement was used to determine the bandwidth, group delay and I/Q amplitude imbalance. Afterwards, the receiver sensitivity was measured under back to back conditions using binary PSK (BPSK) modulated signals. These measurements help to determine the bandwidth and the achievable data rates depending on the receiver input power.

In a real application scenario, a coherent LO distribution from Tx to Rx is virtually impossible. Unsynchronized LO signals will be used at the transmitter and the receiver site. To recover the OOK data signals, the I/Q functionality of the receiver is exploited. A power detection by the means of the sum of squares, $I^2 + Q^2$ after the Rx enables the data recovery even after an incoherent transmission. Any amplitude imbalance between

the I and Q channel degrades the quality of the recovered signal and hence the achievable data rates.
Higher order modulations increase the spectral efficiency and are also getting more and more used in optical communication systems. Amplitude modulations like amplitude-shift keying (ASK) or QAM require linear transmitter and receiver circuits while constant envelope modulations are less susceptible to nonlinear behavior.

5.1 RF Front-end Characterization

To characterize the performance of the Rx/Tx module pair without the influence of the radio channel, a coherent back to back configuration was used by Antes et. al. [105] . The modules were connected using a WR-3 waveguide attenuator to ensure linear operation of the receiver. The LO signal was generated by a single synthesizer and distributed to two $\times 6$ frequency multipliers. LO coherence was achieved by placing a phase shifter in one branch between the synthesizer and the frequency multiplier. Figure 5.1 shows a block diagram of the employed measurement setup. A standard VNA was used to measure the S-parameters between the IF terminals of the Rx/Tx modules. The reference plane was calibrated to the IF terminals using an electronic calibration module.

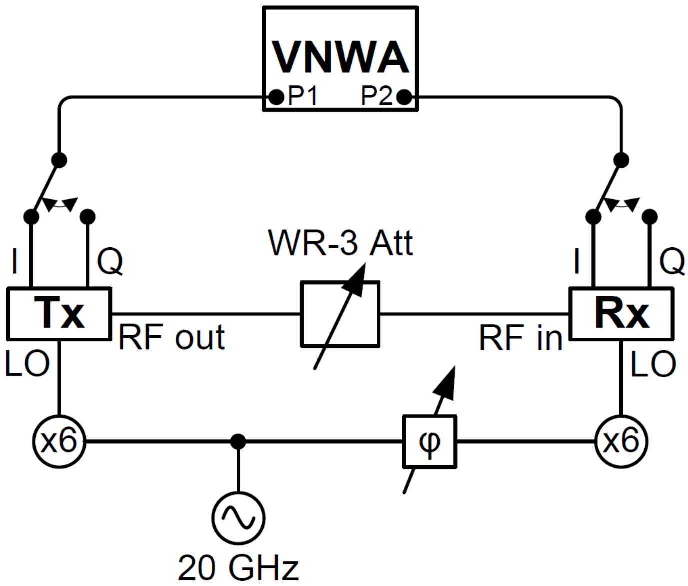

Fig. 5.1: Block diagram of the back to back S-parameter measurement setup used to characterize the RF link at 240 GHz.

This setup was used to determine the IF port matching (S_{11}, S_{22}) and the transmission (S_{21}), which provides in detail information about the bandwidth and group delay of the Rx/Tx modules. All permutations of I/Q channel combinations have been examined by connecting port 1 of the VNA to either the I or the Q channel of the transmitter while port 2 is connected to the I or Q channel of the receiver. The phase shifter was adjusted each time to achieve maximum power in the measured receiver channel. An overlay of the measurements of the port matching is shown in figure 5.2a while the measured S_{21} is plotted in figure 5.2b. All I/Q channel combinations achieve similar performance with respect to bandwidth and return loss. The IF port matching over a large bandwidth from 0 to 40 GHz is a challenge and requires complex matching networks. Due to the on-chip integration a tradeoff between return loss and chip area has to be made. To keep the required area reasonable low, on-chip inductors were not used but a R-C network was used to separate the IF from the RF and LO signals and achieve a return loss of more than 6 dB for frequencies up to 12 GHz. An IF bandwidth of more than 20 GHz is achieved for all I/Q combinations. An important finding of these measurements is the equality between the I/Q channel combinations which implies a low I/Q amplitude imbalance necessary for the transmission of complex modulated signals as well as the power detection at the receiver using the sum of squares ($I^2 + Q^2$).

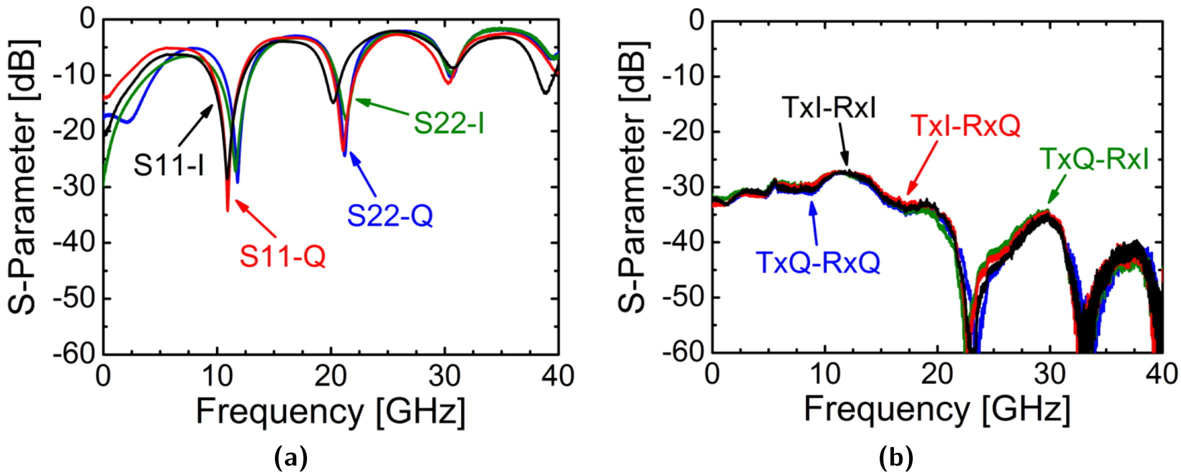

Fig. 5.2: Measured port matching (a) and frequency response (b) of the Rx-Tx chain in a back to back configuration.

The group delay has been calculated based on the measured S_{21} parameter. As discussed in chapter 4.4.3, the ripple of the group delay is of special interest. The different group delays for all I/Q channel combinations are shown in figure 5.3. Over the entire bandwidth, the variation stays below 5 ns for all I/Q combinations.

After characterization of the RF modules with respect to their frequency response and group delay, the performance of the Rx/Tx set in a real data transmission scenario is investigated in the next chapter. The modules are therefore connected in a back to back configuration and different data rates and power levels are fed into the Tx module.

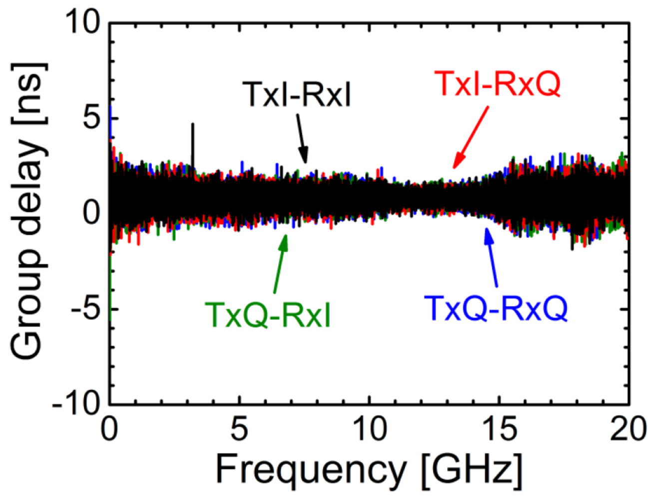

Fig. 5.3: Measured group delay of the 240 GHz link in a back to back configuration.

5.2 Receiver Sensitivity

Receiver sensitivity measurements were performed to estimate the required signal strength at the receiver for a given data rate by the author et. al. [104]. A back to back configuration, similar to the front-end characterization was employed for the measurements. A block diagram of the measurement setup is shown in figure 5.4. The Rx/Tx modules were connected using a WR-3 waveguide attenuator to vary the Rx input power. A coherent LO configuration with a single synthesizer was used. The 20 GHz signal from the synthesizer was split equally in amplitude and fed into two $\times 6$ frequency multipliers. A coaxial phase shifter in one of the branches to the frequency multipliers assures coherent operation.

A four channel pulse pattern generator (PPG) with a maximum data rate of 12.5 Gbit per channel served as a signal source. To generate higher data rates, a four channel multiplexer (MUX) supporting data rates from 20 to 40 GHz was attached to the PPG. On the receiver side, IF amplifiers were used to increase the signal level. Since the employed broadband amplifiers feature AC coupled in- and outputs BPSK modulated signals with no DC content were chosen as modulation format. The amplified IF signals are analyzed using a digital communication analyzer (DCA) and a bit error rate tester (BERT). The

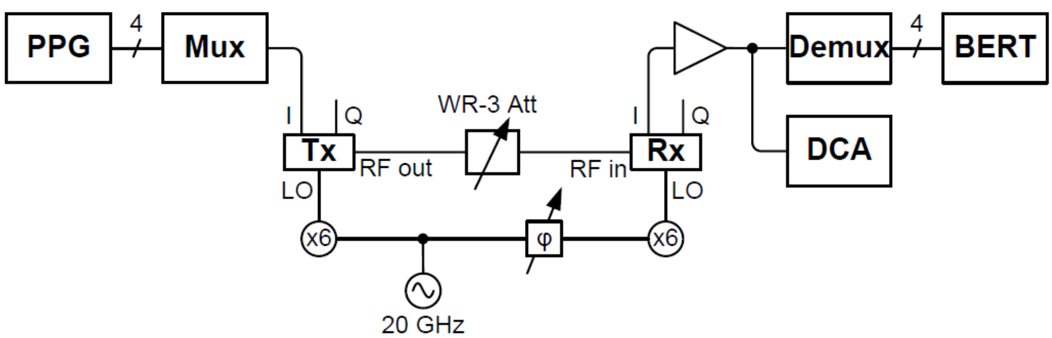

Fig. 5.4: Measurement setup for the receiver sensitivity measurements with data rates of up to 40 Gbit/s.

DCA is able to measure eye diagrams of the multiplexed signals to gain information about the signal to signal levels, clock jitter and signal to noise ratio. A de-multiplexer (DEMUX) was used to separate the individual data channels at the receiver and feed them into the BERT to measure the bit error rate for different combinations of data rate and receiver input power. Figure 5.5 shows the measured bit error rate (BER) as a function of the Rx input power for different data rates from 25 to 40 Gbit/s. A BER of 1.7×10^{-4} was achieved for an Rx input power level of -29 dBm at 40 Gbit/s. This is, so far, the highest reported data rate transmitted by a entirely MMIC based wireless link in the mmW frequency range in a single-input single-output (SISO) configuration. For 25 Gbit/s a BER of 1.1×10^{-11} was measured with an input power level of -28.5 dBm. This confirms the measured IF and RF bandwidth of the waveguide modules and proves the ability of the Rx/Tx pair to support data rates of up to 40 Gbit/s using simple BPSK modulated signals.

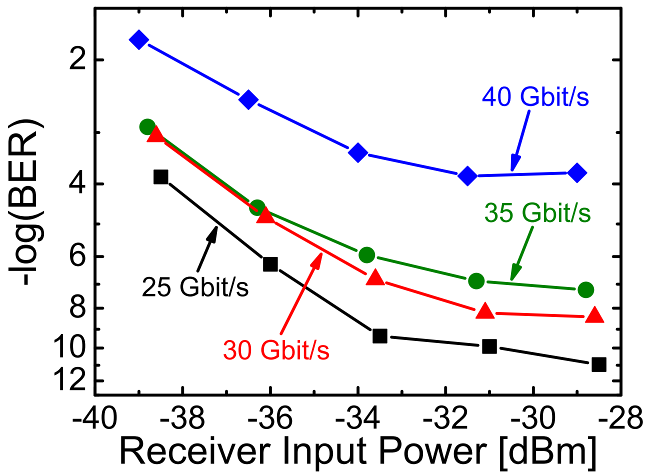

Fig. 5.5: Measured BER as a function of the receiver input power for different data rates.

5.3 Transmission of On-Off-Keyed Signals

Since OOK is commonly used in optical communication networks with data rates of several Gbit/s, the direct up and down conversion of these signals after an optical-electrical conversion is only possible using a very broadband RF front-end. The receiver sensitivity and the S-parameter measurements of the Rx/Tx modules prove that the Rx/Tx modules provide the necessary bandwidth for data rates up to 40 Gbit/s.

These measurements were, however, performed using a coherent measurement setup as it won't be available in the field. The LO signals of the transmitter and the receiver will be out of phase and exhibit also a frequency offset in a real application scenario. A two amplitude level OOK modulated signal may be recovered after the Rx using the sum of squares ($I^2 + Q^2$). This equals a power detection of the signal and requires in case of a down conversion to zero-IF, DC coupling on the Rx side. DC coupling entails several disadvantages like DC offsets as well as the need for broadband DC coupled IF amplifiers.

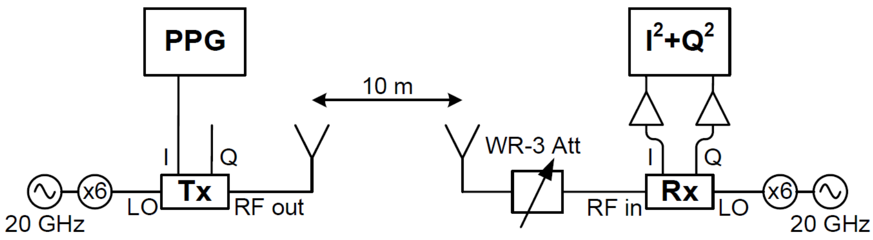

Fig. 5.6: Diagram of the measurement setup used to transmit a 10 Gbit/s OOK modulated signal over a distance of 10 m.

To overcome these problems, a near zero-IF approach is used. Instead of down converting to zero-IF, the LO of the receiver and the transmitter have a slight offset in the order of several kHz. Figure 5.6 shows the measurement setup used to transmit a 10 Gbit/s OOK modulated signal over a distance of 10 m in an incoherent way.

The LO signals were generated by two synthesizers with subsequent $\times 6$ frequency multipliers and have a slight offset resulting in a very low IF of 200 kHz. The OOK modulated baseband signal is generated by a PPG and DC coupled to the IF-I channel of the transmitter. At the RF ports of the Rx and Tx modules, WR-3 horn antennas with attached lenses are used. The plane convex lenses are made of high-density polyethylene (HD-PE) and reduce the path loss and improve the link alignment. The lenses are optimized of a center frequency of 240 GHz using the commercial ray tracing program Zemax. To keep the LNA of the receiver in linear operation, a WR-3 waveguide attenuator is placed between the receiving antenna and the Rx module. Omitting this attenuator would allow to bridge longer distances not limited by the size of the laboratory. The received I and Q signals are recorded using a high speed real time oscilloscope with a sample rate of 80 GS/s. The $I^2 + Q^2$ operation was performed offline using Matlab. Due to the down conversion to a near zero IF of 200 kHz (period of 5 µs), the received IF-I and IF-Q signals exhibit an envelope of the IF frequency (figure 5.7).

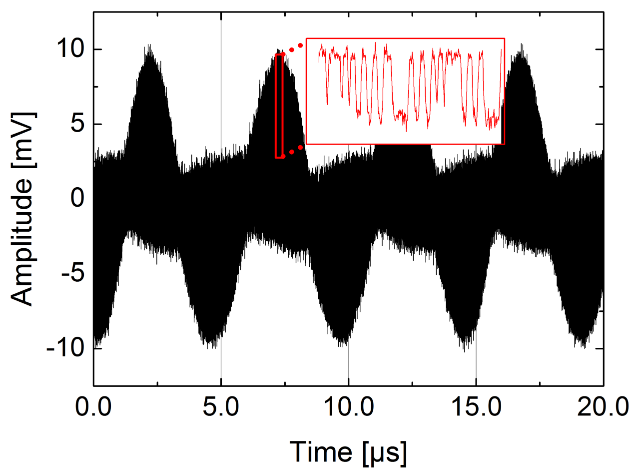

Fig. 5.7: Received IF-I signal at the receiver. The 10 Gbit/s OOK modulated signal was down converted to a near zero IF of 200 kHz with a period of 5 µs.

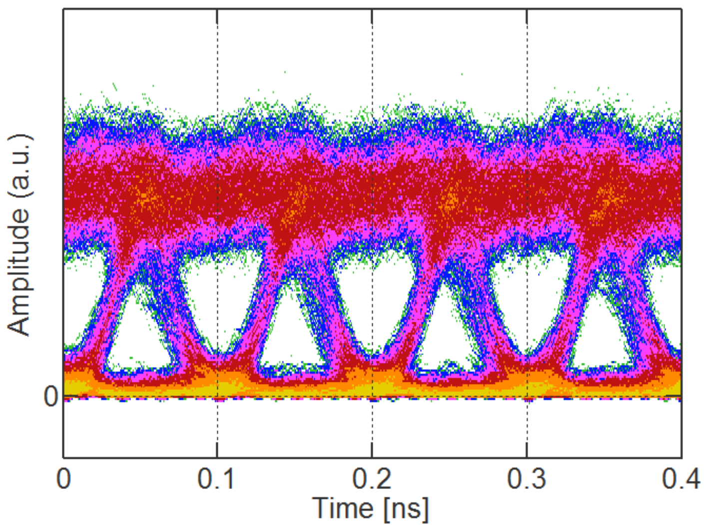

Fig. 5.8: Recovered 10 Gbit/s eye diagram after the sum of squares operation ($I^2 + Q^2$) of an OOK signal transmitted over a distance of 10 m.

The data is modulated on the IF signal and alternates between the IF-I and the IF-Q channel depending on the phasing of the LO at the Rx/Tx modules. Power detection on both IF channels is able to recover the baseband data signal. Due to the amplitude modulation, any amplitude mismatch between the IF-I and IF-Q channel will lead to additional noise on the recovered signal which degrades the performance and limits the achievable data rates. The sum of squares operation ($I^2 + Q^2$) is performed on the recorded IF channel data. Figure 5.8 shows the recovered eye diagram of the 10 Gbit/s OOK modulated signals after the sum of squares operation. A total of 10 kbits has been evaluated for the eye diagram. Due to the I/Q imbalance of about 1 dB, the logic one level is exposed to noise but the eye pattern remains open and suggests that higher data rates could be achieved.

5.4 Transmission of 16-QAM Signals

After the transmission of the two amplitude level OOK modulated signals, multilevel signals were examined. These experiments have been performed together with staff from the IHE at the KIT [91]. QAM is used in many communication applications like digital video broadcasting (DVB) and makes use of the I/Q functionality of the transmitter as well as the receiver. Compared to phase modulations, QAM imposes higher demands on the amplifier linearity. To test the ability of the 240 GHz link to support these signals, a 16-QAM modulated signal with a symbol rate of 5 Gbd (20 Gbit/s) has been used.
Figure 5.9 illustrates the employed measurement setup. The data signal was generated using a state of the art arbitrary waveform generator (AWG) which was connected to the I/Q inputs of the transmitter. The LO signals were again generated by a synthesizer with subsequent frequency multipliers by 6. An estimation of the link quality was made by a back to back configuration, where the modules are directly connected using a waveguide attenuator to ensure linear operation of the receiving amplifier. The output signals of the

IF channels have been amplified using two phase matched 24 dB broadband amplifiers and recorded using the same high speed real time scope (30 GHz, 80 GS/s) as used for the incoherent transmission of OOK modulated signals (chapter 5.3). The vector signal analysis software from Agilent has been used to measure the signal quality after down conversion into baseband.

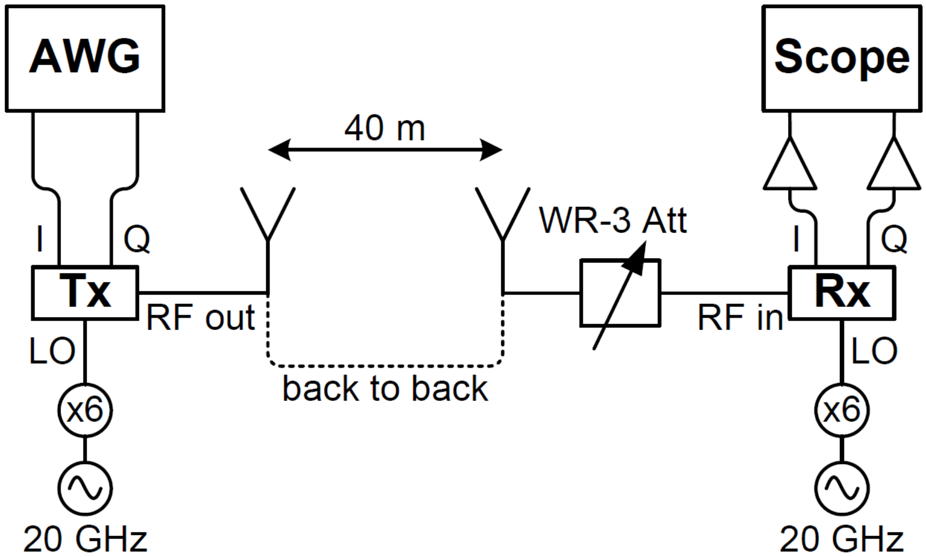

Fig. 5.9: Block diagram of the measurement setup for the transmission of QAM and PSK modulated signals. The measurements have been performed with a back to back connection (dashed lines) and wirelessly over a distance of 40 m.

Figure 5.10 shows the colored ideal locations of the symbols employing a 16-QAM modulation together with the constellation diagram of the received signal using the back to back setup. In an error free transmission, the constellation points of the received signal would lie directly on the colored locations. Clearly, the received symbols cannot be assigned to the 16 ideal symbols in the constellation diagram. The measured points form a circle in the constellation diagram of constant amplitude. Instead of discrete and distinguishable amplitude levels of a QAM modulation, only a small variation in the amplitude of the received signal is visible which indicates a saturated amplifier stage. Due to the employed waveguide attenuator at the Rx input, ensuring linearity in the Rx, this is most likely caused by the Tx output stage.

Due to the lack of a real broadband power amplifier in this frequency range, a LNA is used to post amplify the RF signal after the mixer in the Tx. Since the LNA is designed for high gain and moderate output power, it can be easily driven into saturation by large IF input signals to the mixer. Figure 5.11 is based on figure 4.65 and shows the measured output power of the transmitter as a function of the applied IF power for a fixed LO power level of 7 dBm. The colored lines refer to the colored dots in the constellation diagram (figure 5.10). The transfer curve is non linear and the output power changes only by 2.3 dB for an input change of 9.6 dB. This prohibits the transmission of modulation formats which rely on linear amplitude modulation (e.g., higher order QAM, 4-ASK,...). Reducing the IF input power to achieve a more linear behavior of the Tx module, worsens the signal to noise ratio to a level where a detection at the Rx becomes impossible due to the noise on the received signal. Besides the utilization of a power amplifier, a possible

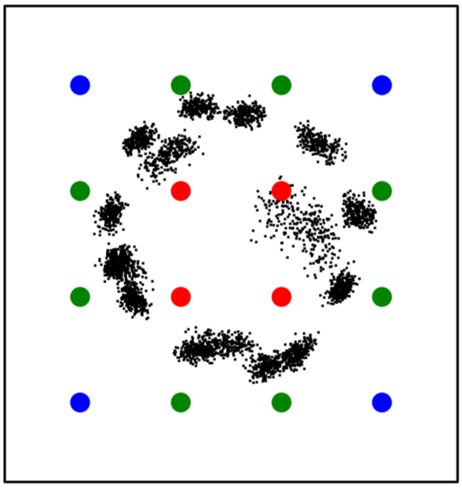

Fig. 5.10: Recovered constellation diagram of the 16-QAM modulated signal. The colored dots are the ideal symbol location of equal amplitudes. The black dots is the received signal.

solution to this problem is a redesign of the transmitter MMIC with reduced gain in the output amplifier to relax the compression of the last amplification stage.

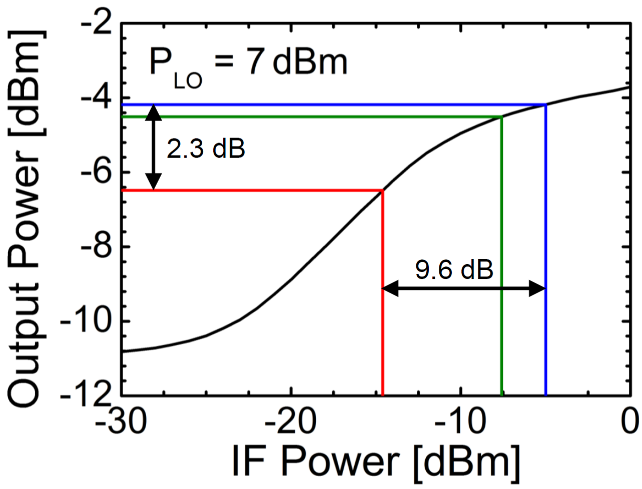

Fig. 5.11: Measured output power as a function of the IF power of the Tx module. A change of 9.6 dB of the input power results only in a change e of 2.3 dB at the output.

5.5 Transmission of PSK Signals

Due to the Tx nonlinearity, the transmission of multilevel amplitude modulated signals is hardly possible. Instead, phase modulated signals have been used to increase the spectral efficiency and the data rate.
QPSK and 8-PSK were examined with symbol rates of 5 and 10 GBd by Antes et. al. [105]. The incoherent measurement set up was the same as used with the QAM modulated signals (figure 5.9). The quality of the transmission has been analyzed using a back to back configuration as well as a wireless connection over a distance of 40 m. To ease proper link alignment, a combination of WR-3 antennas and HD-PE lenses has been used as described in chapter 5.3.
The PSK modulated signals were generated using an AWG with a sample rate of 10 GS/s which allows a maximum symbol rate of 10 GBd. For a QPSK modulation this equals a data rate of 20 Gbit/s and 30 Gbit/s with 8-PSK, respectively. Since the S-parameter and module measurements prove the wireless link to support an IF bandwidth of more than 20 GHz, higher symbol rates and thus higher data rates could be achieved if an AWG featuring a higher sampling rate would have been available.
Figure 5.12 shows the measured constellation diagrams for the QPSK modulated signals. To analyze the signal quality at the receiver side, the error vector magnitude (EVM) has been measured. The EVM is calculated based on the vector between the ideal location of a symbol in the constellation diagram and the location of the received symbol:

$$EVM = \sqrt{\frac{P_{error}}{P_{reference}}} \cdot 100\% \tag{5.1}$$

Where P_{error} is the root mean square (RMS) power of the error vector and $P_{reference}$ is, with this single carrier transmission, the power level of the constellation point with the highest power.
The plotted constellation diagrams are averaged over 51200 symbols and the QPSK transmission achieves an EVM better than 11% in all configurations.

The measurement results for the 8-PSK modulation are plotted in figure 5.13. An EVM value better than 16% has been achieved in all transmission cases. The radio channel has only a slight influence on the EVM and the constellation diagrams. In some cases, the EVM even improved in the wireless transmission over 40 m. This is most likely caused by an imperfect attenuation in the back to back setup. Due to the high gain in the receiver, the input power in this direct connection is probably still too high even after the WR-3 attenuator and causes nonlinear behavior of the receiving amplifier.
These measurements show the ability of the Rx/Tx module to transmit higher order phase modulated signals with data rates of 30 Gbit/s with distributed unsynchronized receiver and transmitter. The comparison between the back to back setup and the wireless transmission over 40 m show only a small effect of the line of sight channel on the signal quality.

After characterization of the Tx and Rx modules in the laboratory, a long range data transmission over a distance of 1 km was performed by the scientific staff of the KIT. The main challenge is the compensation of the high free space path loss around 240 GHz. According to [81], the path loss at 240 GHz over a distance d of 1 km equals:

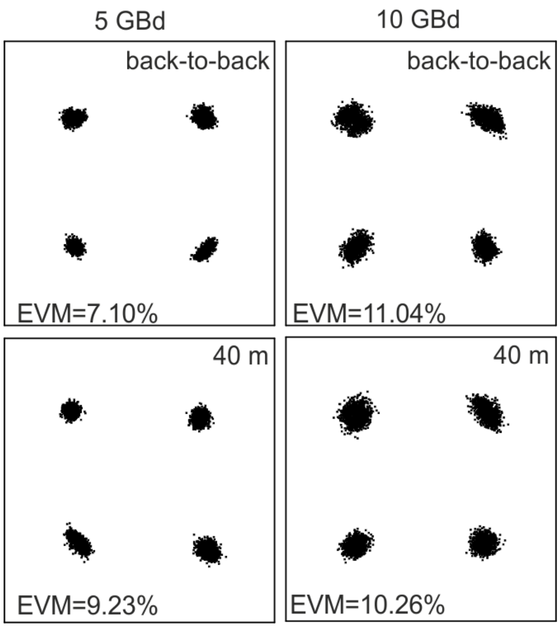

Fig. 5.12: Constellation diagram of the received 5 and 10 GBd QPSK modulation. The upper diagrams show the results using a back to back configuration while the lower constellation diagrams employ a wireless transmission over 40 m.

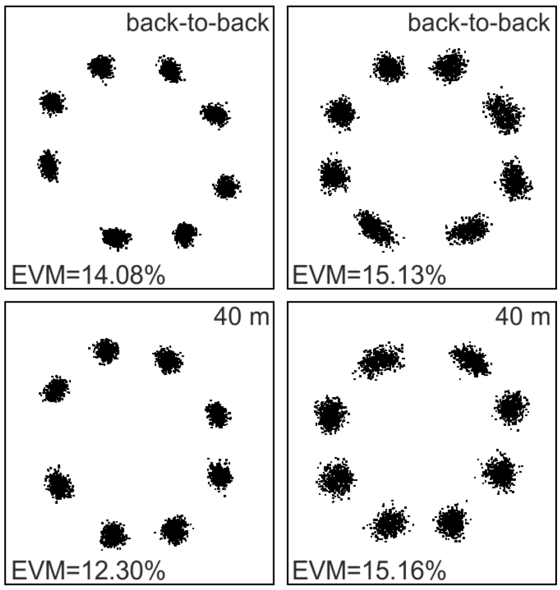

Fig. 5.13: Measured constellation diagram for the 5 and 10 GBd symbol rate using 8-PSK modulation. The upper diagrams have been measured using a back to back set up and the lower diagrams are for a wireless transmission over a distance of 40 m.

$$L_0 = 20log\left(\frac{4\pi f_c d}{c}\right) \tag{5.2}$$

$$L_0 = 140\ dB/km \tag{5.3}$$

In addition to the free space path loss, the attenuation by atmospheric gases has to be taken into account. According to the recommendation of the International Telecommunication Union (ITU), the atmospheric attenuation of a radio link at 240 GHz for a temperature of 293 K and 59% humidity equals 3.65 dB/km [92].
To compensate the path loss and the atmospheric attenuation, the modules need to be combined with a high gain antenna. A Cassegrain type antenna has been chosen to provide high gain and high directivity at a reasonable size. Figure 5.14 shows a photograph of the Cassegrain antenna manufactured at RPG. The calculated gain of the antenna is 55.1 dBi with a half power beamwidth (HPBW) of 0.35°.

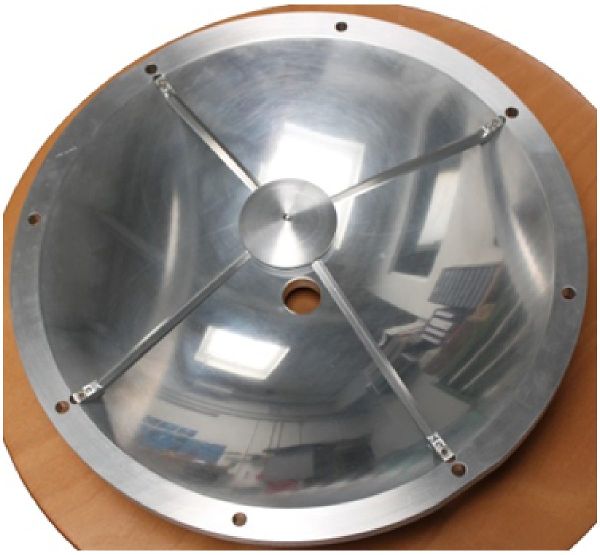

Fig. 5.14: Photograph of the Cassegrain antenna manufactured by RPG.

Based on the transmitter output power, the path losses and the antenna gain, a link budget for the radio link at 240 GHz over a distance of 1 km can be summarized. Table 5.1 shows the link budget and the calculated receive power for the radio link.

Tx Power	-3.6 dBm
Tx Antenna Gain	55.1 dB
Path Loss	140 dB/km
Atmospheric Attenuation	3.65 dB
Rx Antenna Gain	55.1 dB
Receive Power	-37.05 dBm

Table 5.1: Link budget for the wireless data transmission around 240 GHz.

Since the Rx and Tx are separated physically, the usage of a common LO source as used with the receiver sensitivity measurement in section 5.2 was not possible. To transmit the data with two unsychronized LO sources at the Rx and the Tx site, a QPSK modulation was employed. A data rate of 24 Gbit/s was achieved using a symbol rate of 12 Gbd. The measured EVM was 22.6% which equals a BER of less than 10^{-5}. The measured constellation diagram is shown in figure 5.15.

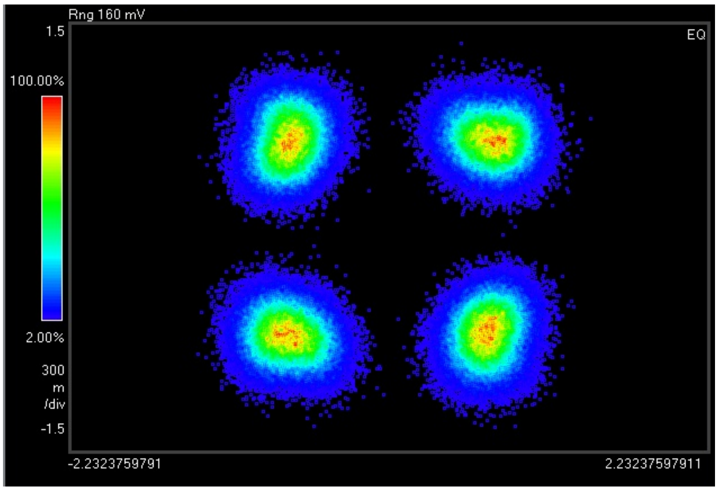

Fig. 5.15: Measured constellation diagram of the QPSK modulated signal with a symbol rate of 12 GBd at the receiver transmitted over a distance of 1.1 km at 240 GHz.

5.6 Summary

After the realization and evaluation of 240 GHz quadrature receiver and transmitter modules in chapter 4, the in-system characterization and evaluation of these modules was covered in this chapter. Figure 5.16 summarizes the achieved data rates and distances for the different employed modulation formats.

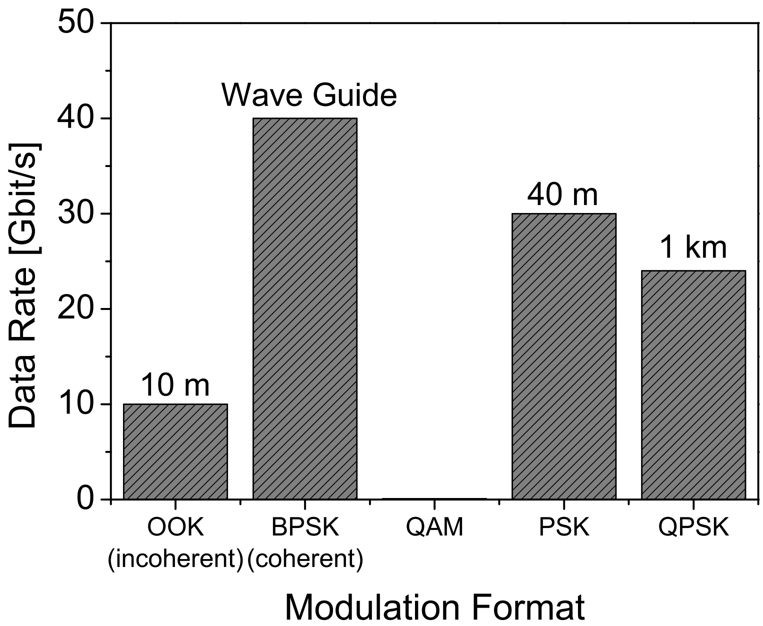

Fig. 5.16: Achieved data rates depending on the employed modulation format and the distance of the wireless transmission.

IF to IF S-parameter measurements provide in depth information about the conversion gain, group delay and amplitude imbalances between the different I/Q channel combinations. The S-parameter show virtually no difference between the possible IF channel combinations and proves the very low imbalance of the IF channels in the transmitter and the receiver. Low I/Q imbalanced is essential for complex modulation formats like QAM or PSK as well as the power detection by the sum of squares ($I^2 + Q^2$).
BPSK modulated signals with data rates of up to 40 Gbit/s are transmitted with a waveguide attenuator between the Tx and the Rx module using a common LO source. BERs better than 10^{-4} at 40 Gbit/s underscore the ability of the 240 GHz receiver and transmitter modules to support high capacity wireless transmission in the mmW frequency range.
In most application scenarios, the data transmission will be performed using two unsychronized LO sources and physically separated Rx and Tx modules. Data rates of up to 10 Gbit/s with OOK modulation and up to 30 Gbit/s using BPSK modulation are measured over distances of 10 m and 40 m, respectively, with independent LO sources. After integration into the weather-proof casing from RPG featuring 55.1 dBi antenna gain, long range transmissions over a distance of 1.1 km were executed by the scientific staff from the KIT. A maximum symbol rate of 12 GBd was achieved with a QPSK modulation. This equals a data rate of 24 Gbit/s over a distance of 1.1 km. Figure 5.17 illustrates the reported state of the art of wireless data transmission and the achieved results using the circuits from this work. Due to the nonlinear behavior of the Tx module, it is hardly possible to transmit broadband multilevel signals. To overcome this issue, the Tx module was replaced by Koenig et. al. by a photonic transmit mixer [106]. The 100 Gbit/s rate was achieved using this photonic mixer to transmit signals using 16QAM modulation which are then received and down converted by the 240 GHz receiver module.

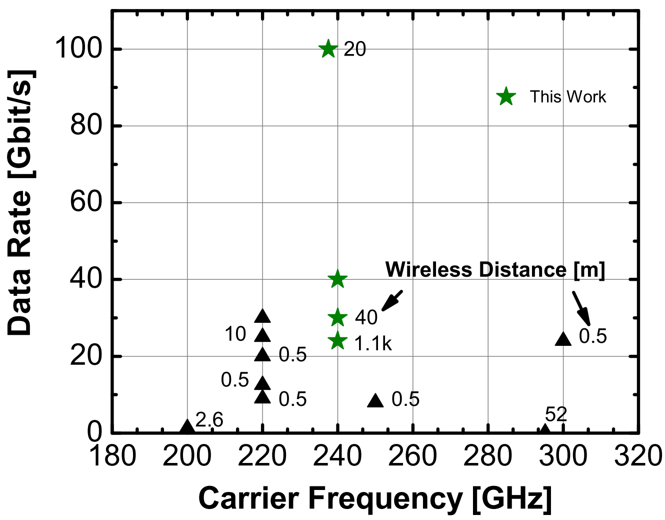

Fig. 5.17: Overview of reported wireless transmission experiments in the mmW frequency range as a function of the carrier frequency.

A comparison of the achieved data rates and employed modulation types of reported data transmission experiments in the frequency range between 200 and 300 GHz is summarized in table 5.2. The results of this work extend the state of the art with respect to data rate as well as distance of the radio link. This is the first time data rates of 40 Gbit/s are transmitted in a SISO configuration over a wireless link.

f_c [GHz]	Data Rate [Gbit/s]	Distance [m]	Modulation Format	Year and Ref.
200[1]	1.25	2.6	ASK	2010 [33]
220	12.5	0.5	-	2011 [30]
220	30	-	BPSK	2012 [34]
220	25	10	OOK	2012 [99]
220	20	0.5	OOK	2012 [94]
220	9	0.5	OFDM-QPSK	2012 [94]
250[1]	8	0.5	ASK	[35]
295.2	0.096	52	OFDM-64QAM	2010 [36]
300[1]	24	0.5	ASK	2012 [37]
240	30	40	8-PSK	this work
240	40	-	BPSK	this work
240	24	1100	QPSK	this work

[1]Employing a photonic transmitter.

Table 5.2: Reported wireless transmission experiments between 200 and 300 GHz based on mmW technology

6 Summary

Wireless communication in the upper millimeter wave frequency range is able to satisfy the increasing demand for broadband wireless connections and opens up new application scenarios beyond those addressed by today's commercially available systems. This thesis explores the design of extremely broadband monolithically integrated millimeter wave mixers to realize wideband receiver and transmitter MMICs. To use the large available bandwidth in the millimeter wave frequency range, new mixers with very large IF and RF bandwidth need to be developed. The advances in compound semiconductor technology allow the design of active integrated circuits which operate at frequencies above 200 GHz. The metamorphic high electron mobility transistor, developed at the Fraunhofer IAF features transit and oscillation frequencies of several hundred GHz. Based on this very fast semiconductor technology, different active and passive mixer stages in the upper millimeter wave frequency range have been successfully designed, manufactured and analyzed to exploit the advantages of the large absolute bandwidth available at these frequencies. Simulations and measurements on manufactured MMICs are used to investigate the advantages and disadvantages of the different mixer topologies. The realized active mixers have shown higher conversion gain but require a more sophisticated circuit design compared to passive mixer cells. The presented Gilbert cell mixer from chapter 4.2.2 is the first Gilbert cell mixer fabricated in the mHEMT technology in the mmW frequency range. It features a conversion gain of more than 12 dB at 77 GHz and even more than 18 dB when the RF balun is excluded. Passive mixers have shown superior performance with respect to bandwidth and linearity compared to their active counter parts. The advantages of small size, robustness through lower complexity and above all, larger operational bandwidth made the passive mixer cells the first choice for the realization of fully integrated receiver and transmitter MMICs.

Passive couplers and hybrids are key components to form multifunctional fully integrated communication MMICs. Different couplers were designed to enable the realization of balanced and I/Q mixers and to investigate the performance of different coupling structures with respect to bandwidth, losses and feasibility of integration. Wideband Lange couplers for frequencies above 200 GHz have shown excellent performance with respect to amplitude and phase balance over a large frequency range. Together with their lower space requirements compared to other coupling structures, they are best suited for the design of integrated balanced and I/Q mixers.

Combined with the Lange coupler and an LNA, a single balanced resistive mixer is used to create a fully integrated chipset for gigabit communication above 200 GHz. This first subharmonic receiver/transmitter chipset operating at a center frequency of 240 GHz with I/Q functionality is a major achievement in this context. A radio link around 240 GHz, based on these MMICs was able to transmit data with up to 40 Gbit/s for the first time in a single-input single-output (SISO) configuration. In a long range experiment, they allowed the transmission of up to 24 Gbit/s over a distance of 1.1 km using BPSK modulation. The broadband IF and RF bandwidth enable the seamless integration into fiber optical networks which still use simple modulation formats like OOK. Furthermore enables the I/Q functionality of the Rx and Tx the transmission of complex modulation formats like PSK. These key results extend the existing state of the art of wireless data transmission above 200 GHz and prove the ability to close the gap between wireless and wired data transmission at multi gigabit data rates.

6.1 Outlook

The presented transceiver circuits around 240 GHz are the first subharmonic mmW receiver and transmitter MMICs supporting I/Q functionality combined with a very broadband IF and RF bandwidth. Due to the lack of a power amplifier which supports the same RF bandwidth as the receiver, the transmitter employs currently the LNA to post amplify the upconverted RF signal. This solution does not fulfill the required linearity to transmit multilevel signals like QAM as shown in section 5.4.
LNAs are usually designed to provide high gain and are typically operated under small signal conditions. The combination of high gain and low output power is the root cause for the non-linear behavior of the transmitter MMIC. Replacing the LNA in the transmitter by a linear power amplifier may enable the transmission of higher order modulations like 256-QAM in the future.
The 240 GHz receiver module was already combined with a photonic transmitter at 237.5 GHz and was able to receive data with up to 100 Gbit/s in a SISO configuration over a distance of 20 m [106]. This experiment uses a 16-QAM modulation with a symbol rate of 25 Gbd and proves the ability of the receiver to support higher order modulations at exceptionally high data rates. In a next step, a linear transmitter circuit would enable the realization of an all MMIC based wireless link supporting data rates of 100 Gbit/s and beyond.

Acknowledgement

This work would not have been possible without the help of several people. First of all, I would like to thank my academic supervisor Prof. Dr. Ingmar Kallfass for giving me the chance to work on a PhD thesis at the cutting edge of high frequency circuit design. During the entire time he supported me with scientific advices, hours of technical discussions and countless consultation hours.

I am very grateful to Prof. Dr. Oliver Ambacher, head of the Fraunhofer IAF, for giving me the opportunity to work as a doctoral student at the high frequency devices and circuits department and supporting me with valuable scientific advices. Dr. Michael Schlechtweg, head of the the high frequency devices and circuits department at the Fraunhofer IAF from whom experience I have been able to profit during my research work.
A great amount of continuous support came from the entire staff of the high frequency devices and circuits department and I would like to thank every single colleague for the support given to me through the time at Fraunhofer IAF. I am obliged to Dr. Axel Tessmann for many hours of technical discussions far beyond solely MMIC design. Reliable measurements at mmW frequencies require precise work and a lot of experience and I am grateful for the support which I have experienced here by Hermann Massler and Sandrine Wagner who spent many hours in the lab for measurement setup and circuit characterization. I would also like to express my gratitude to the staff of the technology and epitaxy department of the Fraunhofer IAF for excellent epitaxial growth and wafer processing. In particular, I thank Dr. Arnulf Leuther for all the time and effort during device processing and in depth explanation of the device physics.

Most of the data transmission experiments were carried out at the KIT together with the scientific staff from IHE and IPQ and it was a pleasure to work together with Jochen Antes from the IHE who kept me motivated by his great team spirit and effort he put into our measurement campaigns. Swen König and Florian Boes from the IPQ helped me with their in-depth knowledge of photonics and optical data transmission as well as a their positive attitude.
After working on this topic for several years, the view of a non-involved person is invaluable and I would like to express my gratitude to Dr. Friederike Brendel for proofreading the manuscript and supporting me with a lot of tips and encouragement.
After all, a very special thank you is due to Michael Kuri for the help in all situations of life and especially to Daniel Bruch who backed me up during all kinds of struggle and gave me continuous support through ups and downs in all areas of life.

Finally, I would like to thank Silke Zaulig and my entire family for the support and encouragement over the last years - I couldn't have done it without you.

7 Appendix

7.1 Metamorphic HEMT

7.1.1 Layer Composition

Figure 7.1 shows the layer structure of the 50 nm and the 35 nm mHEMT [54].

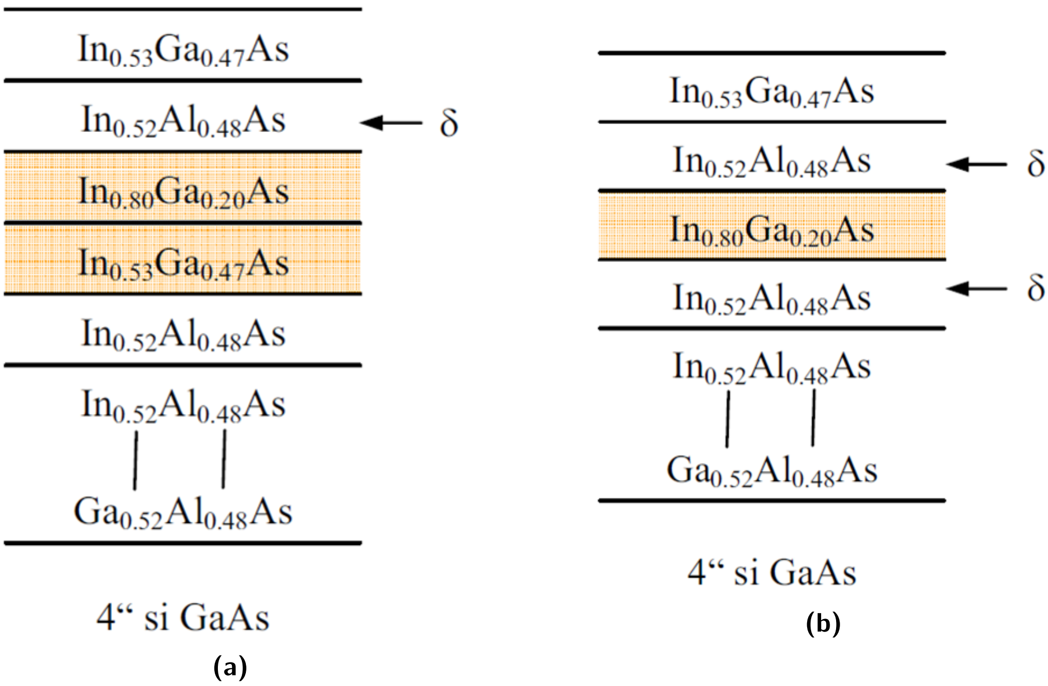

Fig. 7.1: Layer structure of the 50 and 35 nm mHEMT heterostructure. The 35 nm mHEMT layer sequence includes a double-side doped single $In_{0.80}Ga_{0.2}As$ channel to avoid short channel effects [54].

7.2 Verilog A Model of a Resistive FET Mixer

```
`include "disciplines.vams"
`include "constants.vams"

module ResFET(g,d,s);
          electrical g,d,s;
    real Rds,vin;
    parameter real a = 12;
    parameter real b = 10.1;
    parameter real c = 12.8;

    analog begin

      Rds = a+b*exp(-c*V(g,s));
      I(d,s) <+ V(d,s)/Rds;

    end

endmodule
```

References

[1] Cisco Systems Inc. Cisco Visual Networking Index: Forecast and Methodology, 2011 - 2016, May 2012.

[2] IEEE. *Wireless LAN Medium Access Control (MAC) and Physical Layer (PHY) Specifications (IEEE Std 802.11-2012)*. Institute of Electrical and Electronics Engineers, Inc., March 2012.

[3] Ericsson AB. MINI-LINK PT 6010 ETSI datasheet, 2011.

[4] EasyA. Website of the easy-a project. http://www.easy-a.de.

[5] WiGig Alliance. Defining the future of multi-gigabit wireless communications, 2010.

[6] Sebastian Priebe. *Towards THz Communications: Propagation Studies, Indoor Channel Modeling and Interference Investigations*. PhD thesis, Technische Universität Braunschweig, 2013.

[7] W. Deal, X.B. Mei, K.M.K.H. Leong, V. Radisic, S. Sarkozy, and R. Lai. THz Monolithic Integrated Circuits Using InP High Electron Mobility Transistors. *IEEE Transactions on Terahertz Science and Technology*, 1(1):25–32, sept. 2011.

[8] A. Leuther, S. Koch, A. Tessmann, I. Kallfass, T. Merkle, H. Massler, R. Loesch, M. Schlechtweg, S. Saito, and O. Ambacher. 20 nm metamorphic HEMT with 660 GHz ft. In *Compound Semiconductor Week (CSW/IPRM), 2011 and 23rd International Conference on Indium Phosphide and Related Materials*, pages 1–4, may 2011.

[9] H. Rucker, B. Heinemann, and A. Fox. Half-Terahertz SiGe BiCMOS technology. In *Silicon Monolithic Integrated Circuits in RF Systems (SiRF), 2012 IEEE 12th Topical Meeting on*, pages 133–136, jan. 2012.

[10] R. Lai, X.B. Mei, W.R. Deal, W. Yoshida, Y.M. Kim, P.H. Liu, J. Lee, J. Uyeda, V. Radisic, M. Lange, T. Gaier, L. Samoska, and A. Fung. Sub 50 nm InP HEMT Device with Fmax Greater than 1 THz. In *Electron Devices Meeting, 2007. IEDM 2007. IEEE International*, pages 609–611, dec. 2007.

[11] W.R. Deal, K. Leong, V. Radisic, S. Sarkozy, B. Gorospe, J. Lee, P. H Liu, W. Yoshida, J. Zhou, M. Lange, R. Lai, and X.B. Mei. Low Noise Amplification at 0.67 THz Using 30 nm InP HEMTs. *IEEE Microwave and Wireless Components Letters*, 21(7):368–370, 2011.

[12] A. Tessmann, A. Leuther, H. Massler, and M. Seelmann-Eggebert. A High Gain 600 GHz Amplifier TMIC Using 35 nm Metamorphic HEMT Technology. In *Compound Semiconductor Integrated Circuit Symposium (CSICS), 2012 IEEE*, pages 1–4, 2012.

[13] W.H. Haydl, W. Heinrich, R. Bosch, M. Schlechtweg, P. Tasker, and J. Braunstein. Design data for millimeter wave coplanar circuits. In *Microwave Conference, 1993. 23rd European*, pages 223–228, 1993.

[14] Lei Wang, Yong-Zhong Xiong, Bo Zhang, Lim Teck-Guan, and Xiaojun Yuan. Lange coupler design for Si-ICs up to 170 GHz in 0.13 um SiGe BiCMOS. In *Radio-Frequency Integration Technology, 2009. RFIT 2009. IEEE International Symposium on*, pages 64–67, 9 2009-dec. 11 2009.

[15] Lei Wang, Yong-Zhong Xiong, Bo Zhang, San-Ming Hu, Teck-Guan Lim, and Xiao-Jun Yuan. 0.7-dB Insertion-Loss D-Band Lange Coupler Design and Characterization in 0.13 um SiGe BiCMOS Technology. *Journal of Infrared, Millimeter, and Terahertz Waves*, 31:1136–1145, 2010.

[16] G. Prigent, E. Rius, H. Happy, K. Blary, and S. Lepilliet. Design of Wide-Band Branch-Line Coupler in the G-Frequency Band. In *Microwave Symposium Digest, 2006. IEEE MTT-S International*, pages 986–989, june 2006.

[17] J. Langst, S. Diebold, H. Massler, A. Tessmann, A. Leuther, T. Zwick, and I. Kallfass. A balanced 150-240 GHz amplifier MMIC using airbridge transmission lines. In *Integrated Nonlinear Microwave and Millimetre-Wave Circuits (INMMIC), 2012 Workshop on*, pages 1–3, 2012.

[18] V. Radisic, W.R. Deal, K.M.K.H. Leong, X.B. Mei, W. Yoshida, Po-Hsin Liu, J. Uyeda, A. Fung, L. Samoska, T. Gaier, and R. Lai. A 10-mW Submillimeter-Wave Solid-State Power-Amplifier Module. *Microwave Theory and Techniques, IEEE Transactions on*, 58(7):1903–1909, july 2010.

[19] Yanfei Mao, K. Schmalz, J. Borngraber, and J.C. Scheytt. A 245 GHz CB LNA and SHM mixer in SiGe technology. In *Silicon Monolithic Integrated Circuits in RF Systems (SiRF), 2012 IEEE 12th Topical Meeting on*, pages 5–8, jan. 2012.

[20] S.E. Gunnarsson, N. Wadefalk, I. Angelov, H. Zirath, I. Kallfass, and A. Leuther. A 220 GHz (G-Band) Microstrip MMIC Single-Ended Resistive Mixer. *Microwave and Wireless Components Letters, IEEE*, 18(3):215–217, march 2008.

[21] E. Ojefors, B. Heinemann, and U.R. Pfeiffer. A 220 GHz subharmonic receiver front end in a SiGe HBT technology. In *Radio Frequency Integrated Circuits Symposium (RFIC), 2011 IEEE*, pages 1–4, june 2011.

[22] Yu Yan, Y.B. Karandikar, S.E. Gunnarsson, B.M. Motlagh, S. Cherednichenko, I. Kallfass, A. Leuther, and H. Zirath. Monolithically Integrated 200-GHz Double-Slot Antenna and Resistive Mixers in a GaAs-mHEMT MMIC Process. *Microwave Theory and Techniques, IEEE Transactions on*, 59(10):2494–2503, oct. 2011.

[23] I. Kallfass, A. Tessmann, H. Massler, A. Leuther, M. Schlechtweg, and O. Ambacher. A 200 GHz active heterodyne receiver MMIC with low sub-harmonic LO power requirements for imaging frontends. In *Microwave Integrated Circuits Conference, 2009. EuMIC 2009. European*, pages 45–48, sept. 2009.

[24] Maarten Tytgat, Michiel Steyaert, and Patrick Reynaert. A 186 to 212 GHz Downconverter in 90 nm CMOS. *Journal of Infrared, Millimeter, and Terahertz Waves*, 33:1085–1103, 2012.

[25] O. Inac, B. Cetinoneri, M. Uzunkol, Y.A. Atesal, and G.M. Rebeiz. Millimeter-wave and thz circuits in 45-nm soi cmos. In *Compound Semiconductor Integrated Circuit Symposium (CSICS), 2011 IEEE*, pages 1–4, oct. 2011.

[26] E. Ojefors and U.R. Pfeiffer. A 650 GHz SiGe receiver front-end for terahertz imaging arrays. In *Solid-State Circuits Conference Digest of Technical Papers (ISSCC), 2010 IEEE International*, pages 430–431, feb. 2010.

[27] E. Ojefors, B. Heinemann, and U.R. Pfeiffer. Subharmonic 220- and 320-GHz SiGe HBT Receiver Front-Ends. *Microwave Theory and Techniques, IEEE Transactions on*, 60(5):1397–1404, may 2012.

[28] A. Tessmann, H. Massler, U. Lewark, S. Wagner, I. Kallfass, and A. Leuther. Fully Integrated 300 GHz Receiver S-MMICs in 50 nm Metamorphic HEMT Technology. In *Compound Semiconductor Integrated Circuit Symposium (CSICS), 2011 IEEE*, pages 1–4, 2011.

[29] S.E. Gunnarsson, N. Wadefalk, J. Svedin, S. Cherednichenko, I. Angelov, H. Zirath, I. Kallfass, and A. Leuther. A 220 GHz Single-Chip Receiver MMIC With Integrated Antenna. *Microwave and Wireless Components Letters, IEEE*, 18(4):284–286, april 2008.

[30] M. Abbasi, S.E. Gunnarsson, N. Wadefalk, R. Kozhuharov, J. Svedin, S. Cherednichenko, I. Angelov, I. Kallfass, A. Leuther, and H. Zirath. Single-Chip 220-GHz Active Heterodyne Receiver and Transmitter MMICs With On-Chip Integrated Antenna. *Microwave Theory and Techniques, IEEE Transactions on*, 59(2):466 –478, feb. 2011.

[31] Munkyo Seo, Miguel Urteaga, Adam Young, Jonathan Hacker, Anders Skalare, Robert Lin, and Mark Rodwell. A single-chip 630 GHz transmitter with 210 GHz sub-harmonic PLL local oscillator in 130 nm InP HBT. In *Microwave Symposium Digest (MTT), 2012 IEEE MTT-S International*, pages 1–3, june 2012.

[32] K. Schmalz, J. Borngraber, B. Heinemann, H. Ruecker, and J. C Scheytt. A 245 GHz transmitter in SiGe technology. In *Radio Frequency Integrated Circuits Symposium (RFIC), 2012 IEEE*, pages 195–198, 2012.

[33] G. Ducournau, P. Szriftgiser, D. Bacquet, A. Beck, T. Akalin, E. Peytavit, M. Zaknoune, and J.F. Lampin. Optically power supplied Gbit/s wireless hotspot using 1.55 μm THz photomixer and heterodyne detection at 200 GHz. *Electronics Letters*, 46(19):1349–1351, 16 2010.

[34] J. Antes, S. Konig, A. Leuther, H. Massler, J. Leuthold, O. Ambacher, and I. Kallfass. 220 GHz Wireless Data Transmission Experiments up to 30 Gbit/s. In *Microwave Symposium Digest (MTT), 2012 IEEE MTT-S International*, pages 1 –3, june 2012.

[35] H.-J. Song, K. Ajito, A. Hirata, A. Wakatsuki, T. Furuta, N. Kukutsu, and T. Nagatsuma. Multi-gigabit wireless data transmission at over 200-GHz. In *Infrared, Millimeter, and Terahertz Waves, 2009. IRMMW-THz 2009. 34th International Conference on*, pages 1–2, sept. 2009.

[36] C. Jastrow, S. Priebe, B. Spitschan, J. Hartmann, M. Jacob, T. Kurner, T. Schrader, and T. Kleine-Ostmann. Wireless digital data transmission at 300 GHz. *Electronics Letters*, 46(9):661–663, 29 2010.

[37] H.-J. Song, K. Ajito, Y. Muramoto, A. Wakatsuki, T. Nagatsuma, and N. Kukutsu. 24 Gbit/s data transmission in 300 GHz band for future terahertz communications. *Electronics Letters*, 48(15):953–954, 19 2012.

[38] Pei-Lin Chen, Shenq-Tsong Chang, Shuen-Te Ji, Shu-Chuan Lin, Han-Hsuan Lin, Ho-Lin Tsay, Po-Hsuan Huang, Wei-Chieh Chiang, Wei-Cheng Lin, San-Liang Lee, Hen-Wai Tsao, Jin-Pu Wu, and Jingshown Wu. Demonstration of 16 channels 10 Gb/s WDM free space transmission over 2.16 km. In *IEEE/LEOS Summer Topical Meetings, 2008 Digest of the*, pages 235 –236, july 2008.

[39] A. Hirata, M. Harada, and T. Nagatsuma. 120-GHz wireless link using photonic techniques for generation, modulation, and emission of millimeter-wave signals. *Lightwave Technology, Journal of*, 21(10):2145–2153, oct. 2003.

[40] B.D. Jackson, G. de Lange, T. Zijlstra, M. Kroug, J.W. Kooi, J.A. Stern, and T.M. Klapwijk. Low-noise 0.8-0.96- and 0.96-1.12-THz superconductor-insulator-superconductor mixers for the herschel space observatory. *Microwave Theory and Techniques, IEEE Transactions on*, 54(2):547–558, feb. 2006.

[41] Wenlei Shan, Shengcai Shi, T. Matsunaga, M. Takizawa, A. Endo, T. Noguchi, and Y. Uzawa. Design and Development of SIS Mixers for ALMA Band 10. *Applied Superconductivity, IEEE Transactions on*, 17(2):363–366, june 2007.

[42] Ilja N. Bronstein, Konstantin A. Semendjajew, Gerhard Musiol, and Heiner Mühlig. *Taschenbuch der Mathematik*. Deutsch (Harri), 2000.

[43] K. Yhland. Simplified Analysis of Resistive Mixers. *Microwave and Wireless Components Letters, IEEE*, 17(8):604–606, 2007.

[44] R.M. Fano. *Theoretical Limitations on the Broadband Matching of Arbitrary Impedances*. Technical report: Research Laboratory of Electronics. MIT Res. Lab. of Electronics, 1948.

[45] Thomas H. Lee. *The Design of Cmos Radio-Frequency Integrated Circuits*. Cambridge Univ Pr, 2006.

[46] Stephen A. Maas. *Nonlinear Microwave and RF Circuits, 2nd Edition*. Artech House Publishers, 2003.

[47] Barrie Gilbert. A precise four-quadrant multiplier with subnanosecond response. *Solid-State Circuits, IEEE Journal of*, 3(4):365–373, 1968.

[48] C.-H. Jan, M. Agostinelli, H. Deshpande, M.A. El-Tanani, W. Hafez, U. Jalan, L. Janbay, M. Kang, H. Lakdawala, J. Lin, Y.-L. Lu, S. Mudanai, J. Park, A. Rahman, J. Rizk, W.-K. Shin, K. Soumyanath, H. Tashiro, C. Tsai, P. Vandervoorn, J.-Y. Yeh, and P. Bai. RF CMOS technology scaling in High-k/metal gate era for RF SoC (system-on-chip) applications. In *Electron Devices Meeting (IEDM), 2010 IEEE International*, pages 27.2.1–27.2.4, dec. 2010.

[49] C.-H. Jan, P. Bai, S. Biswas, M. Buehler, Z.-P. Chen, G. Curello, S. Gannavaram, W. Hafez, J. He, J. Hicks, U. Jalan, N. Lazo, J. Lin, N. Lindert, C. Litteken, M. Jones, M. Kang, K. Komeyli, A. Mezhiba, S. Naskar, S. Olson, J. Park, R. Parker, L. Pei, I. Post, N. Pradhan, C. Prasad, M. Prince, J. Rizk, G. Sacks, H. Tashiro, D. Towner, C. Tsai, Y. Wang, L. Yang, J.-Y. Yeh, J. Yip, and K. Mistry. A 45nm low power system-on-chip technology with dual gate (logic and I/O) high-k/metal gate strained silicon transistors. In *Electron Devices Meeting, 2008. IEDM 2008. IEEE International*, pages 1–4, dec. 2008.

[50] S.T. Nicolson, A. Tomkins, K.W. Tang, A. Cathelin, D. Belot, and S.P. Voinigescu. A 1.2V, 140GHz receiver with on-die antenna in 65nm CMOS. In *Radio Frequency Integrated Circuits Symposium, 2008. RFIC 2008. IEEE*, pages 229–232, 2008.

[51] C.-L. Ko, C.-H. Li, C.-N. Kuo, M.-C. Kuo, and D.-C. Chang. A 210-GHz Amplifier in 40-nm Digital CMOS Technology. *Microwave Theory and Techniques, IEEE Transactions on*, 61(6):2438–2446, 2013.

[52] R.J. Gutmann and D.J. Fryklund. Characterization of Linear and Nonlinear Properties of GaAs MESFET's for Broad-Band Control Applications. *Microwave Theory and Techniques, IEEE Transactions on*, 35(5):516–521, may 1987.

[53] S.E. Gunnarsson, D. Kuylenstierna, and H. Zirath. Analysis and Design of Millimeter-Wave FET-Based Image Reject Mixers. *Microwave Theory and Techniques, IEEE Transactions on*, 55(10):2065–2074, oct. 2007.

[54] A. Leuther, A. Tessmann, I. Kallfass, H. Massler, R. Loesch, M. Schlechtweg, M. Mikulla, and O. Ambacher. Metamorphic HEMT technology for submillimeter-wave MMIC applications. In *Indium Phosphide Related Materials (IPRM), 2010 International Conference on*, pages 1–6, 2010.

[55] A. Leuther, A. Tessmann, I. Kallfass, R. Losch, M. Seelmann-Eggebert, N. Wadefalk, F. Schafer, J.D. Gallego Puyol, M. Schlechtweg, M. Mikulla, and O. Ambacher. Metamorphic HEMT technology for low-noise applications. In *Indium Phosphide Related Materials, 2009. IPRM '09. IEEE International Conference on*, pages 188–191, may 2009.

[56] A. Leuther, A. Tessmann, H. Massler, R. Losch, M. Schlechtweg, M. Mikulla, and O. Ambacher. 35 nm metamorphic HEMT MMIC technology. In *Indium Phosphide and Related Materials, 2008. IPRM 2008. 20th International Conference on*, pages 1–4, may 2008.

[57] S. Diebold, R. Weber, M. Seelmann-Eggebert, H. Massler, A. Tessmann, A. Leuther, and I. Kallfass. A Fully-Scalable Coplanar Waveguide Passive Library for Millimeter-Wave Monolithic Integrated Circuit Design. In *41st European Microwave Conference (EuMC), 2011*, pages 293–296, oct. 2011.

[58] Ching-Cheng Tien, C. K C TZUANG, S.-T. Peng, and Chung-Chi Chang. Transmission characteristics of finite-width conductor-backed coplanar waveguide. *Microwave Theory and Techniques, IEEE Transactions on*, 41(9):1616–1624, 1993.

[59] A. Leuther, A. Tessmann, M. Dammann, C. Schworer, M. Schlechtweg, M. Mikulla, R. Losch, and G. Weimann. 50 nm MHEMT Technology for G- and H-Band MMICs. In *Indium Phosphide Related Materials, 2007. IPRM '07. IEEE 19th International Conference on*, pages 24–27, may 2007.

[60] Simon M. Sze and Kwok K. Ng. *Physics of Semiconductor Devices*. Wiley-Interscience, 2006.

[61] A. Tessmann. 220-GHz metamorphic HEMT amplifier MMICs for high-resolution imaging applications. *Solid-State Circuits, IEEE Journal of*, 40(10):2070–2076, 2005.

[62] P.H. Siegel, R.P. Smith, M.C. Graidis, and S.C. Martin. 2.5-THz GaAs monolithic membrane-diode mixer. *Microwave Theory and Techniques, IEEE Transactions on*, 47(5):596–604, may 1999.

[63] S.M. Sze. *Physics of Semiconductor Devices*. John Wiley and Sons (WIE), 1981.

[64] B. Alderman, H. Sanghera, C. Price, B. Thomas, and D.N. Matheson. Fabrication of Reproducible Air-Bridged Schottky Diodes for use at Frequencies near 200 GHz. In *Infrared and Millimeter Waves, 2007 and the 2007 15th International Conference on Terahertz Electronics. IRMMW-THz. Joint 32nd International Conference on*, pages 848 –849, sept. 2007.

[65] Seok Ho Bang, Sang Jin Lee, Mun Kyo Lee, Dong Sik Ko, Sung-Woon Moon, Yong Hyun Baek, Min Han, Seok Gyu Choi, Tae Jong Baek, Byoung-Chul Jun, Dong Chul Park, Sam-Dong Kim, and Jin Koo Rhee. Comparison of Dot Schottky and MHEMT Diodes for 94 GHz Mixer Applications. In *Millimeter Waves, 2008. GSMM 2008. Global Symposium on*, pages 52 –55, april 2008.

[66] C.E. Shannon. Communication in the Presence of Noise. *Proceedings of the IRE*, 37(1):10–21, 1949.

[67] Agilent Technologies. Fundamentals of RF and Microwave Noise Figure Measurements, 2010.

[68] H.T. Friis. Noise Figures of Radio Receivers. *Proceedings of the IRE*, 32(7):419–422, 1944.

[69] Agilent Technologies. Noise Figure Measurement Accuracy - The Y-Factor Method, 2010.

[70] E.J. Wilkinson. An N-Way Hybrid Power Divider. *Microwave Theory and Techniques, IRE Transactions on*, 8(1):116–118, january 1960.

[71] S. Horst, R. Bairavasubramanian, M.M. Tentzeris, and J. Papapolymerou. Modified Wilkinson Power Dividers for Millimeter-Wave Integrated Circuits. *Microwave Theory and Techniques, IEEE Transactions on*, 55(11):2439–2446, nov. 2007.

[72] Seymour B. Cohn. A Class of Broadband Three-Port TEM-Mode Hybrids. *IEEE Transactions on Microwave Theory and Techniques*, 16(2):110–116, 1968.

[73] Stephen A. Maas. *Microwave Mixers (Artech House Antennas and Propagation Library) (Artech House Microwave Library)*. Artech Print on Demand, 1993.

[74] Kai Chang. *Microwave Passive and Antenna Components, Volume 1, Handbook of Microwave and Optical Components*. Wiley-Interscience, 1989.

[75] F.C. de Ronde. Octave-Wide Matched Symmetrical, Reciprocal, 4- And 5 Ports. In *Microwave Symposium Digest, 1982 IEEE MTT-S International*, pages 521–523, june 1982.

[76] M. Kirschning and R.H. Jansen. Accurate Wide-Range Design Equations for the Frequency-Dependent Characteristic of Parallel Coupled Microstrip Lines. *Microwave Theory and Techniques, IEEE Transactions on*, 32(1):83–90, jan 1984.

[77] Agilent Technologies. *Agilent EEsof Advanced Design System 2009 Update 1 Documentation*.

[78] C. H Huang, C. H Chen, and T.-S. Horng. Design of integrated planar marchand balun using physical transformer model. In *Microwave Conference, 2009. APMC 2009. Asia Pacific*, pages 1004–1007, 2009.

[79] E. Valletta, J. Van Beek, A. Den Dekker, N. Pulsford, H. F F Jos, L.C.N. de Vreede, L.K. Nanver, and J.N. Burghartz. Design and characterization of integrated passive elements on high ohmic silicon. In *Microwave Symposium Digest, 2003 IEEE MTT-S International*, volume 2, pages 1235–1238 vol.2, 2003.

[80] Nathan Marchand. Transmission line conversion transformers. *Electronics*, 17:142–145, 1944.

[81] David M. Pozar. *Microwave Engineering*. Wiley, 2011.

[82] I. Kallfass, H. Massler, and A. Leuther. A 210 GHz, Subharmonically-Pumped Active FET Mixer MMIC for Radar Imaging Applications. In *Compound Semiconductor Integrated Circuit Symposium, 2007. CSIC 2007. IEEE*, pages 1–4, 2007.

[83] Federal Communications Commission. REPORT AND ORDER (FCC 03-248) Allocations and Service Rules for the 71-76 GHz, 81-86 GHz and 92-95 GHz Bands, 11 2003.

[84] V.H. Le, H.T. Duong, A.T. Huynh, C.M. Ta, F. Zhang, R.J. Evans, and E. Skafidas. A CMOS 77-GHz Receiver Front-End for Automotive Radar. *Microwave Theory and Techniques, IEEE Transactions on*, PP(99):1–11, 2013.

[85] W. Perndl, H. Knapp, M. Wurzer, K. Aufinger, T.F. Meister, J. Bock, W. Simburger, and A.L. Scholtz. A low-noise, and high-gain double-balanced mixer for 77 GHz automotive radar front-ends in SiGe bipolar technology. In *Radio Frequency Integrated Circuits (RFIC) Symposium, 2004. Digest of Papers. 2004 IEEE*, pages 47–50, 2004.

[86] B. Dehlink, H. D Wohlmuth, H.-R. Forstner, H. Knapp, S. Trotta, K. Aufinger, T.F. Meister, J. Bock, and A.L. Scholtz. A highly linear SiGe double-balanced mixer for 77 GHz automotive radar applications. In *IEEE Radio Frequency Integrated Circuits (RFIC) Symposium, 2006*, page 4 pp., 2006.

[87] I. Kallfass, H. Massler, A. Leuther, A. Tessmann, and M. Schlechtweg. A 210 GHz Dual-Gate FET Mixer MMIC With > 2 dB Conversion Gain, High LO-to-RF Isolation, and Low LO-Drive Requirements. *Microwave and Wireless Components Letters, IEEE*, 18(8):557–559, 2008.

[88] A. Tessmann, A. Leuther, H. Massler, W. Bronner, M. Schlechtweg, and G. Weimann. Metamorphic H-Band Low-Noise Amplifier MMICs. In *Microwave Symposium, 2007. IEEE/MTT-S International*, pages 353–356, 2007.

[89] V. Radisic, K.M.K.H. Leong, X. Mei, S. Sarkozy, W. Yoshida, and W.R. Deal. Power Amplification at 0.65 THz Using InP HEMTs. *Microwave Theory and Techniques, IEEE Transactions on*, 60(3):724–729, 2012.

[90] A.A. Abidi. Direct-Conversion Radio Transceivers for Digital Communications. *Solid-State Circuits, IEEE Journal of*, 30(12):1399–1410, 1995.

[91] Florian Boes. 100 Gbit/s Millimeter-Wave Photonic Wireless Link. Master's thesis, Karlsruhe Institute of Technology, 2013.

[92] ITU. Recommendation p.676-9 attenuation by atmospheric gases.

List of Publications

[93] **Lopez-Diaz, D.**, I. Kallfass, A Tessmann, R. Weber, H. Massler, A. Leuther, M. Schlechtweg, and O. Ambacher. High-Performance 60 GHz MMICs for Wireless Digital Communication in 100 nm mHEMT Technology. *International Journal of Microwave and Wireless Technologies*, 3:107–113, 3 2011.

[94] S. Koenig, J. Antes, **Lopez-Diaz, D.**, I. Kallfass, T. Zwick, C. Koos, W. Freude, and J. Leuthold. High-Speed Wireless Bridge at 220 GHz Connecting Two Fiber-Optic Links Each Spanning up to 20 km. In *Optical Fiber Communication Conference*, page OM2B.1. Optical Society of America, 2012.

[95] I. Kallfass, A. Tessmann, H. Massler, **Lopez-Diaz, D.**, A. Leuther, M. Schlechtweg, and O. Ambacher. A 300 GHz Active Frequency-Doubler and Integrated Resistive Mixer MMIC. In *Microwave Integrated Circuits Conference, 2009. EuMIC 2009. European*, pages 200–203, sept. 2009.

[96] I. Kallfass, J. Antes, T. Schneider, F. Kurz, **Lopez-Diaz, D.**, S. Diebold, H. Massler, A. Leuther, and A. Tessmann. All Active MMIC-Based Wireless Communication at 220 GHz. *Terahertz Science and Technology, IEEE Transactions on*, 1(2):477–487, 2011.

[97] J. Antes, **Lopez-Diaz, D.**, A. Tessmann, A. Leuther, H. Massler, T. Zwick, O. Ambacher, and I. Kallfass. MMIC Based Wireless Data Transmission of a 12.5 Gbit/s Signal using a 220 GHz Carrier. In *Microwave Conference (EuMC), 2011 41st European*, pages 238–241, 2011.

[98] I. Kallfass, A. Tessmann, J. Antes, **Lopez-Diaz, D.**, M. Kuri, H. Massler, T. Zwick, and A. Leuther. Wireless DVB-C transmission at 220 GHz using active single-chip receive and transmit MMICs. In *Microwave Symposium Digest (MTT), 2011 IEEE MTT-S International*, pages 1–4, 2011.

[99] I. Kallfass, J. Antes, **Lopez-Diaz, D.**, S. Wagner, A. Tessmann, and A. Leuther. Broadband Active Integrated Circuits for Terahertz Communication. *European Wireless, 2012. EW. 18th European Wireless Conference*, pages 1–5, april 2012.

[100] **Lopez-Diaz, D.**, I. Kallfass, A. Tessmann, H. Massler, A. Leuther, M. Schlechtweg, and O. Ambacher. Monolithic Integrated 210 GHz Couplers for Balanced Mixers and Image Rejection Mixers. In *Integrated Nonlinear Microwave and Millimeter-Wave Circuits (INMMIC), 2010 Workshop on*, pages 58 –61, april 2010.

[101] **Lopez-Diaz, D.**, I. Kallfass, A. Tessmann, A. Leuther, H. Massler, M. Schlechtweg, and O. Ambacher. Subharmonically Pumped 210 GHz I/Q Mixers. In *Compound*

Semiconductor Integrated Circuit Symposium (CSICS), 2010 IEEE, pages 1–4, 2010.

[102] **Lopez-Diaz, D.**, I. Kallfass, A. Tessmann, H. Massler, A. Leuther, M. Schlechtweg, and O. Ambacher. A Balanced Resistive 210 GHz Mixer with 50 GHz IF Bandwidth. In *Microwave Integrated Circuits Conference (EuMIC), 2010 European*, pages 190–193, 2010.

[103] **Lopez-Diaz, D.**, I. Kallfass, A. Tessmann, A. Leuther, S. Wagner, M. Schlechtweg, and O. Ambacher. A Subharmonic Chipset for Gigabit Communication around 240 GHz. In *Microwave Symposium Digest (MTT), 2012 IEEE MTT-S International*, pages 1–3, 2012.

[104] **Lopez-Diaz, D**, A Tessmann, A. Leuther, S. Wagner, M. Schlechtweg, O. Ambacher, S. Koenig, J. Antes, F. Boes, F. Kurz, R. Henneberger, and I. Kallfass. A 240 GHz Quadrature Receiver and Transmitter for Data Transmission up to 40 Gbit/s. In *European Microwave Integrated Circuits Conference, 2013 EuMIC 2013.*, 2013.

[105] J. Antes, S. Konig, **Lopez-Diaz, D.**, Boes F., A Tessmann, R. Henneberger, O. Ambacher, T. Zwick, and I. Kallfass. Transmission of an 8-PSK Modulated 30 Gbit/s Signal using an MMIC-based 240 GHz Wireless Link. In *Microwave Symposium Digest (MTT), 2013 IEEE MTT-S International*, pages 1 –3, june 2013.

[106] S. Koenig, **Lopez-Diaz, D.**, J. Antes, F. Boes, R. Henneberger, A. Leuther, A Tessmann, R. Schmogrow, D. Hillerkuss, R. Palmer, T. Zwick, C. Koos, W. Freude, O. Ambacher, J. Leuthold, and I. Kallfass. Wireless sub-THz communication system with high data rate. *Nature Photonics*, 7:977–981, 2013.

Daniel Lopez-Diaz
daniel@lopez-diaz.de

Klagenfurter Strasse 4
A-9500 Villach
Austria

EDUCATION

PhD student, Fraunhofer Institute for Applied Solid State Physics IAF, Freiburg, Germany
High Frequency Devices and Circuits Department (Feb. 2009 – Apr. 2013)
Thesis: "Broadband Transceiver Circuits for Millimeter-Wave Wireless Communication"
Advisor: Prof. Dr. I. Kallfass, University of Stuttgart, Germany

Dipl-Ing. (MS equivalent), Karlsruhe Institute of Technology, Germany
Electrical Engineering, Focused on "System-on-Chip" (Oct 2008)
Thesis: "Characterization and comparison of different stall detect methods on DC stepper motors for dashboard applications", Carried out at Freescale Semiconductor, Munich, Germany
Advisor: Prof. Dr. M. Siegel, Karlsruhe Institute of Technology, Germany

RESEARCH EXPERIENCE

Doctoral Research: Department of High Frequency Devices and Circuits, Fraunhofer IAF, 2009-2013 (Research Advisor: Prof. Dr. I. Kallfass)

- Design and layout of RF MMICs with operation frequencies > 200 GHz
- MMIC based wireless data transmission with up to 100 Gbit/s
- Development of digital blocks for signal processing in VHDL
- Management of joint research projects
- Publication / review of scientific papers

PROFESSIONAL EXPERIENCE

Senior Engineer RF Design, Lantiq A GmbH, Villach, Austria, May 2013 – present
Design of building blocks for WLAN RFICs in a deep submicron CMOS technology. In contrast to the MMIC design at millimeter-wave frequencies, large-scale integration, low power and high yield considerations poses significant design challenges.

Scientific Staff Member, Fraunhofer IAF, Freiburg. Germany, Feb. 2009 – Apr. 2013
Designed chipsets for radar and wireless high speed data transmission above 200 GHz using an in-house metamorphic HEMT process based on 4" GaAs substrates. Mainly focused on broadband mixer circuits for direct conversion architectures. Designed active and passive mixers from 80 GHz to 280 GHz with intermediate frequencies of up to 50 GHz. Low conversion loss and LO drive requirements combined with a flat frequency response were the main design challenges. Created receive and transmit chipsets for world record wireless data transmissions around 240 GHz.

Design Engineer, Freescale Semiconductor Inc., Munich, Germany, Nov. 2008 – Dec. 2008
Worked for Freescale for two month after finishing the diploma thesis. Responsibilities included:

- Generation of liberty files for the chip integration of a 180 nm pad library
- Evaluation of analog blocks on a 90 nm CMOS test chip

PATENTS

US Patent US 8716971 B2

European Patent EP 2384539 A0

Herausgeber: Prof. Dr. Oliver Ambacher

In the present work, broadband millimeter wave (mmW) receiver and transmitter circuits for wireless communication in the frequency range around 240 GHz are investigated. The absolute available bandwidths in the mmW frequency range allow high data rates and thus potentially close the technological gap between fast but wired and the comparatively slow and wireless communication. For this purpose, monolithic integrated millimeter wave mixer circuits (MMICs) are designed and analyzed, based on the metamorphic high electron mobility transistor, developed at the Fraunhofer Institute for Applied Solid State Physics (IAF). To simplify the signal generation of the local oscillator, subharmonic mixer circuits are of special interest. Together with other building blocks, these circuits are then integrated in multi-functional receiver and transmitter MMICs for wireless digital communication. These active transmitter and receiver MMICs form the functional core of a 240 GHz radio link, which is able to transmit data with up to 40 Gbit/s in a single-input single-output configuration. As part of a long range demonstrator, they allowed the transmission of up to 24 Gbit/s over a distance of 1.1 km.

ISBN 978-3-8396-0834-0

9 783839 608340